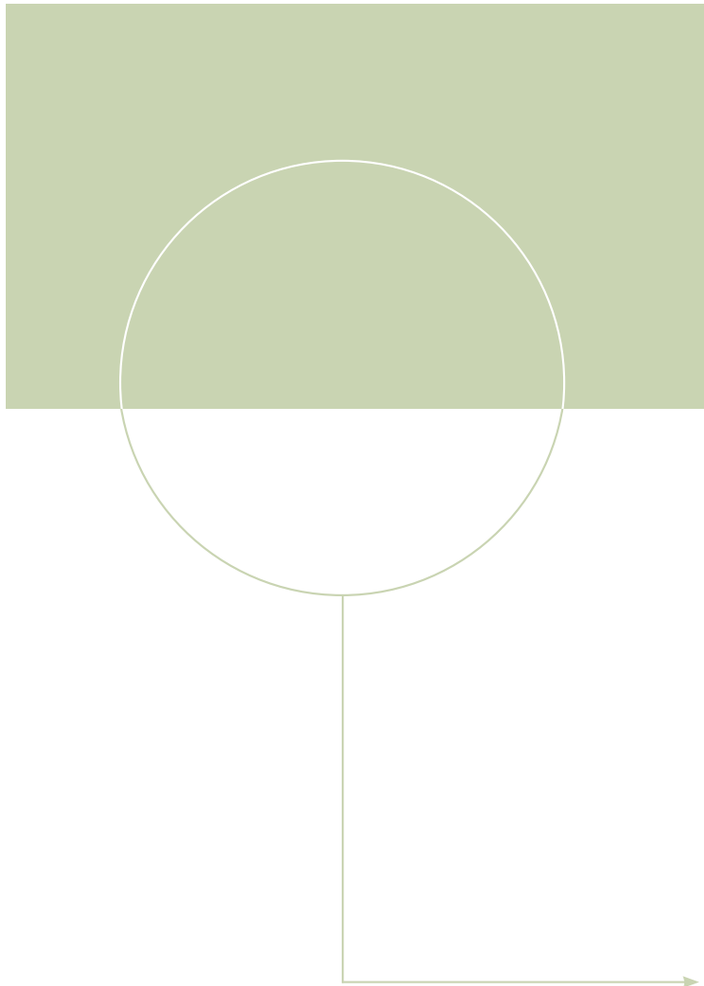

Master's thesis

2020

Betina Hansen

NTNU
Norwegian University of
Science and Technology
Faculty of Engineering
Department of Civil and Environmental Engineering

Betina Hansen

Verification of the Vertical Bearing Capacity of Excavation Support Systems with Numerical Analyses

April 2020

NTNU
Norwegian University of
Science and Technology

NTNU
Norwegian University of
Science and Technology

NTNU
Norwegian University of
Science and Technology

Verification of the Vertical Bearing Capacity of Excavation Support Systems with Numerical Analyses

Betina Hansen

Civil and Environmental Engineering
Submission date: April 2020
Supervisor: Steinar Nordal
Co-supervisor: Werner Felber

Norwegian University of Science and Technology
Department of Civil and Environmental Engineering

Preface

This thesis is written during the winter of 2019/2020 as the last part of my Master of Science degree in Civil and Environmental Engineering, for the geotechnical department at the Norwegian University of Science and Technology. The thesis is given by and performed in cooperation with Boley Geotechnik in Munich, Germany.

I would like to express my gratitude to Boley Geotechnik for providing me with office space during my thesis, and to my supervisor Werner Felber and colleagues Jonas Wieser and Chuantao Chen for guidance. I would also like to thank NTNU supervisor Steinar Nordal for his much appreciated advice. Lastly, I would like to express my appreciation to NTNU for making working during the Corona Crisis as comfortable as possible.

Trondheim, 24-04-20

Betina Hansen

Betina Hansen

Summary and conclusions

This thesis is based on an underground railway station in Munich that is to be built. Retaining structures has frequently been studied as lateral retaining structures, but the use of this structure for permanent vertical load bearing as well, is increasing. There are different methods to calculate the vertical capacity and different methods provide different results. The safety factors for the vertical capacity are calculated numerically by using PLAXIS 2D to calculate the earth pressures acting on the wall on the active side, and the maximum possible resistance forces that can act on the passive side. These results are used to calculate the safety factor for the vertical capacity. Earth pressures are calculated analytically according to the German Standard. In order to compare the different methods, it is investigated to what degree the variation of friction angles, cohesion and earth pressures angles affect the results of the different methods. In addition, the safety factors are calculated in three different ways for each method. One where resistance forces on the passive side and below the required embedment depth on the active side in addition to the tip resistance are obtained from the geotechnical report and the active earth pressures are obtained from analytical or numerical calculations, one where only the tip resistance and passive earth pressure is obtained from the geotechnical report and all forces on the soil side is obtained from analytical and numerical calculations and one where only the tip resistance is obtained from the geotechnical report.

In the load situation used in the reference model, it is found that the wall is moving downwards relative to the soil, creating nearly only upwards acting earth pressures. This means that a negative earth pressure angle on the active soil side needs to be used for the analytical calculations in order to obtain results similar to the numerical results. It is also found that variation of the friction angle gives the largest spread of results within one method, while varying the earth pressure angle gives the largest spread of results between the different methods. The cohesion creates some, but little variation in the earth pressures and safety factors. The safety factor calculation where all resistance forces are obtained from the geotechnical report, provides results with least spread between the different methods. The plate model provides slightly more conservative safety factors due to the foot plate hindering the relative movement between the soil and the lower part of the wall, which leads to smaller vertical earth pressures in the clay layer on both sides of the wall.

Sammendrag og konklusjoner

Denne avhandlingen er basert på en undergrunns jernbanestasjon som skal bygges i Munchen. Støttekonstruksjoner har ofte blitt studert som laterale støttekonstruksjoner, men bruken av denne type struktur for permanent vertikalt lastbæring i tillegg, øker. Den vertikale kapasiteten kan beregnes på flere måter og de ulike måtene gir ulike resultater. Sikkerhetsfaktorene for den vertikale kapasiteten beregnes numerisk ved å bruke PLAXIS 2D for å beregne jordtrykkene som virker på veggen på den aktive siden, og maksimale mulige motstandskrefter som kan virke på den passive siden. Disse resultatene brukes til å beregne sikkerhetsfaktoren for vertikal kapasiteten. Jordtrykk blir beregnet analytisk i henhold til den tyske standarden. For å sammenligne de forskjellige metodene, blir det undersøkt i hvilken grad variasjonen av friksjonsvinkler, kohesjon og jordtrykkvinkler påvirker resultatene av de forskjellige metodene. I tillegg beregnes sikkerhetsfaktorene på tre forskjellige måter for hver metode. En der motstandskrefter på den passive siden og under den nødvendige vegg dybden på den aktive siden i tillegg til spissmotstanden er hentet fra den geotekniske rapporten og de aktive jordtrykkene er hentet fra analytiske eller numeriske beregninger, en der bare spissmotstanden og det passive jordtrykket er hentet fra den geotekniske rapporten, og alle krefter på jordssiden er hentet fra analytiske og numeriske beregninger, og en der bare spissmotstanden er hentet fra den geotekniske rapporten.

I referansemodellens belastningssituasjon, ble det funnet at veggen beveger seg nedover i forhold til jorda, og skaper nesten bare oppovervirkende jordtrykk. Dette betyr at en negativ jordtryksvinkel på den aktive jordsiden må brukes til de analytiske beregningene for å oppnå resultater som ligner de numeriske resultatene. Det er også funnet at variasjon av friksjonsvinkelen gir størst spredning av resultater innen en metode, mens variasjon av jordtrykkvinkelen gir den største spredningen av resultater mellom de forskjellige metodene. Kohesjonen skaper noe, men liten variasjon i jordtrykk og sikkerhetsfaktorer. Beregningen av sikkerhetsfaktorer der alle motstandskrefter oppnås fra den geotekniske rapporten, gir resultater med minst spredning mellom de forskjellige metodene. Platemodellen gir litt mer konservative sikkerhetsfaktorer på grunn av at fotplaten hindrer den relative bevegelsen mellom jorden og den nedre delen av veggen, noe som fører til mindre oppovervirkende vertikale jordtrykk i leirlaget på sidene av veggen.

Contents

List of Figures

List of Tables

Chapter 1

Introduction

1.1 Background

In order to design excavation support systems, geotechnical stability calculations have to be performed. In general, the vertical capacity of excavation support systems can be verified with analytical calculations, comparing acting forces to resisting forces. As a part of the calculations, the verification of vertical bearing capacity of the excavation supports must be confirmed. Most of the European Standards uses the concept of partial safety factors. The design of excavation support systems in analytical calculations is carried out with the earth pressure theories of Rankine and Coulomb. Numerical FEM calculations allows one to perform simulations of more complex situations and more factors can be taken into account. However, the implementation of safety factors for different loads and load scenarios is not always possible in numerical analysis. It is also not possible to straight forward verify the vertical capacity with numerical calculation considering that simulations are in static equilibrium at the end of each calculation phase.

In this thesis the verification of the vertical capacity of excavation support systems will be investigated using analytical and numerical methods. Based on the current practice for design approaches, taking analytical methods and available standards into account, numerical simulations are carried out on a deep excavation example. The example of the excavation support system is based on a railway project in Munich.

For the simulation of the soil behaviour, the non-linear elasto-plastic material model “Hardening Soil with Small Strain Stiffness" (HSS) is used. The necessary model parameters will be taken from the Geotechnical Report of the project. The FE calculations are carried out with the

software PLAXIS 2D 2018.

Problem formulation

A part of the design of excavation support systems, is the verification of the vertical bearing capacity. In FE-calculations, the calculation model will be in equilibrium after each calculation phase. This means that it will verify the bearing capacity in the current situation. The goal of this thesis is to investigate the vertical capacity of an excavation wall with analytical and numerical analysis. Different approaches to designing an excavation support wall analytically and numerically are investigated. A number of parameters are varied one by one, both in the numerical and in the corresponding analytical models. Different design approaches provides different results. These results, as well as the impact from the parameter variations are analyzed. Results, such as normal and shear stresses, displacements, relative displacements and safety factors are investigated and compared in order to see the differences between the design approaches.

1.2 Objectives

The main objectives of this thesis are

1. In which way can a diaphragm wall be modelled with plate elements in order to obtain results similar to a continuum model?
2. To what degree does the bottom plate in the numerical plate model affect the results?
3. What are the challenges with numerical calculations considering partial safety factors?
4. To what degree does the change of friction angles, cohesion and earth pressure angle affect the safety factors?
5. Which parameter has the largest impact on the safety factors?

1.3 Structure of the thesis

The rest of the report is structured as follows. Chapter 2 presents the theoretical background of the thesis in order to gain knowledge of current design approaches for deep excavation support systems in analytical and numerical analysis. In Chapter 3 the Finite-Element-Software,

the Material models and the used parameters are described. Chapter 4 describes the project which the thesis is based on and Chapter 5 presents the analytical and numerical calculation models used. Chapter 6 describes the process of choosing the reference model and the results and findings can be found in Chapter 7. Chapter 8 contains summary, conclusions and recommendations for further work.

Chapter 2

Theoretical Background

Retaining structures such as diaphragm walls, sheet pile walls and soldier piles have mostly been used for lateral retaining in excavations for underground structures such as shipyards, buildings and as in this case, metro stations. The diaphragm wall as a lateral retaining structure has frequently been studied the past years. However, with time, construction techniques and design develops. The use of this structure for permanent vertical load bearing in addition to lateral retaining increases. This chapter will present how calculation of the vertical capacity of such a wall can be handled analytically and numerically. This chapter also compares the analytical method according to the German standard with the method taught at The Norwegian University of Science and Technology.

2.1 Literarure review

For analytical verification of vertical capacity of excavation support systems, the German standard is used, and for the numerical calculations the EAB is used. Other than this there is not found much literature on this topic. However, this thesis can be seen as an investigation of the analytical and numerical approach to finding the vertical capacity.

2.2 Types and application areas of excavation support systems

There are different ways of retaining the earth in order to dig a deep excavation. Depending on the soil and environmental conditions, the water table conditions, the safety of adjacent

buildings and the economy, different earth retaining systems can be selected. Different systems are described below:

Sheet pile walls

The use of sheet pile walls are normally restricted in urban areas due to effect of vibrations, difficulty of driving the piles due to boulders and hard layers, presence of buried pipes and public utilities and environmental problems. They are designed to resist lateral forces (Eskandari and Kalantari, 2011). Sheet pile walls are used to construct deep excavation foundations, waterfront structures and erosion protection. A steel sheet pile wall can be constructed water tight. It is used in temporary and permanent structures (Sadeghi et al., 2018). Sheet pile walls can be cantilevered, anchored or strutted. Sheet pile walls can be made of wood, steel or reinforced concrete. Figure 2.1 shows two different types of sheet pile sections.

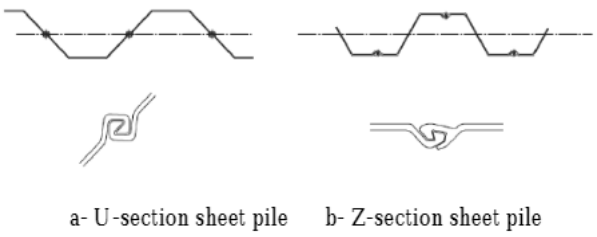

Figure 2.1: Sheet pile section types (Sadeghi et al., 2018)

Pile walls

Pile walls can be cast in situ or they can be precast. During installation, there is less noise and vibration than for installation of sheet pile walls. Pile walls have greater stiffness than sheet pile walls (Godavarthi et al., 2011). Three different types of piles walls are presented below and illustrated in Figure 2.1:

• Contiguous pile wall: Piles installed with gaps between. Due to low installation costs, they are more economical than diaphragm walls for small and medium excavations. The diameter and spacing of the piles depends on soil type, ground water level and magnitude of design pressures. Contiguous pile walls are suitable in urban areas.

• Secant pile wall: Intersecting piles. The space between the piles are smaller than the pile diameter. Secant pile walls are used for minimizing movement in wet and weak soils and to

build cut off walls for controlling groundwater inflow.

• Tangent pile wall: A series of piles installed alongside each other, touching. Less stiff than secant pile wall, and less effective keeping groundwater out of excavation.

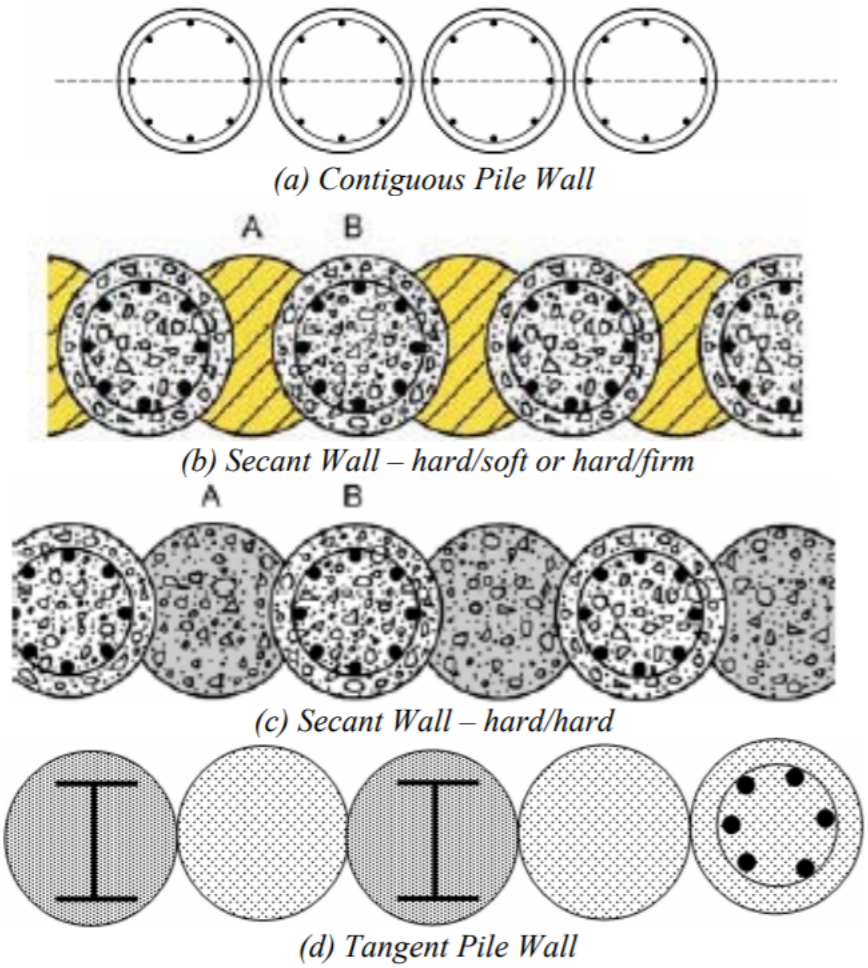

Figure 2.2: Types of pile walls (Godavarthi et al., 2011)

Diaphragm walls

Diaphragm walls are used for deep excavations when major construction work is performed under the water table. When installing the wall, bentonite or polymer-based slurries are filled in the trench as it is excavated in order to prevent soil incursions. As Figure 2.3 illustrates; when the excavation is finished, the slurry is replaced by reinforcement and concrete. The structure formed is the diaphragm wall. Such a wall can be used both as support in a temporary excavation and as a part of a permanent structure. This kind of support system provides high structural support and water tightness. Advantages with diaphragm walls is that they can be used in many

different soil types and rocks, it can reach large depths, it is water tight, it may be installed near existing structures and it is suitable for urban areas. (Soilmec, 2019)

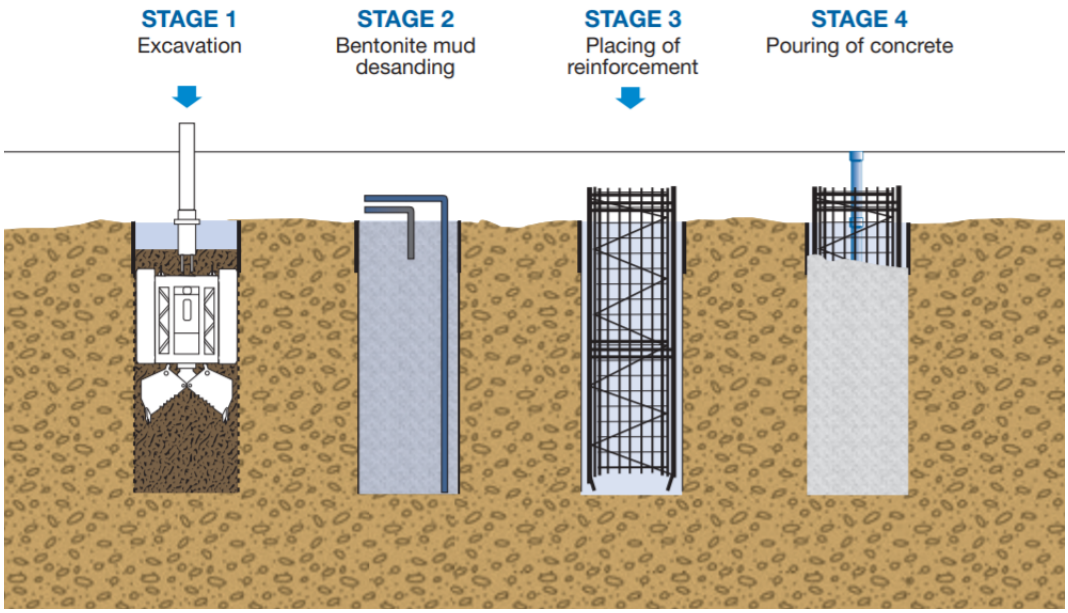

Figure 2.3: Construction sequence of diaphragm walls (Soilmec, 2019).

2.3 Verification of the vertical capacity in general

To ensure the vertical capacity of a wall, the vertical resistance forces must be larger than the downwards acting forces such as the weight of the wall, earth pressures and external loads. The resistance forces acts mostly as friction forces along the sides of the walls, but also at the bottom tip. Figure 2.4 illustrates the forces acting on the wall.

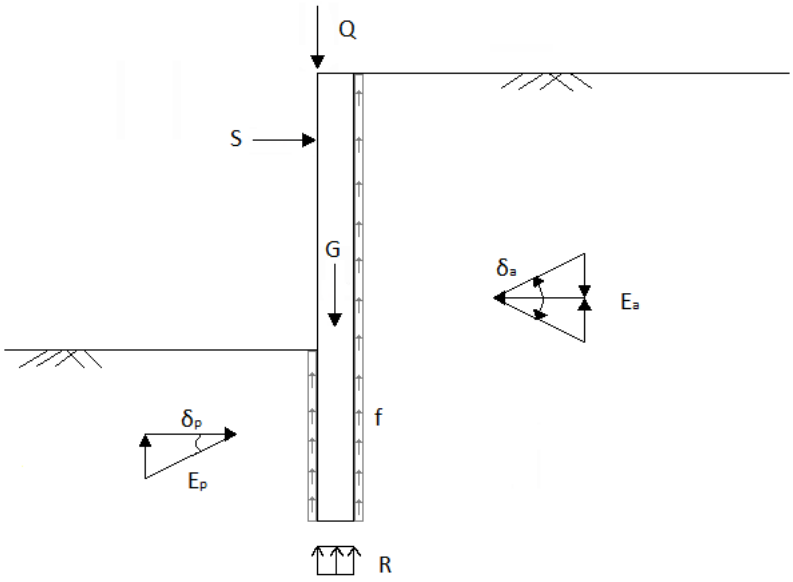

Figure 2.4: Acting forces on retaining wall

Downwards acting forces

The external force, Q, is the resultant of forces such as the weight of and potential service loads on struts and the downward acting forces of anchors. G is the weight of the wall. The direction of friction forces, f, and whether the earth pressure angle, δ_a is positive or negative depends on the relative movement between the soil and the wall. In the case where the soil moves downwards relative to the wall, the earth pressure angle is positive. Thus, a downward acting earth pressure, $E_{a,y}$, develops behind the wall and the friction force acts downwards instead of as a resistance (see Figure 2.5). There might also be terrain and service loads outside of the excavation that can affect the earth pressure angle. External forces acting on slabs and struts is acting on the side of the wall, causing a bending moment in the wall.

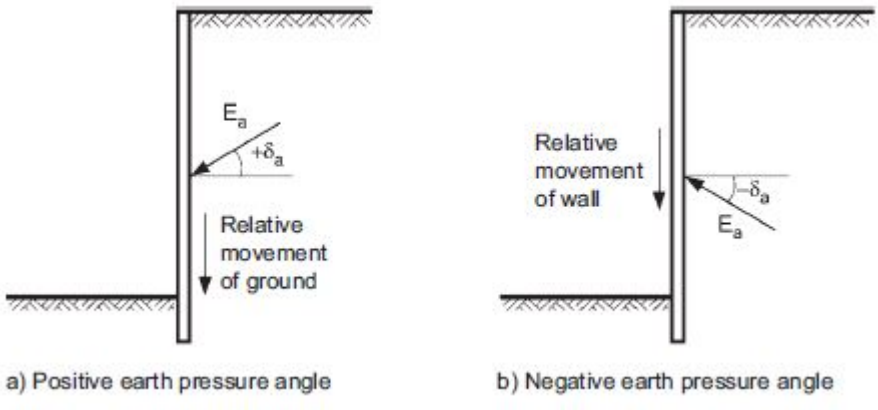

Figure 2.5: Earth pressure angle for active earth pressure (DGGT, 2013)

Resistance forces

The resistance forces, as illustrated in Figure 2.4 are the tip resistance, R, and the friction forces, f, along the sides of the wall in situations where the wall is moving downwards relative to the soil. Additionally, when ground water is present, it will cause an uplift force.

2.4 Earth pressure definitions

Earth pressure denotes the stress components (normal and shear) that occurs in a vertical interface between soil and structure (Aarhaug, 1984). In the case of an excavation, where a wall (eg. diaphragmant wall or sheet pile wall) is installed and the earth is excavated, a situation similar to the one in Figure 2.8 is obtained. In earth pressure calculations, it is usually differed between three states, depending on the movement of the wall:

- Earth pressure at rest: An at rest-earth pressure is obtained if the wall can resist horizontal displacement.

- Active earth pressure: As illustrated in Figure 2.8, when the wall is moving away from the soil, active earth pressure developes. As the wall moves away from the soil, the earth pressure gradually decreases from the at rest-pressure to a lower limit is reached. At this limit, the soil fails and here we obtain the active earth pressure (Aarhaug, 1984). This is illustrated in Figure 2.6. These areas of active earth pressure is defined by the areas where the horizontal stresses are smaller than the vertical stresses in an earth element close to the

structure (Emdal et al., 2013).

- Passive earth pressure: If the wall starts at rest and moves towards the soil, and the soil is compressed until failure is reached along a passive failure surface. In this situation, as shown in Figure 2.8, passive earth pressure develops. As Figure 2.6 shows, the the displacement needed to reach passive earth pressure and the size of the pressure is significantly larger than the for the active earth pressure. The areas of passive earth pressure are defined by where the horizontal stresses are larger than the vertical stresses (Emdal et al., 2013).

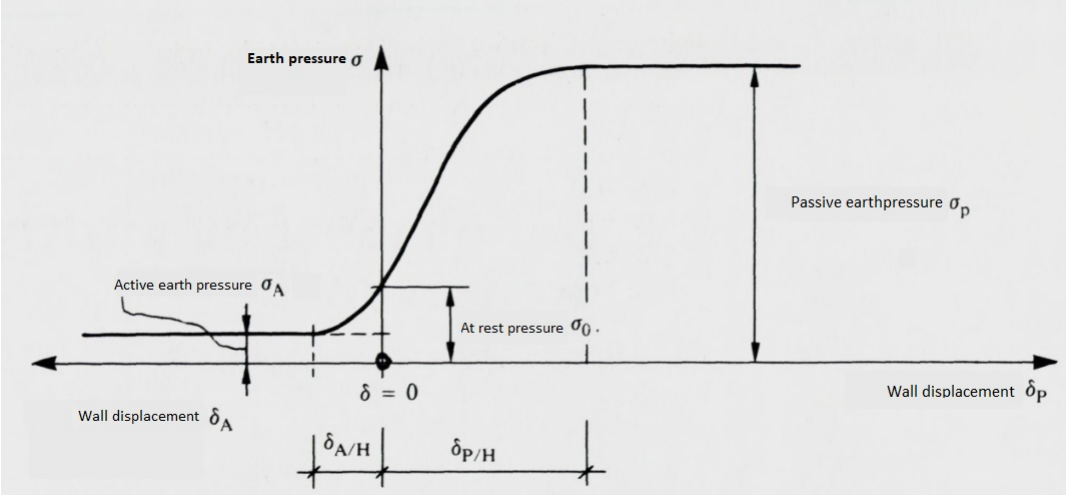

Figure 2.6: Relation between horizontal displacement and earth pressure (adapted from Aarhaug, 1984)

Any wall will act like a cantilever wall, like in Figure 2.8 until the first strut is installed. One method used to describe earth pressure on sheet pile walls is the British method and it is described by Padfield and Mair (1984). The wall is in this case assumed to rotate around a point on the lower end of the wall. The deformation of the wall is illustrated in Figure 2.8. The upper end will move into the excavation, creating an active earth pressure behind the wall, down to the rotation point. Between the excavation bottom and the rotation point in front of the wall, a passive earth pressure is created. The wall will deform in the opposite direction below the rotation point, leading to a passive earth pressure behind the wall and an active in front. To calculate the earth pressure according to this method, an iteration process is necessary. However, the method can, according to Padfield and Mair (1984), be simplified. The earth pressure below the rotation point can be replaced by a resultant force acting in the rotation point. This

is illustrated in Figure 2.7. In order to determine the required embedment depth d_0, moment equilibrium about O is calculated. Experience shows that this simplification gives a depth, d, that is a little short. Therefore the depth, d, is made 20 % longer than what is required according to calculations. This makes the simplified method slightly more conservative than The British Method (Padfield and Mair, 1984).

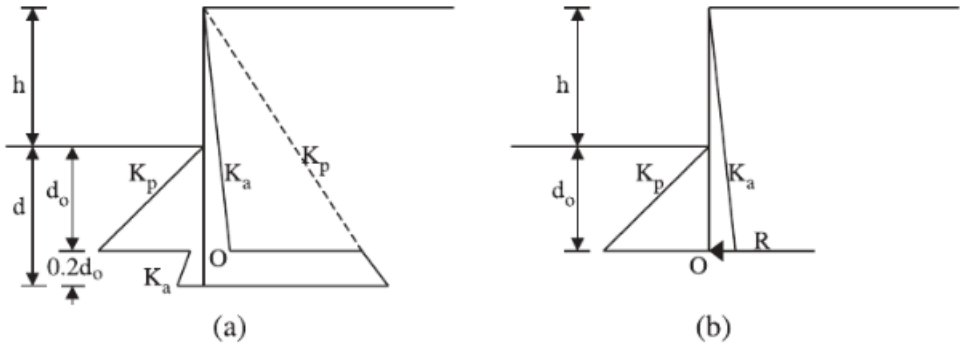

Figure 2.7: (a) Idealized earth pressure distribution and (b) simplified earth pressure distribution according to Padfield and Mair (1984) (Osman and Bolton, 2011)

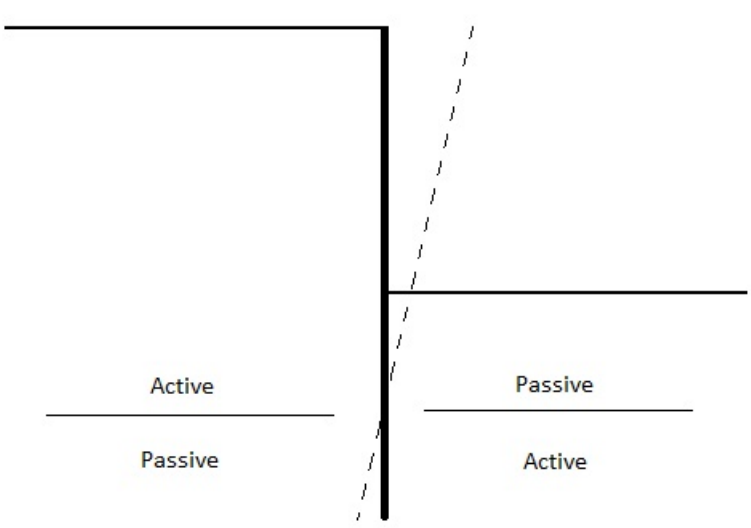

Figure 2.8: Excavation example: Earth pressures due to wall displacement

2.5 Analytical calculation of vertical bearing capacity

As explained in the German "Recommendations on Excavations" (EAB) (DGGT, 2013, section R84), sufficient bearing capacity is obtained when the sum of design values of the components

directed downwards, V_d does not exceed the sum of design values of the resistance forces R_d:

$$V_d \leq R_d$$

Examples of downward directed forces are the weight of the wall and struts, service loads on struts, downward acting forces from anchors, downward acting earth pressures and friction forces and terrain loads. Examples of resistance forces are tip resistance, upward acting earth pressures like passive earth pressures or earth pressures below the required embedment depth.

Characteristic actions directed downwards shall be converted into design values using the partial safety factors γ_Q and γ_G. The resistance forces are converted by partial safety factors for resistance forces. The partial safety factors are given in tables 2.1, 2.2 and 2.3, and the values are obtained from Deutsches Institut für Normung (DIN) (2010). The combination of partial safety factors is chosen according to Design Approach 2 in the German Standard. According to the German Standard, Design Approach 2 is to be applied for determination of internal forces, as well as for the verification of sufficient earth resistance, for the verification of safety against sliding soil and ground failure, for the verification of load-bearing capacity of piles and anchors and for the verification of stability in slip surfaces. The Second Design Approach is referred to as GEO-2 in the safety factor tables.

The application of partial safety factors differs between permanent (BS-P), variable (BS-T), accidental (BS-A), favorable (günstigen) and unfavorable (ungünstigen) loads and between application to structural and geotechnical parts. In this approach, partial factors are applied to actions or affects of actions from the structure and to the soil strength.

Table 2.1: Partial factors on actions or the effect of actions (Deutsches Institut für Normung (DIN), 2010)

Einwirkung bzw. Beanspruchung	Formelzeichen	Bemessungssituation		
		BS-P	BS-T	BS-A
HYD und UPL: Grenzzustand des Versagens durch hydraulischen Grundbruch und Aufschwimmen				
Destabilisierende ständige Einwirkungen[a]	$\gamma_{G,dst}$	1,05	1,05	1,00
Stabilisierende ständige Einwirkungen	$\gamma_{G,stb}$	0,95	0,95	0,95
Destabilisierende veränderliche Einwirkungen	$\gamma_{Q,dst}$	1,50	1,30	1,00
Stabilisierende veränderliche Einwirkungen	$\gamma_{Q,stb}$	0	0	0
Strömungskraft bei günstigem Untergrund	γ_H	1,35	1,30	1,20
Strömungskraft bei ungünstigem Untergrund	γ_H	1,80	1,60	1,35
EQU: Grenzzustand des Verlusts der Lagesicherheit				
Ungünstige ständige Einwirkungen	$\gamma_{G,dst}$	1,10	1,05	1,00
Günstige ständige Einwirkungen	$\gamma_{G,stb}$	0,90	0,90	0,95
Ungünstige veränderliche Einwirkungen	γ_Q	1,50	1,25	1,00
STR und GEO-2: Grenzzustand des Versagens von Bauwerken, Bauteilen und Baugrund				
Beanspruchungen aus ständigen Einwirkungen allgemein[a]	γ_G	1,35	1,20	1,10
Beanspruchungen aus günstigen ständigen Einwirkungen[b]	$\gamma_{G,inf}$	1,00	1,00	1,00
Beanspruchungen aus ständigen Einwirkungen aus Erdruhedruck	$\gamma_{G,E0}$	1,20	1,10	1,00
Beanspruchungen aus ungünstigen veränderlichen Einwirkungen	γ_Q	1,50	1,30	1,10
Beanspruchungen aus günstigen veränderlichen Einwirkungen	γ_Q	0	0	0
GEO-3: Grenzzustand des Versagens durch Verlusts der Gesamtstandsicherheit				
Ständige Einwirkungen[a]	γ_G	1,00	1,00	1,00
Ungünstige veränderliche Einwirkungen	γ_Q	1,30	1,20	1,00
SLS: Grenzzustand der Gebrauchstauglichkeit				
γ_G = 1,00 für ständige Einwirkungen bzw. Beanspruchungen				
γ_Q = 1,00 für veränderliche Einwirkungen bzw. Beanspruchungen				

[a] einschließlich ständigem und veränderlichem Wasserdruck.

[b] nur im Sonderfall nach 7.6.3.1 A (2).

Table 2.2: Partial factors for soil parameters (Deutsches Institut für Normung (DIN), 2010)

Bodenkenngröße	Formelzeichen	Bemessungssituation		
		BS-P	BS-T	BS-A
HYD und UPL: Grenzzustand des Versagens durch hydraulischen Grundbruch und Aufschwimmen				
Reibungsbeiwert tan φ' des dränierten Bodens und Reibungsbeiwert tan φ_u des undränierten Bodens	$\gamma_{\varphi'}$, $\gamma_{\varphi u}$	1,00	1,00	1,00
Kohäsion c' des dränierten Bodens und Scherfestigkeit c_u des undränierten Bodens	$\gamma_{c'}$, γ_{cu}	1,00	1,00	1,00
GEO-2: Grenzzustand des Versagens von Bauwerken, Bauteilen und Baugrund				
Reibungsbeiwert tan φ' des dränierten Bodens und Reibungsbeiwert tan φ_u des undränierten Bodens	$\gamma_{\varphi'}$, $\gamma_{\varphi u}$	1,00	1,00	1,00
Kohäsion c' des dränierten Bodens und Scherfestigkeit c_u des undränierten Bodens	$\gamma_{c'}$, γ_{cu}	1,00	1,00	1,00
GEO-3: Grenzzustand des Versagens durch Verlust der Gesamtstandsicherheit				
Reibungsbeiwert tan φ' des dränierten Bodens und Reibungsbeiwert tan φ_u des undränierten Bodens	$\gamma_{\varphi'}$, $\gamma_{\varphi u}$	1,25	1,15	1,10
Kohäsion c' des dränierten Bodens und Scherfestigkeit c_u des undränierten Bodens	$\gamma_{c'}$, γ_{cu}	1,25	1,15	1,10

Table 2.3: Partial resistance factor for retaining structures (Deutsches Institut für Normung (DIN), 2010)

Widerstand	Formelzeichen	Bemessungssituation		
		BS-P	BS-T	BS-A
STR und GEO-2: Grenzzustand des Versagens von Bauwerken, Bauteilen und Baugrund				
Bodenwiderstände				
— Erdwiderstand und Grundbruchwiderstand	$\gamma_{R,e}$, $\gamma_{R,v}$	1,40	1,30	1,20
— Gleitwiderstand	$\gamma_{R,h}$	1,10	1,10	1,10
Pfahlwiderstände aus statischen und dynamischen Pfahlprobebelastungen				
— Fußwiderstand	γ_b	1,10	1,10	1,10
— Mantelwiderstand (Druck)	γ_s	1,10	1,10	1,10
— Gesamtwiderstand (Druck)	γ_t	1,10	1,10	1,10
— Mantelwiderstand (Zug)	$\gamma_{s,t}$	1,15	1,15	1,15
Pfahlwiderstände auf der Grundlage von Erfahrungswerten				
— Druckpfähle	γ_b, γ_s, γ_t	1,40	1,40	1,40
— Zugpfähle (nur in Ausnahmefällen)	$\gamma_{s,t}$	1,50	1,50	1,50
Herausziehwiderstände				
— Boden- bzw. Felsnägel	γ_a	1,40	1,30	1,20
— Verpresskörper von Verpressankern	γ_a	1,10	1,10	1,10
— Flexible Bewehrungselemente	γ_a	1,40	1,30	1,20
GEO-3: Grenzzustand des Versagens durch Verlust der Gesamtstandsicherheit				
Scherfestigkeit				
— Siehe Tabelle A 2.2				
Herausziehwiderstände				
— Siehe STR und GEO-2				

2.5.1 Earth pressure calculations according to the German Standard DIN 4085

In order to calculate the vertical bearing capacity, we need to know with what angle the earth pressure acts on the wall. The earth pressure angle δ, is the angle between the normal of the wall and the direction of the earth pressure. δ is caused by the interaction between soil and structure and it cannot exceed the value of the friction angle of the structure. The size of δ depends on the following:

- the stress state in the soil
- the relative movement between soil and structure
- the shear strength on the contact surface between soil and structure

- the equilibrium of vertical forces, including the influence of stiffeners and anchors

Active and Passive Earth Pressures

Calculation of Active Earth pressure

The total active earth pressure is given by the sum of earth pressure due to the soil density, cohesion and surface loads.

$$E_a = E_{ag} + E_{ac} + E_{ap} \tag{2.1}$$

The horizontal and vertical components are given by:

$$E_{ah} = E_a \cos\delta_a \tag{2.2}$$

$$E_{av} = E_{ah} \tan\delta_a \tag{2.3}$$

The earth pressure angle δ_a can be found according to EAB (DGGT, 2013, section R89 (5)).

The horizontal components is expressed as follows:

$$E_{agh}(z) = \gamma z K_{agh} \tag{2.4}$$

$$E_{aph} = p_v K_{aph} \tag{2.5}$$

$$E_{ach} = -cK_{ach} \tag{2.6}$$

The earth pressure coefficients can be calculated by:

$$K_{agh} = K_{aph} = \frac{\cos\phi}{1 + \sqrt{\frac{\sin\phi}{\sin\phi\cos\delta_a}}} \tag{2.7}$$

$$K_{ach} = \frac{2\cos\phi\cos\delta_a}{1 + \sin\phi + \delta_a} \tag{2.8}$$

In a case with several soil layers, the earth pressures should be calculated for each layer separately.

The development of the active earth pressure coefficients with the variation of ϕ and $\delta = \frac{1}{2}\phi$ is illustrated in Figure 2.9

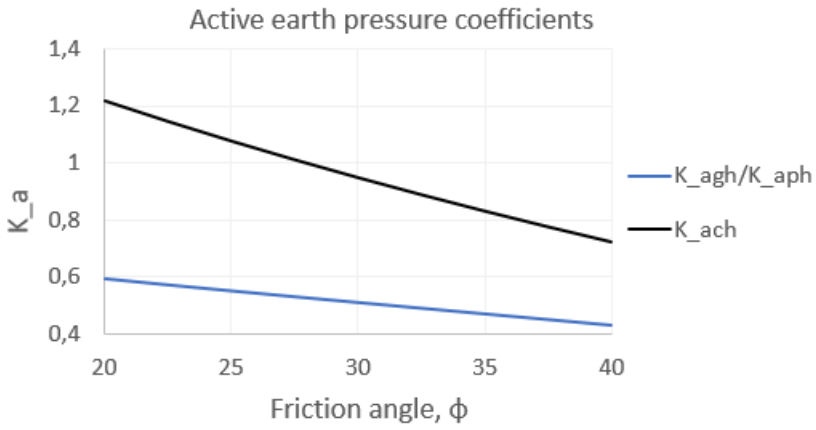

Figure 2.9: Active earth pressure coefficients for different values of ϕ and δ.

Calculation of Passive Earth pressure

The total passive earth pressure is given by the sum of earth pressure due to the soil density, cohesion and surface loads.

$$E_p = E_{pg} + E_{pp} + E_{pc} \tag{2.9}$$

The horizontal and vertical components are given by:

$$E_{ph} = E_p \cos\delta_p \tag{2.10}$$

$$E_{pv} = E_{ph} \tan\delta_p \tag{2.11}$$

The earth pressure angle δ_p can be found according to the EAB (DGGT, 2013, section R89 (5)). The horizontal components is expressed as follows:

$$E_{pgh}(z) = \gamma z K_{pgh} \tag{2.12}$$

$$E_{pph} = p_v K_{pph} \tag{2.13}$$

$$E_{pch} = c K_{pch} \tag{2.14}$$

The earth pressure coefficients can be calculated from:

$$K_{pgh} = \cos\delta_p \cdot \frac{1+\sin\phi}{1-\sin\phi} \cdot i_{pg} \cdot g_{pg} \cdot t_{pg} \tag{2.15}$$

$$K_{pph} = \cos\delta_p \cdot \frac{1+\sin\phi}{1-\sin\phi} \cdot i_{pp} \cdot g_{pp} \cdot t_{pp} \tag{2.16}$$

$$K_{pch} = \cos\delta_p \cdot 2 \cdot \sqrt{\frac{1+\sin\phi}{1-\sin\phi}} \cdot i_{pc} \cdot g_{pc} \cdot t_{pc} \tag{2.17}$$

The coefficients i_p, g_p and t_p are given in Table 2.4.

The development of the passive earth pressure coefficients with the variation of ϕ and $\delta = \frac{1}{2}\phi$ is illustrated in Figure 2.11

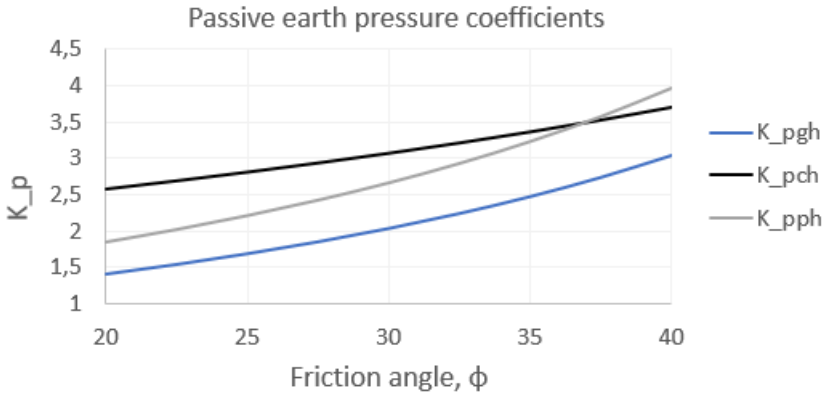

Figure 2.10: Passive earth pressure coefficients for different values of ϕ and δ.

Table 2.4: Coefficients according to Pregel/Sokolowski (Deutsches Institut für Normung (DIN), 2017)

δ_p	i_{pg}	i_{pp}	i_{pc}
≤ 0	$(1-0{,}53\cdot\delta_p)^{(0{,}26+5{,}96\cdot\varphi)}$	$(1-1{,}33\cdot\delta_p)^{(0{,}08+2{,}37\cdot\varphi)}$	i_{pp}
>0	$(1+0{,}41\cdot\delta_p)^{-7{,}13}$	$(1-0{,}72\cdot\delta_p)^{2{,}81}$	$(1+4{,}46\cdot\delta_p\cdot\tan\varphi)^{(-1{,}14+0{,}57\cdot\varphi)}$

g_{pg}	g_{pp}	g_{pc}
$(1+0{,}73\cdot\beta)^{2{,}89}$	$(1+1{,}16\cdot\beta)^{1{,}57}$	$(1+0{,}001\cdot\beta\cdot\tan\varphi)^{(205{,}4+2\,232\cdot\varphi)}$

t_{pg}	t_{pp}	t_{pc}
$(1+0{,}72\cdot\alpha\cdot\tan\varphi)^{(-3{,}51+1{,}03\cdot\varphi)}$	$\frac{e^{-2\cdot\alpha\cdot\tan\varphi}}{\cos\alpha}$	t_{pp}

Parameters

c	[kN/m^2]	Cohesion
E	[kN/m^2]	Earth pressure
K	[-]	Earth pressure coefficient
ϕ	[°]	Friction angle
δ	[°]	Earth pressure angle
γ	[kN/m^3]	Soil density
p_v	[kN/m^2]	Evenly ditributed vertikal surface loads
β	[°]	Inclination of terrain behind the wall
α	[°]	Inclination of wall

Indexes

- a Active state
- p Passive state
- h Horizontal component
- v Vertical component
- g As a result of soil density
- c As a result from cohesion

2.5.2 Earth pressure calculations according to NTNU teaching

In comparison to the earth pressure calculation approach according to the German standard, a different approach is taught at NTNU.

In the German Standard the earth pressure angle is considered. This earth pressure angle is dependent on the roughness of the wall, r. The NTNU approach uses this roughness as an input parameter instead of the earth pressure angle. The roughness, as well as the earth pressure angle can be mobilized in different degrees on the active and the passive side, and they can vary along the wall. However, this is simplified to keeping the roughness constant along one side of the wall.

When the earth pressure behind an excavation wall causes the wall to deform into the excavation, active earth pressure develops behind the wall. As the wall is deforming, the soil behind the wall will move downwards relative to the wall, and the wall friction will cause the soil to stick to the wall in the active situation.

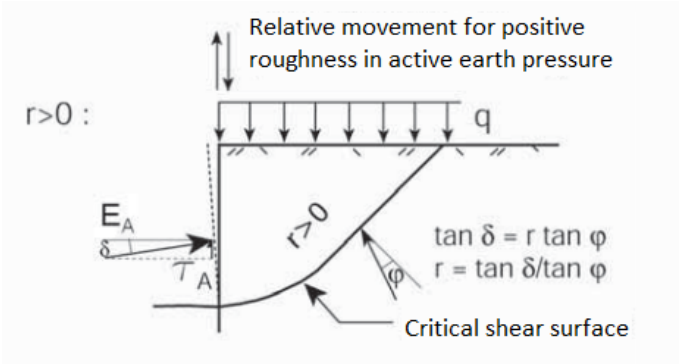

Figure 2.11: Positive roughness with active earth pressure. Translated from Veidirektoratet (2014)

E_a	[kN/m^2]	Resulting active earth pressure force
τ_a	[kN/m^2]	Active shear stress
δ	[°]	Earth pressure angle
ϕ	[°]	Friction angle
δ	[°]	Earth pressure angle
r	[-]	Roughness

The roughness r can be defined as the relationship between the earth shear strength and the shear stress τ mobilized along the support wall. The roughness relation is positive if the soil moves downwards relative to the wall, causing downward acting earth pressure, and negative if the wall moves downwards relative to the soil, causing upward acting earth pressure.

$$r = \frac{(p'_A + a) * \tan\delta}{(p'_A + a) * \tan\phi_d} = \frac{\tan\delta}{\tan\phi_d} \tag{2.18}$$

In an active state, the earth pressure components are given by:

$$p'_A + a = K_A * (p'_V + a) \tag{2.19}$$

$$p'_V = q + \bar{\gamma} * z \tag{2.20}$$

$$\tau_A = r * \tan\phi_d * (p'_A + a) \tag{2.21}$$

In a passive state, the earth pressure components are given by:

$$p'_p + a = K_p * (p'_V + a) \tag{2.22}$$

$$p'_V = q + \bar{\gamma} * z \tag{2.23}$$

$$\tau_p = r * \tan\phi_d * (p'_p + a) \tag{2.24}$$

Here p_a and p_p denotes active and passive earth pressures, while E_a and E_p denotes the resulting acting active and passive earth pressure forces. The earth pressure coefficients K_a and

K_p depends on the mobilized friction $\tan\phi_d$ and the roughness. The mobilized friction can be expressed in the following two ways:

$$\tan\phi_d = f * \tan\phi \tag{2.25}$$

$$\tan\phi_d = \frac{\tan\phi}{\gamma_M} \tag{2.26}$$

The degree of mobilization (f) is used in situations where a smaller part of shear stresses are mobilized than what corresponds to the material factor γ_M. Values for f and γ_M can be found in chapter 9.2 in Veidirektoratet (2014).

The earth pressure coefficients are dependent on the roughness of the wall, r, and the mobilized friction angle, ϕ_d. For a positive roughness relation, 0 < r < 1, the active and passive earth pressure coefficient can be expressed as follows:

$$K_P = \frac{(1+f_\omega^2) * N_+}{1+f_\omega^2 * N_+} * e^{2\omega\tan\phi_d} \tag{2.27}$$

$$K_A = \frac{(1+f_\omega^2) * N_+}{1+f_\omega^2 * N_+} * e^{-2\omega\tan\phi_d} \tag{2.28}$$

For a positive roughness relation, 0 < r < 1, the active and passive earth pressure coefficient can be expressed as follows:

$$K_P = \left(\frac{1}{\sqrt{1+\tan^2\phi_d} - \tan\phi_d * \sqrt{1+r^2}}\right)^2 \tag{2.29}$$

$$K_A = \left(\frac{1}{\sqrt{1+\tan^2\phi_d} + \tan\phi_d * \sqrt{1+r^2}}\right)^2 \tag{2.30}$$

The earth pressure coefficients can also be obtained from the diagram in Figure 2.12.

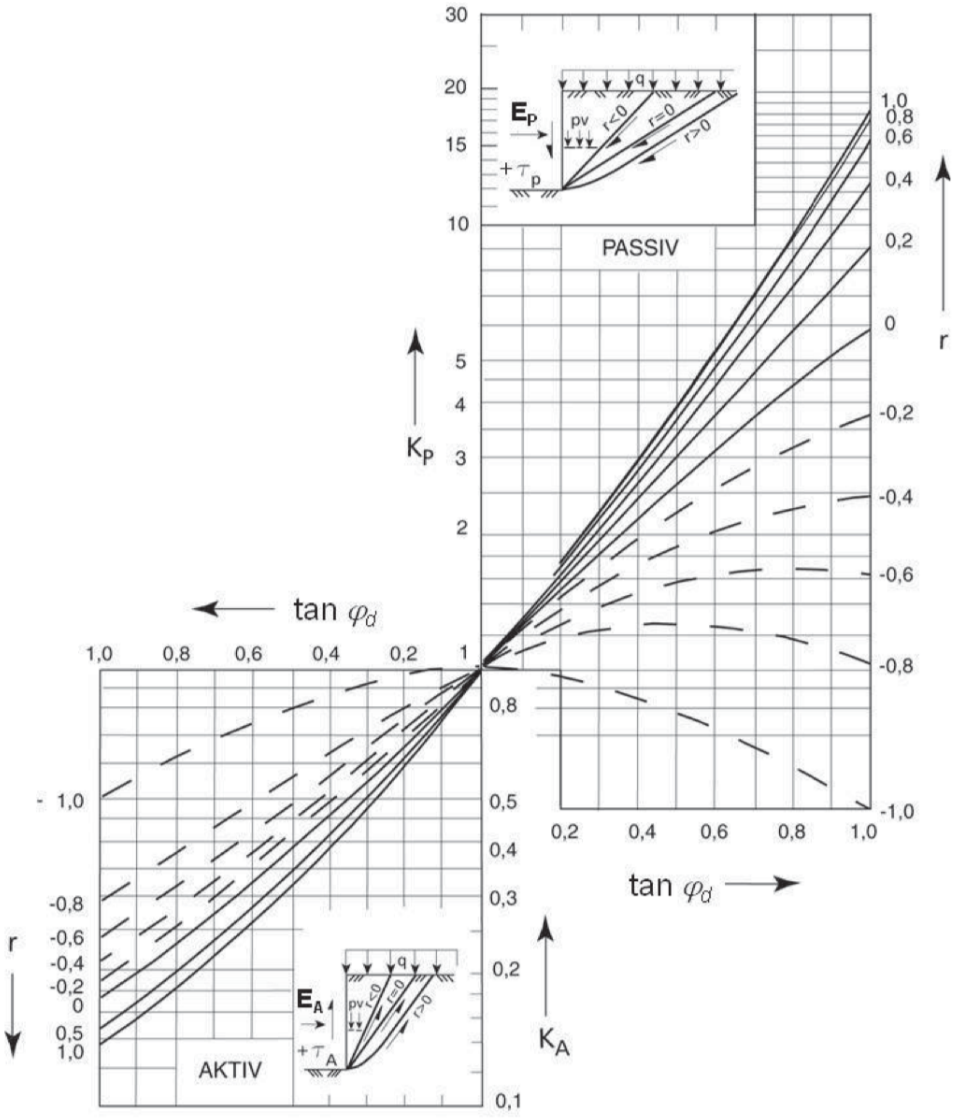

Figure 2.12: Earth pressure coefficients according to NTNU

2.5.3 Comparison of the German Standard approach and the NTNU approach

In the German Standard, the earth pressure is denoted E and in the NTNU approach, the earth pressure is denoted p'.

The earth pressure is expressed with cohesion c in the German Standard and with attraction a in the NTNU approach. The attraction can be expressed with cohesion:

$$a = c \tan \phi \tag{2.31}$$

In order to compare the different approaches, the earth pressures from the NTNU approach for calculating active earth pressure is expressed with cohesion and Equation 2.20 is substituted into Equation 2.19:

$$p'_A + c\tan\phi = K_A * (q + \gamma z + c\tan\phi) \tag{2.32}$$

$$p'_A = K_A q + K_a \gamma z + c\tan\phi(K_a - 1) \tag{2.33}$$

Where q is surface loads. This is comparable with Equation 2.1 where the surface loads are expressed with p_v:

$$E_a = K_{aph} q + K_{agh} \gamma z - cK_{ach} \tag{2.34}$$

Both in Equation 2.33 and 2.34 has three parts: one for surface loads, one for vertical terrain loads and one cohesion part. In the active earth pressure calculations, $K_{aph} = K_{agh}$ and K_{ach} is different. In the NTNU approach, there is only one active earth pressure coefficient, depending on the assumed roughness relation. The cohesion part in the NTNU approach is, as in the German Standard approach, also multiplied with a different value then the other two parts. In the NTNU approach, this value is $K_a - 1$.

The active earth pressure coefficients are compared below. The earth pressure coefficients from the NTNU approach is illustrated with roughness values 0,5 and -0,5.

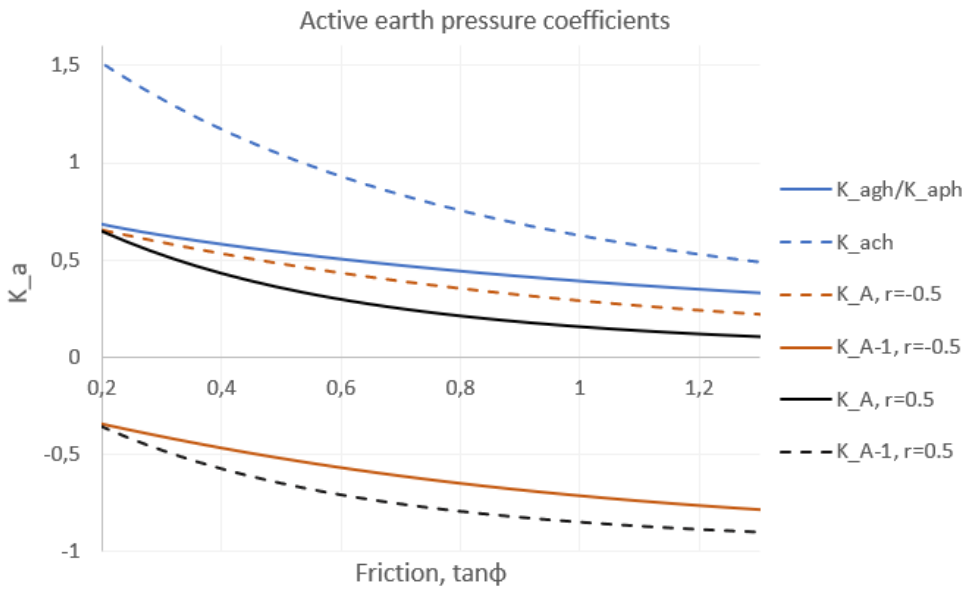

Figure 2.13: Comparison of active earth pressure coefficients from the German Standard and NTNU approaches

The same can be done for the passive earth pressure. For the NTNU approach, equations 2.31 and 2.23 is substituted into Equation 2.22:

$$p'_P = K_P q + K_P \gamma z + c \tan\phi (K_P - 1) \tag{2.35}$$

The corresponding equation from the German Standard is:

$$E_p = K_{pph} q + K_{pgh} \gamma z + c K_{pch} \tag{2.36}$$

The passive earth pressure coefficients are compared below.

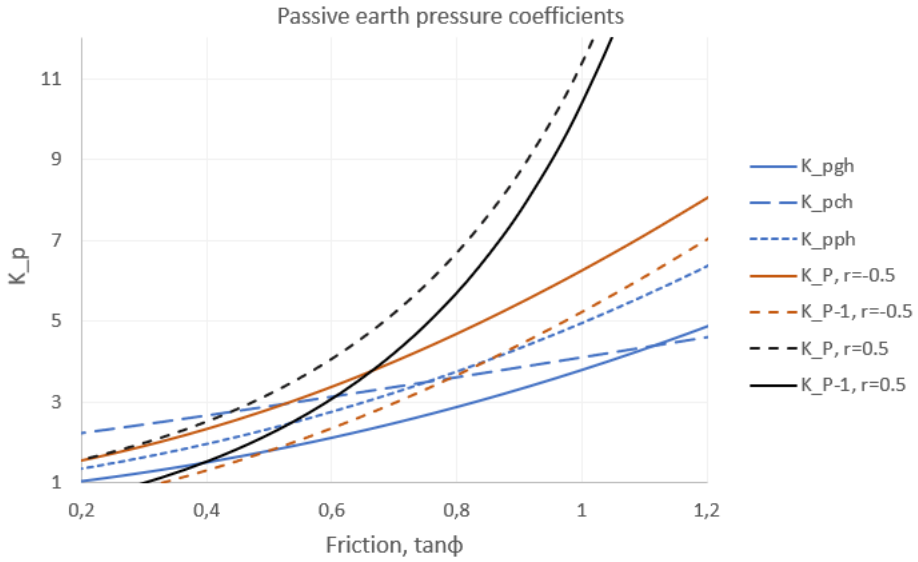

Figure 2.14: Comparison of passive earth pressure coefficients from the German Standard and NTNU approaches

In the range $\tan\phi = 0,2 - 1,2$, for the active earth pressure coefficients for surface and vertical terrain loads, the values from the German Standard (GS) is 0-0,1 larger than the corresponding coefficient for r=-0,5 and 0-0,2 larger than the corresponding coefficient for r=0,5 from the NTNU calculation. This results in a larger active earth pressure when calculating according to GS. The coefficient for the cohesion part from GS is positive, but the cohesion part is subtracted from the earth pressure. The cohesion part is added to the earth pressure in the NTNU approach, but c is multiplied with $K_A - 1$, which is a negative value causing the cohesion to be a negative contribution to the earth pressure. According to GS, the cohesion coefficient varies from 1,5 for $\tan\phi = 0,2$, to 0,5 for $\tan\phi = 1,2$. According to the NTNU approach, the absolute value of $K_A - 1$ varies from 0,36-0,9. The absolute value of the cohesion coefficients are developing in opposite directions.

All the passive earth pressure coefficients are in the same range until $\tan\phi = 0,5$. From here, the coefficients for r=0,5 increase far more rapidly then the rest. K_P for r=-0,5 is increasing slightly faster than K_{pgh} and K_{pph}. K_P varies from 1,6-8,1, K_{pgh} varies from 1,0-4,8 and K_{pph} from 1,5-6,3, meaning the passive earth pressure from the NTNU approach is the largest and therefore less conservative. The cohesion coefficient from GS starts at 2,2, and the one from NTNU starts below zero. At $\tan\phi$=0,77, the cohesion coefficients crosses and the one from the NTNU approach is larger from here on.

The cohesion contribution is normally small compared to the other two. Therefore, figures 2.13 and 2.14 shows that, considering the earth pressure coefficients, the calculation according to the German Standard is more conservative then the calculation according to the NTNU approach. However, partial safety factors also plays a role.

The safety factors are calculated as explained in chapter 2.6.3.

2.6 Numerical Approaches

The Finite Element Method has over the last decennia evolved into a daily used engineering tool and it has obtained a position next to traditional design methods. FEM offers significant advantages in complex situations.

Design codes deals mainly with ultimate limit state (ULS) design, while FEM mostly deal with analysis of stresses and deformations related to working load conditions, which is more relatable to the serviceability limit state (SLS). SLS requirements are often considered in deformation sensitive situations which has increased the use of FEM in geotechnical design (Brinkgreve and Post, 2013).

2.6.1 Soil-Structure Interaction

In contrast to the analytical method where the characteristic earth pressure angle is an input parameter, it is now a result of the computation. It can be found as the angle between the wall normal and the resultant of the vertical and horizontal earth pressure forces. The earth pressure angle depends on the degree of mobilisation, the relative movement between wall and soil, the selection of slip surface type and of the characteristic wall friction angle which again depends on the shear strength of the soil and the surface roughness of the wall (DGGT, 2013).

The interaction between soil and structure is modelled by an interface element which is placed between soil and structure. In Plaxis, a parameter R_{inter} can be entered. This parameter relates the soil strength to the interface strength according to the following equations:

$tan\phi_{interface} = R_{inter}\, tan\phi_{soil}$ and $c_{inter} = R_{inter} c_{soil}$

Thus, R_{inter} reduces the friction and cohesion of the interface compared to the friction and cohesion of the adjacent soil. As equation 2.18 shows, the roughness r, used in the NTNU cal-

culations depends on $tan\phi$ in the interface region. This roughness is therefore also affected by the R_{inter}.

2.6.2 Partial Safety Factors in FEM

Methods for dealing with FEM in geotechnical design according to design codes have been developed. Strength reduction was traditionally used to evaluate the global safety factors. Eurocode 7 (EC7, 2014) introduces three different design approaches, DA1, DA2 and DA3. The different approaches applies different partial safety factors to soil properties, actions and resistances. DA1 has two different combinations, DA1-1 and DA1-2. Generally, DA1-1 and DA2 are load factoring approaches and DA1-2 and DA3 are material factoring approaches. DA2 require application of partial safety factors to permanent unfavourable actions. This includes the earth pressure acting on the wall, which is problematic when it comes to numerical analyses because the earth pressure is not an input parameter, but a result of the analyses. However, according to Eurocode 7 and DA2, the partial safety factors can be applied to the effect of the action instead of the action it self. This way, the analysis is performed using characteristic values for loads and parameters and the partial safety factors are applied to the results in order to obtain design values. Countries defines in their own National Annex which design approach is to be used in which situation.

2.6.3 Vertical Capacity

The vertical component of the earth pressure along the side of the wall can according to the EAB be obtained by integrating the vertical stresses along the wall in cases where downward acting vertical forces can be transmitted to the subsurface with sufficient safety. The magnitude of the tip resistance depends on the cross section area of the tip. Slender walls are often modelled as vertical plates without a thickness. These plates has no end bearing. However, Plaxis can still consider this end bearing by selecting the option "prevent punching" in the material data set. By selecting this option, an area around the bottom of the plate will exclude plastic behaviour. This option will not represent true end bearing capacity, but it will prevent unrealistic vertical movement (Brinkgreve et al., 2017). The tip resistance calculated by PLAXIS using the "prevent punching" function can easily get too large, and it is therefore important to check whether or not it is reasonable.

Safety factor calculation

The safety factor for the vertical capacity is calculated according to the DGGT (2013) and is obtained by dividing downward acting forces F, with resistance forces R:

$$SF = \frac{F}{R} \tag{2.37}$$

Meaning that SF > 1 indicates failure.

The passive earth pressure is a resistance force and is obtained by integrating the maximum possible shear stresses σ_{max} along the excavation side of the wall. The active earth pressure is obtained by integrating the acting earth pressures, τ_1, along the wall. σ_{max} and τ_1 are interface stresses. The active earth pressure is considered a downward acting force, which means that in the case of upward acting earth pressure, the active earth pressure is subtracted from F.

Chapter 3

Software Description

3.1 Finite Element Method

The finite element method is a widely used numerical solving method. It is not an exact method, but it gives a good approximation of solutions to problems that cannot be solved exactly. When used in geotechnical problems, the soil body and structural elements are devided into elements with a certain number of nodes. These elements decides the behaviour of the model.

3.1.1 Plaxis 2D

Plaxis 2D performs finite element analyses on stability, deformation and water flow for different types of geotechnical applications (Brinkgreve et al., 2017). Calculations can be performed in plane strain or in axisymmetry.

Elements

In Plaxis, one can chose between using 6-node elements or 15-node elements. The 6-node elements can establish a complete second degree polynomial; thus, the first derivative of the deformation, which represents strain, can express the linear normal stress distribution exact. However, the polynomial degree is too low to represent the quadratic varying shear stress. The 15-node element on the other hand, can establish a complete 4th degree polynomial (Mathisen, 2018). Therefore it can represent both the linear varying normal stress and the quadratic varying shear stress. In other words, the freedom of movement achieved by the 15-node element is larger than that achieved by the 6-node element due to the larger number of shape functions

present. The 6-node elements are also fairly accurate and can give good results for standard deformation analyses, given that a sufficient number of elements is used. However, in situations where failure plays a role or axisymetry is used, the 15-node element should be chosen (Brinkgreve et al., 2017).

Mesh

Before finite element calculations can be performed, the defined geometry must be divided into finite elements. The composition of such elements is called a mesh (Brinkgreve et al., 2017). The element sizes must be defined. Plaxis offers five different standard sizes, but around structures, the element sizes will automatically be made smaller. The mesh can also manually be made finer or coarser in necessary areas.

Interfases

As mentioned in Paragraph 2.6.1, the interaction between soil and structure or between two soil polygons is modelled by interfaces. Each interface can be assigned properties such as permeability, virtual thickness and material mode. The virtual thickness is assigned to interfaces to define the interface material properties. A larger virtual thickness generates more elastic deformations. Generally, interface elements should generate little elastic deformations. However, too small virtual thickness can lead to numerical problems (Brinkgreve et al., 2017).

3.2 Material Models

In order to control and optimize geotechnical engineering tasks, finite element analyses are frequently used. Despite soil being a highly nonlinear material, linear constitutive models are often and carelessly used in numerical analyses. Soil can exhibit both elastic and plastic nonlinearities which cannot be represented by elastic material models. The Hardening Soil (HS) model and the Hardening Soil Small Strain (HSS) model takes the non-linear behaviour of the soil into account.

The HSS model is applied for the soil elements and elastic material model for the structural elements in the Plaxis 2D model of the deep excavation. These material models and their input parameters are presented below. As the HSS model is based on the HS model, the HS model is

also presented. Input parameters, formulas and expressions are according to Brinkgreve et al. (2017):

3.2.1 Hardening Soil Model

The HS-model contains two yield surfaces, volumetric and deviatoric hardening. Volumetric hardening is a result of compression loading and deviatoric hardening is a result of shear loading. By replacing the theory of elasticity with the theory of plasticity and taking soil dilatancy into consideration as well as introducing a yield cap, the HS-model is able to handle collapse load computations in plastic range and distinguish between loading and unloading. In contrast to the Mohr-Coulomb model, plastic strains causes the yield surface of HS to expand, as illustrated in Figure 3.1. In other words, the stiffness is stress dependent and the yield surface is therefore not fixed in the principal stress space.

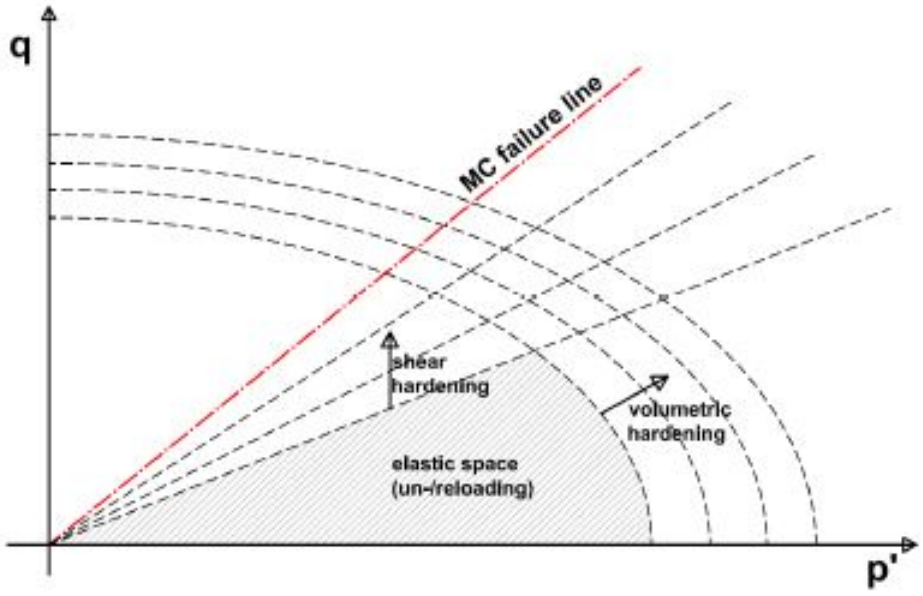

Figure 3.1: Yield surfaces of Hardening soil model in p'-q- plane (T. Voit, 2016)

Similar to MC-model, the limiting states of stress are described by the cohesion c, the friction angle ϕ and the dilatancy angle ψ. In addition, the hardening soil model increases the soil description accuracy by considering three different soil stiffnesses. Figure 3.2 illustrates the hyperbolic function describing the nonlinear stress-strain relation for primary loading. The figure shows that for unloading and reloading, the soil behaves elastic and the stiffness is much higher

than for the primary loading.

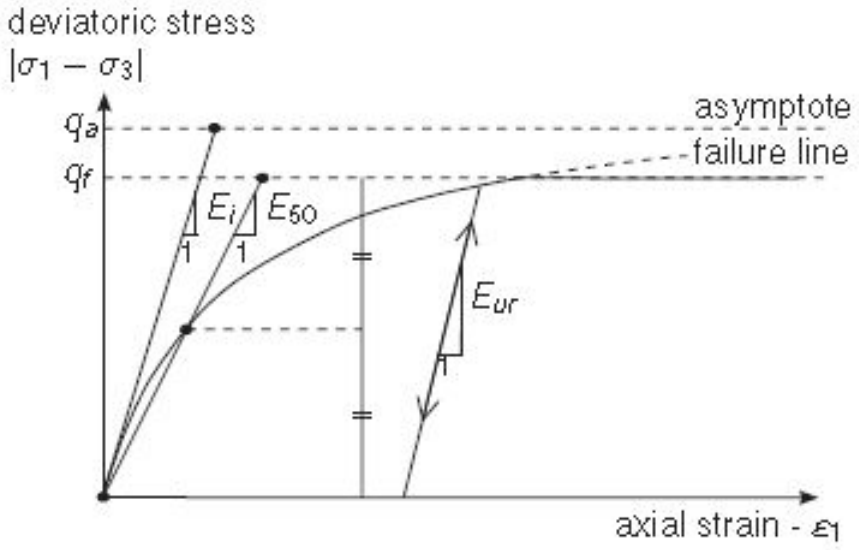

Figure 3.2: Deviatoric stress-strain relation (Brinkgreve et al. 2015)

E_{50}	[kN/m^2]	Stiffness at 50% of the strength for primary loading
E_{ur}	[kN/m^2]	Unloading/reloading stiffness
E_{oed}	[kN/m^2]	Oedometer stiffness

E_{50} is neccessary to obtain the desired hyperbolic function, E_{ur} consideres the unloading/reloading stiffness, and E_{oed} controls the volumetric hardening along with K_0^{nc}. Because of the stress dependency of the soil stiffness, the reference parameters E_{50}^{ref}, E_{ur}^{ref} and E_{oed}^{ref} are required by Plaxis.

The following formulas accounts for stress dependency:

$$E_{50} = E_{50}^{ref}\left(\frac{c'cos\phi' - \sigma_3' sin\phi'}{c'cos\phi' + \sigma_3'^{ref} sin\phi'}\right)^m \tag{3.1}$$

$$E_{ur} = E_{ur}^{ref}\left(\frac{c'cos\phi' - \sigma_3' sin\phi'}{c'cos\phi' + p^{ref} sin\phi'}\right)^m \tag{3.2}$$

$$E_{oed} = E_{oed}^{ref}\left(\frac{c'cos\phi' - \sigma_1' sin\phi'}{c'cos\phi' + p^{ref} sin\phi'}\right)^m \tag{3.3}$$

K_0^{nc}	[-]	K_0 for normal consolidated soil
m	[-]	Expresses stress dependency
c'	[kN/m^2]	Effective cohesion
ϕ	[°]	Effective friction angle

3.2.2 Hardening Soil Model with Small Strain Stiffness

The HSS model builds on the HS model. However, as opposed to the HS model, it considers the fact that there is only a very small strain range where a soil can recover enough to be considered truly elastic. As illustrated in Figure 3.3, the stiffness decays non-linearly as the strain increases.

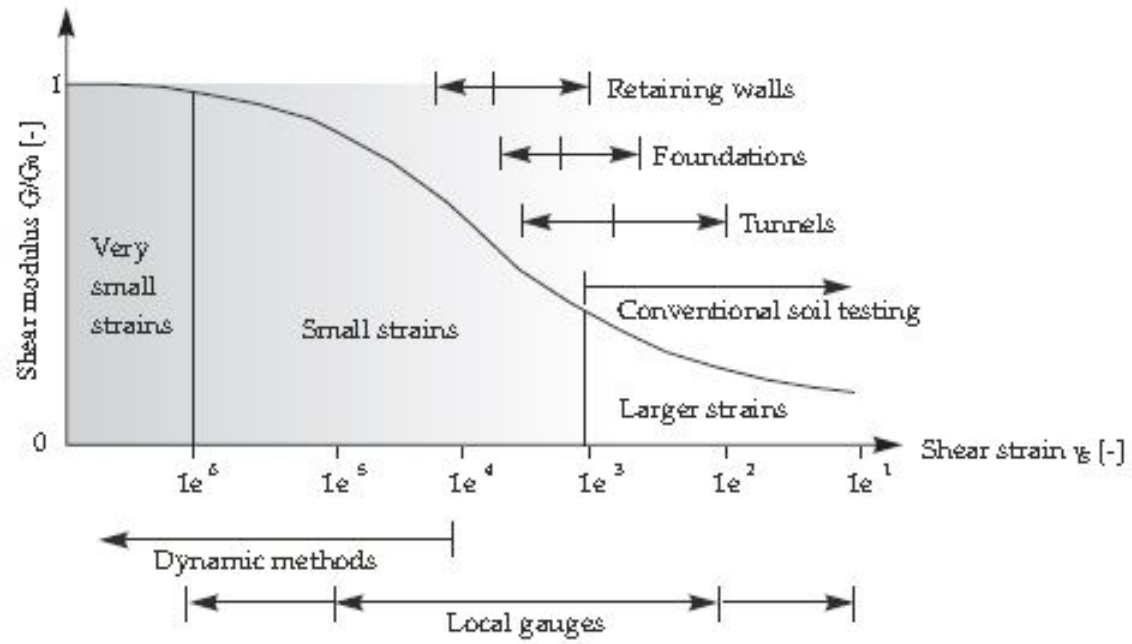

Figure 3.3: Characteristic stiffness-strain behaviour of soil (Brinkgreve et al. 2015)

The HSS model implemented in Plaxis only contains two paramaters in addition to those in the HS model:

- G_0: Shear modulus for very small strain
- G_s: Shear modulus reduced to about 70 % of G_0

Model Parameters

c'	[kN/m^2]	Effective cohesion
ϕ	[°]	Effective friction angle
ψ	[°]	Dilatancy angle
σ_t	[kN/m^2]	Tensile strength and tensile cut-off
E_{50}^{ref}	[kN/m^2]	Secant stiffness in standard deained triaxial test
E_{oed}^{ref}	[kN/m^2]	tangent stiffness for primary oedometer loading
E_{ur}^{ref}	[kN/m^2]	Unloading/reloading stiffness
m	[-]	Expresses stress dependency
υ_{ur}	[-]	Poisson Ratio for unloading/reloading
p^{ref}	[kN/m^2]	Reference stress for stiffness (default p^{ref} = 100 kN/m^2)
K_0^{nc}	[-]	K_0 for normal consolidated soil
R_f	[-]	Failure ratio q_f/q_a (default $R_f = 0,9$)
$\sigma_{tension}$	[kN/m^2]	Tensile strength (Default $\sigma_{tension} = 0$)

3.2.3 Linear Elastic Model

The structural elements is modelled with the linear elastic model. Materials can be represented by this model up to their elastic limit if they satisfy the following linear and elastic conditions:

Linear

- Small strains in material

- Stresses are proportional to strains

Elastic

- Material obtains original shape after unloading and the unloading path corresponds with the loading path

- The rate of loading or straining is irrelevant

Model Parameters

The Linear Elastic model depends on the following parameters:

E	$[kN/m^2]$	Young's modulus
ν	[-]	Poisson Ratio
c	[kN/m^2]	Cohesion
ϕ	[°]	Friction angle
ψ	[°]	Dilatancy angle
σ_t	$[kN/m^2]$	Tensile strength and tensile cut-off
G	$[kN/m^2]$	Shear modulus
E_{oed}	$[kN/m^2]$	Oedometer modulus

3.3 Wall modelling

In this thesis, the wall is modelled in two different ways, as a plate and as a continuum. The continuum wall accounts for the actual wall thickness and is the more accurate version, however, according to Voit (2016), modelling the wall with continuum elements causes less output options concerning structural forces. Due to this, it can be more convenient to use plate elements to model the wall.

Plates are made of line elements in the 2D finite element model. These line elements has three degrees of freedom per node, two translational and one rotational. In this thesis the line elements will interact with 15-node soil elements, therefore the line elements are defined by 5 nodes. These elements bases on Mindlin's beam theory (Bathe, 1982), which allows the beam to deflect due to both shearing and bending. Since the plate elements are defined as structural elements, structural forces can easily be obtained for them (Voit, 2016). However, modelling the wall with plate elements also causes some limitations.

Plate walls have no thickness which removes the resistance that naturally is offered by the soil at the tip, which depends on the cross section area of the tip. In order to deal with this, there is a couple of things that can be done. There is the function in the material model of the plate called "prevent punching". This function will exclude plastic behavior within a zone around the tip of the wall. This is meant to prevent unrealistic vertical movement of the wall and it does not present an actual bearing capacity. Another way of dealing with the slenderness of the plate is to model the wall with a foot plate. A horizontal plate at the bottom of the wall.

Another limitation following the use of the footplate, is that the soil above the footplate will act as an extra vertical weight acting on the wall.

It will be investigated to what extent it is sufficient to model the wall as a plate compared to a continuum wall.

Interface elements

Interface elements are present between the soil and the wall in order to model the interaction between the wall and the soil. The properties of the interface can be found in Table 5.1, 5.2 and 5.4.

3.3.1 Struts

Struts will be installed in two levels. The first will be installed at ground level and the second at 8,5 meters below the surface. Service loads will be acting on the struts. Properties of the struts are given in Table 5.3

Chapter 4

Project description

4.1 Location

An underground railway is to be extended. It is located in Munich at 530,4 m above sea level. In this regard, a new station is to be build. The calculation models will be based on the excavations regarding this project.

4.2 Geology

This is an area characterized by mighty Quaternary gravel deposits. These sediments have primarily been transported north to the Munich area by the melting water of the Pleistocene ice. Since the Quaternary gravel of Munich is a result of deposits from several cold and warm periods with changing sedimentation conditions in the form of dormant and flowing waters, the stratification is described as an extremely carbonate-rich mixture of silt, sand and gravel. Directly under the Quaternary gravel, tertiary clay-silt sedimentation can be found. The groundwater level can be found at approximately 8,4 meters below the terrain surface, but to simplify the problem, groundwater level is assumed to be below the wall.

Drilling performed in regards of the current project in addition to former subsoil investigations, suggests the following layering:

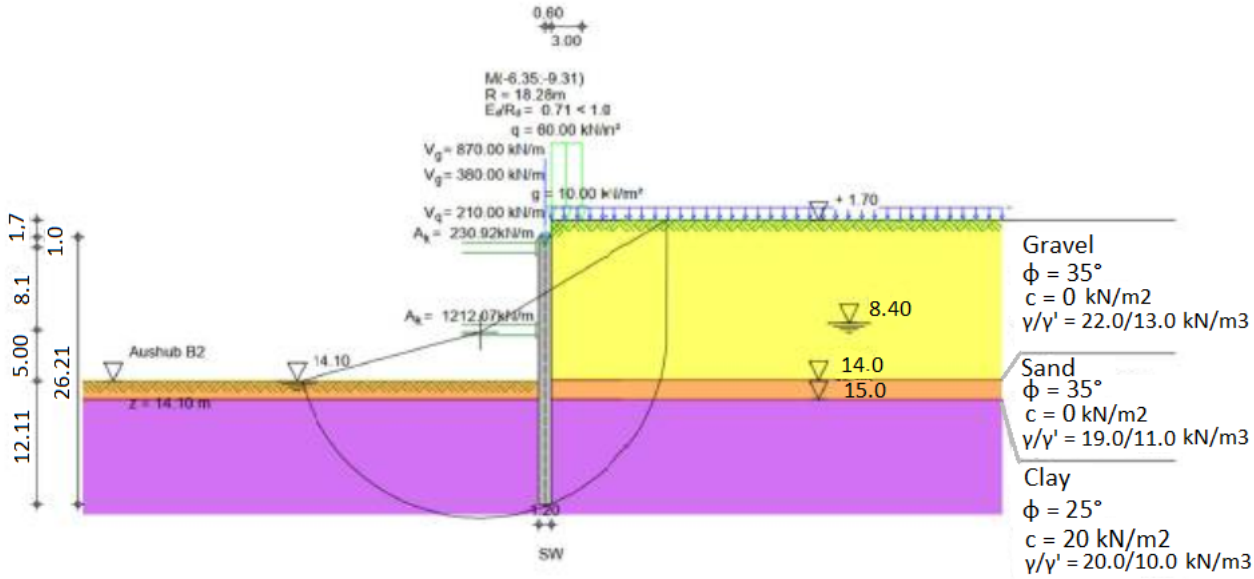

Figure 4.1: Sketch of soil layers from the geotechnical report.

In order to simplify the calculations in this thesis, it is chosen to remove the middle layer of sand and external loads on the outside of the excavation.

4.3 Excavation Support System

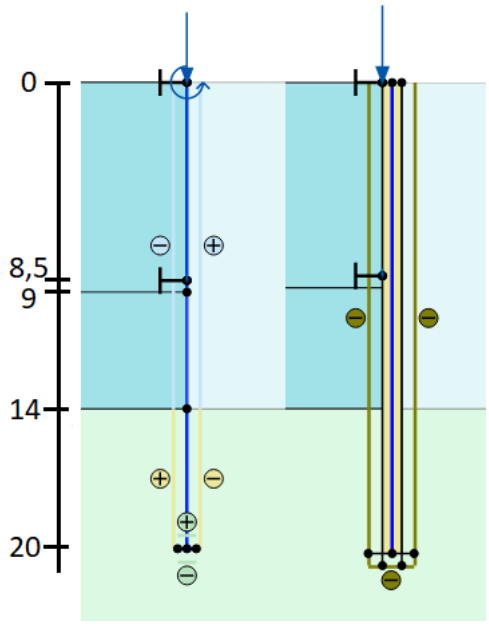

Figure 4.2: Plate and continuum wall models.

The Quaternary gravel layer is 14 meters thick and lays on top of a thick deposit of tertiary clay-silt layer. The required embedment depth of the wall is calculated to be 6 meters based on the geology derived from the geotechnical report, meaning that the wall need to reach 20 meters into the ground since the excavation will be 14 meters deep. This is a little shorter than the wall illustrated in Figure 4.1 from the geotechnical report. The diaphragm wall is supported by two struts, one at surface and the depth of the lower strut is optimized by running PLAXIS simulations with a lower strut at levels -7,5 m, -8 m, -8,5 m and 9 m, in order to chose the level that gives the lowest bending moment in the wall. A lower strut at -8,5 meters gave the lowest maximum bending moment in the wall.

Chapter 5

Calculation Models

This chapter presents the numerical and analytical calculation approaches. In order to get an efficient numerical model, the mesh coarseness is optimized. The mesh coarseness is optimized based on accuracy and calculation time. The plate model is to be modelled in a way that it obtains similar results as the continuum model. Thereafter, the simulation is run with a variation of different parameters. The data for the vertical forces acting on the wall are gathered in order to calculate the safety factors. Analytically, the earth pressures are calculated according to the German standard. The safety factors are calculated in three different ways, using earth pressures obtained from the FEM or analytical calculations, and the Geotechnical report (GTB). These different calculation methods are later referred to as the 1st, 2nd and 3rd calculation:

1. Active earth pressure down to the required embedment depth obtained from FE calculations/calculations according to the German standard and all resisting forces obtained from the Geotechnical Report
2. Active earth pressure obtained from FE calculations/calculations according to the German Standard and passive earth pressure obtained from the Geotechnical Report.
3. Active and passive earth pressures obtained from FE calculations/calculations according to the German standard

In all three methods, the tip resistance will be obtained from the Geotechnical report. The three different calculations are illustrated in figures 5.1 and 5.2.

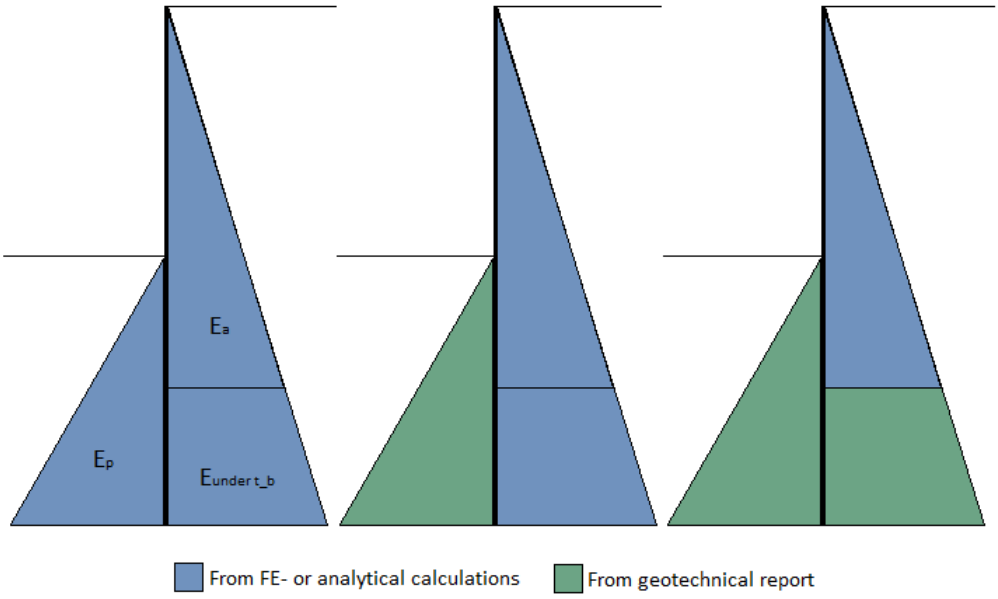

Figure 5.1: Earth pressure combinations, first excavation down to -9m. Left side is excavation side, right side is soil side

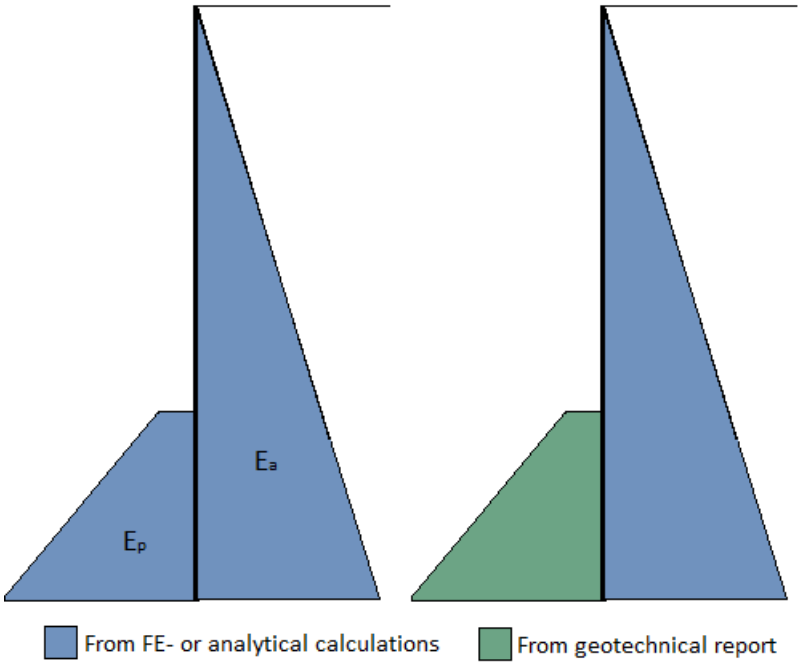

Figure 5.2: Earth pressure combinations, second excavation down to -14m. Left side is excavation side, right side is soil side.

For this model, the required embedment depth is $t_b = 6m$. This means that the wall must

be embedded 6 meters below the excavation level. At stages where the wall is embedded below t_b, the forces beneath t_b are assumed to be resistance forces. t_b is after the first excavation at -15 m with a 5 meter embedment below t_b, and t_b is at -20 m after the second excavation which corresponds with the depth of the embedment.

5.1 Numerical Calculation Model

5.1.1 Geometry of FE Model

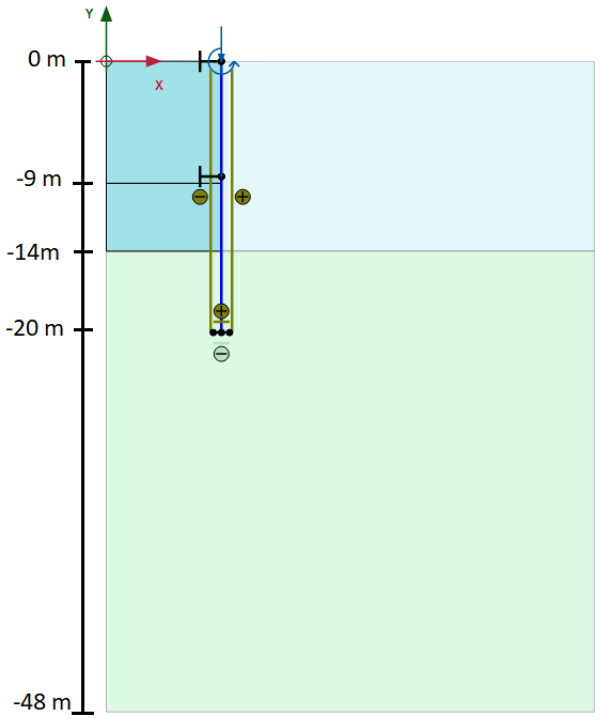

Figure 5.3: FE-model of wall modelled with plate elements in PLAXIS 2D

The overall dimensions are required to ensure that the influence from boundary conditions are negligible. According to the EANG (DGGT, 2014), this requirement is satisfied with the dimensions x * y = 36 * 31 m. In order to support this excavation, 20 m deep and 0,8 m thick walls is installed. The excavation will be 6,02 meters wide and 14 meters deep supported with struts at the excavation surface and at 8,5 m below the surface. Service loads are acting on the struts. Due to symmetry, it is sufficient to model half of the excavation in order to obtain a lower computation time. The excavation is performed in 2 steps of 9m and 5m. Simulations will be run with a plate model and with a continuum model. The continuum model is modelled with a plate in

the center line in order to easily read out the results. According to NTNU professors, the best results are obtained when the weight and stiffness of the wall are divided between the plate and the concrete with 30% and 70% respectively.

5.1.2 Elements

As described in Brinkgreve et al. (2017), the 15-node element should be used in cases of axisymmetri and in situations where failure plays a role. The 15-node element is therefore used in these simulations.

5.1.3 External loads

In addition to the weight of the struts and slabs, there are service and terrain loads acting on them as well. A point load of 530,6 kN/m is added to where the top slab is connected to the wall, and a point load of 52,8 is added to where the strut is connected to the wall. In addition, to compensate for off-centered loads in the continuum model, a bending moment of 212,2 kNm is added to the top of the plate wall.

5.1.4 Soil- and Model Parameters

The parameter values are obtained from the geotechnical report of the railway project. Tables 5.1, 5.2 and 5.3 represents the parameters for the reference model. Parameter variations are given in table 5.4.

Table 5.1: Model parameters for numerical calculations for excavations (HSS)

Parameter	Unit	Layer 1	Layer 2
γ	[kN/m^3]	22	20
γ'	[kN/m^3]	13	10
c'	[kN/m^2]	0	20
ϕ'	[°]	35	25
ψ	[°]	0	0
E_{50}^{ref}	[MN/m^2]	110	60
E_{oed}^{ref}	[MN/m^2]	110	60
E_{ur}^{ref}	[MN/m^2]	250	130
m	[-]	0,4	0,5
ν_{ur}	[-]	0,2	0,2
p^{ref}	[kN/m^2]	100	100
K_0	[-]	0,39	0,8
R_f	[-]	0,9	0,9
R_{inter}	[-]	0,5	0,5
$\gamma_0,7$	[MN/m^2]	$8*10^{-5}$	$2*10^{-4}$
G_0^{ref}	[MN/m^2]	260,4	162,5

Table 5.2: Model parameters for numerical calculations for excavation support system (Elastic)

Continuum (reinforced concrete)			Plate (steel)		
Parameter	Unit	Value	Parameter	Unit	Value
γ	[kN/m^3]	25	EI	[kNm]	$4,75*10^6$
E	[kN/m^2]	$33*10^6$	EA	[MN/m]	39600
ν	[-]	0,2	w	[kN/m/m]	30
G	[MN/m^2]	$13,75*10^6$	ν	[-]	0,2
E_{oed}	[kN/m^2]	$36,67*10^6$			
R_{inter}	[-]	0,5			
K_0	[-]	0,5			

Table 5.3: Model parameters for the struts (Elastic)

Upper strut (reinforced concrete)			Lower strut (steel)		
Parameter	Unit	Value	Parameter	Unit	Value
γ	[kN/m^3]	25	γ	[kN/m^3]	78,5
E	[kN/m^2]	$33 * 10^6$	E	[GPa]	210
A	[m^2/m]	2,1	d	[mm]	1219
$L_{spacing}$	[m]	1	t	[mm]	25
			$L_{spacing}$	[m]	6

5.1.5 Mesh configuration

In order to chose the optimal coarseness of the mesh, the FE model where the diaphragm wall is modelled with plate elements is run with different mesh coarseness. The optimal coarseness is chosen based on accuracy and calculation time. When decreasing the element size, the accuracy is increased, but so is the calculation time. The goal is to find the refinement where the shear stresses along the wall changes significantly little compared to the increase of the calculation time. The coarseness factor in PLAXIS is set to 0,2 along the entire wall, 0,5 in the soil that is excavated and 1,0 in the remaining soil.The FE simulation is run with the standard refinements coarse, medium, fine and very fine which provides 527, 786, 1801 and 3050 elements respectively. The shear stresses from these simulations are compared with the shear stresses from a simulation with a very fine mesh refinement in addition to dividing the coarseness factor of the entire model by two. The different meshes are illustrated in figures 5.4 and 5.5.

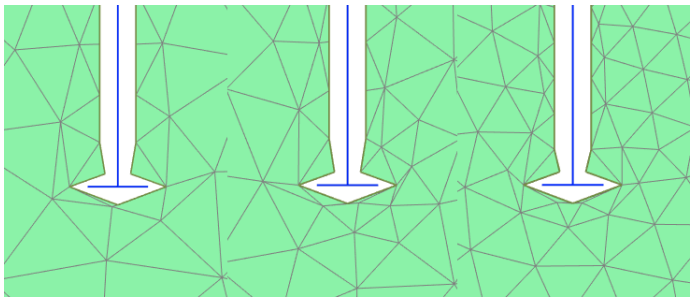

Figure 5.4: Mesh variations. From left: coarse mesh, medium mesh, fine mesh.

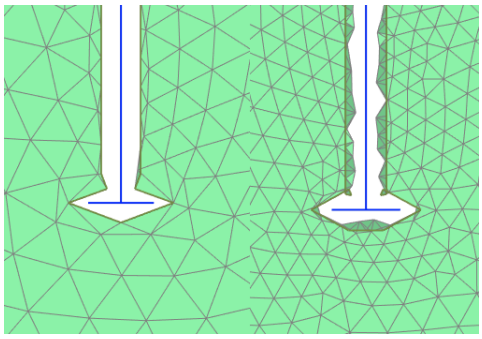

Figure 5.5: Mesh variations. From left: very fine mesh, extra fine mesh.

5.1.6 Calculation phases

The FE calculations are performed in five phases shown in Figure 5.6. The initial phase consists of the original terrain. In the next phase the wall, interfaces and the strut at surface level is activated. The first excavation down to -9 meters is performed in the third phase and the activation of the lower strut happens in the fourth. In the last phase, the last excavation step down to -14 m is performed.

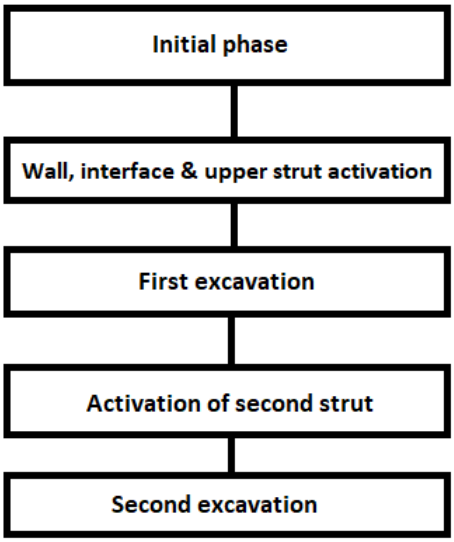

Figure 5.6: Calculation phases

5.1.7 Choice of reference model

A wall modelled with continuum elements is considered more accurate than one modelled with plate elements because it represents the actual size of the wall. However, the plate wall has convenient output options, and is therefor often preferred. In order to optimise the plate wall model compared to the continuum wall model, the vertical earth pressures on the outside of the walls are compared for variations of methods to model the plate wall. The plate wall is first modelled with a 0,8 m wide footplate, which results in vertical earth pressures that differs from the continuum model. The plate wall only has a virtual thickness, which means that all the weight of the wall is concentrated in one line. The idea of a footplate is to prevent this. However, when such a footplate is added to the wall, the extra weight due to the soil above this plate needs to be accounted for by reducing the weight of the wall as long as it is embedded. In order to achieve results more similar to the continuum wall, simulations are run with two different adjusted wall weights. Firstly, the weight of the wall is adjusted by subtracting the weight of the overlying soil from the weight of the wall, and as the soil is excavated, the weight of the excavated soil is re-added to the weight of the wall. This improved the results. However, considering that the weight of the wall and the overlying soil is not fully transferred to the bottom of the wall, but is also partly taken up by the soil along the wall, another model with a wall with its original weight at the part that is no longer embedded, is also investigated. In addition to this, the results are compared with a plate model without a foot plate. The results are illustrated in Figure 6.3.

5.1.8 Parameter variations

Vertical capacity calculations will be performed with variations of parameter values. The parameters that will be varied is the friction angle ϕ, cohesion c and the earth pressure angle δ. The analytical and numerical models will contain the standard parameter values while the three mentioned parameters are changed one by one. Calculations will be performed analytically based on German standards and the relevant geotechnical reports, and twice numerically using the two models described in Chapter 3.3.

Table 5.4: Parameter variations

Parameter	Unit	Referance value	Variation 1	Variation 2	Variation 3	Variation 4	Variation 5
c'	[kN/m^2]	20	15	17,5	20	22,5	25
ϕ_{clay}	[°]	25	20	22,5	25	27,5	30
ϕ_{gravel}	[°]	35	30	32,5	35	37,5	40
R_{inter}	[-]	0,5	0,5	0,6	0,7	0,8	0,9
$\delta_{ss,gravel}$	[°]	19,1	19,1	22,7	25,7	28,9	32,0
$\delta_{ss,clay}$	[°]	17,8	17,8	20,2	23,6	27,6	28,7
$\delta_{es,gravel}$	[°]	9,7	9,7	8,3	7,4	5,2	5,1
$\delta_{es,clay}$	[°]	14,4	14,4	13,1	12,3	10,8	9,7

Friction angle ϕ

The friction angle is varied in steps of 2,5° in each direction from the standard value for both soil layers.

Cohesion c

The cohesion is varied in steps of 2,5 kN/m^2 in each direction of the standard value in the clay layer.

Earth pressure Angle δ

The earth pressure angle δ is a direct input parameter in the analytical model. This is however not the case in the numerical models. In order to vary the earth pressure angle in PLAXIS, the interaction between the soil and the structure is varied. This is done by varying the interface parameter R_{inter}.

According to Brinkgreve et al. (2017), the interface element properties are dependent on the soil model and its parameters of the surrounding soil. The parameters that are necessary to derive the interface properties depends on which soil model is selected. R_{inter} defines the interface strength for the following soil models: the Mohr-Coulomb model, Linear Elastic model, HS model and as in this case HSS model (Brinkgreve et al., 2017). There are three options for setting the interface strength; Rigid, manual and manual with residual strength. The first two are used here. In the rigid option $R_{inter} = 1,0$ and it is used in cases where the interface strength should not be reduced, for instance at extended interfaces at corners of structural objects where there

is no soil-structure interaction. Interface properties will as a result of this remain the same with the exception of Poisson's ratio ν. The R_{inter} value can be entered manually in the interface tab in the material set. Soil-structure interaction is generally weaker than in the surrounding soil. This is obtained by giving R_{inter} a value lower than 1. Suitable values for the interactions between different soil and structure types can be found in literature. By reducing R_{inter}, the interface strength as well as the interface stiffness are reduced (Brinkgreve et al., 2017). The interface behavior in soil-structure interaction is described by an elastic-plastic model and in order to distinguish between elastic and plastic behavior, the Mohr-Coulomb criterion is used. According to Brinkgreve et al. (2017), interface strength properties are linked to the strength properties of the adjacent soil, which means that by reducing the interface strength, the cohesion c_i and friction angle ϕ_i of the interface area is also reduced:

$$c_i = R_{inter} * c_{soil} \tag{5.1}$$

$$\tan\phi_i = R_{inter} \tan\phi_{soil} \tag{5.2}$$

The dilatancy angle ψ is 0 for $R_{inter} = 1$ and $\psi_i = \psi_{soil}$ otherwise.
The interface friction angle ϕ_i corresponds to the largest possible angle the earth can act on the wall with. In order to perform analytical and numerical calculations with the same variation of earth pressure angle, the numerical model is run with five different values of R_{inter}. The earth pressure angle is then calculated from the resulting normal and shear forces acting on the wall due to the soil. These calculated earth pressure angles is then used in the analytical calculations. According to the EAB, the maximum earth pressure angle on a diaphragm wall is half of the friction angle to the adjacent soil. $R_{inter} = 0,5$ is therefore chosen for the reference model, and it is varied from 0,5 - 0,9. Depending on the quality of the installation of the wall, the soil at the bottom of the wall might be disturbed and its strength weakened. Therefore the R_{inter} for the interface of the foot plate is set to and kept at 0,8.

Earth pressure angles are calculated for each soil layer on each side of the wall. The earth pressure angles calculated for the clay layer on the excavation side is larger than the maximum ϕ_i. One reason for this can be that the cohesion provides an extra shear strength to the soil in addition to the shear strength provided by the soil friction angle. The earth pressure angle is calculated as the angle between the wall normal and the resultant of the normal stresses and

shear stresses, meaning that the cohesion can cause the angle between the wall normal and the resultant to be larger than ϕ_i which only depends on ϕ and R_{inter}. This is illustrated in Figure 5.7. The left side of Figure 7.8 also shows how the maximum possible passive shear stresses increase as the cohesion increases.

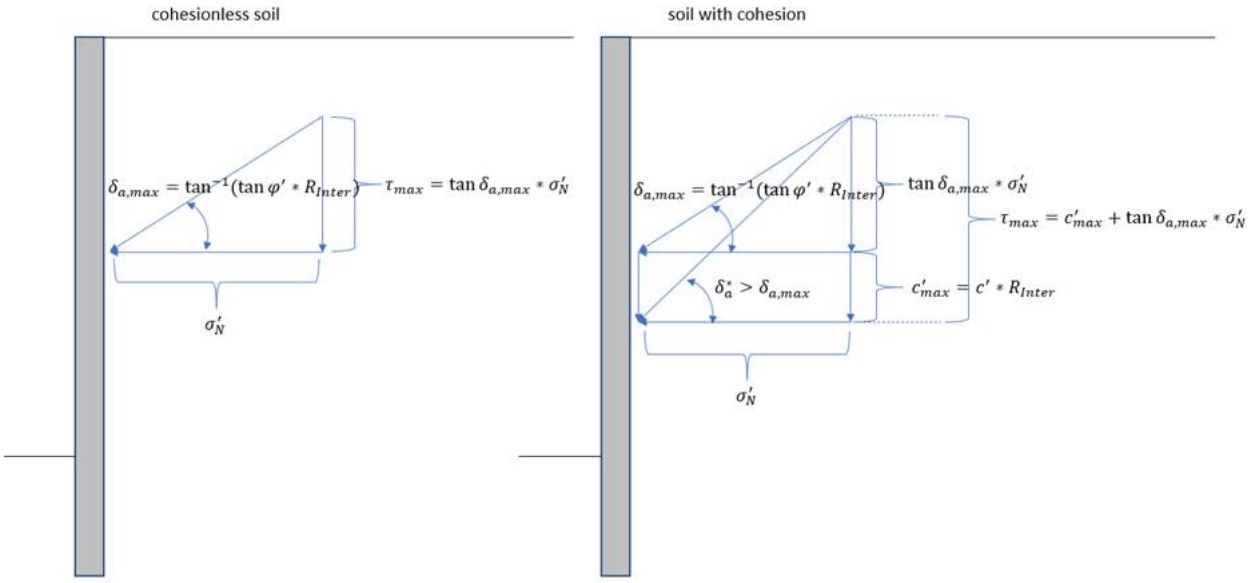

Figure 5.7: Earth pressure angle in soil with cohesion vs without cohesion.

5.2 Analytical Calculation Model

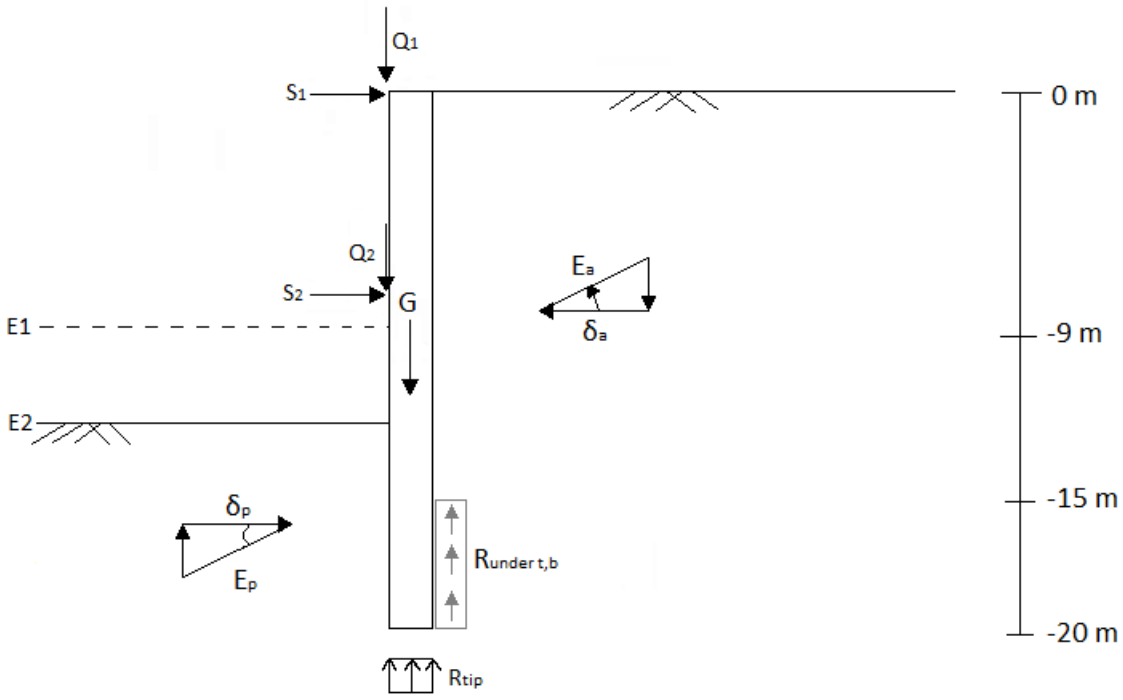

Figure 5.8: Analytical earth pressure model

The downward acting loads in the analytical model is the weight of the wall and struts and the service loads acting on the struts. The upward acting forces are the tip resistance, passive earth pressure and the friction forces below the required embedment depth. The active earth pressure can act both upwards or downwards, depending on the roughness relation between the wall and the soil.

In this case, the required embedment depth is 6 meters, which means that the wall needs to be embedded 6 meters below the excavation surface in order to have a sufficient amount of resistance forces. If the wall is embedded more than 6 meters below the excavation surface, all earth pressure below the required embedment depth can be assumed to act upwards.

Here, the wall reaches down to -20 m. The first excavation is down to -9 m, meaning that the embedment depth is five meters more than the required depth. This provides upwards acting forces at this stage of the excavation. After the second excavation, the embedment depth corresponds to the required depth, the only upward acting forces are therefore the tip resistance and

the passive earth pressure.

For each parameter variation, the active earth pressure will be calculated with three different earth pressure angles:

- $\delta = \frac{1}{2}\phi$, causing the earth pressure to act downwards, corresponding to the case where the soil is moving downwards relative to the wall.
- $\delta = 0$ Corresponding to the case where the wall and soil are not moving or are moving parallel.
- $\delta = -\frac{1}{2}\phi$ corresponding to the case where the wall is moving downwards relative to the soil

Chapter 6

Choice of reference model

In order to obtain the most realistic results, the numerical wall model should be modelled with an actual volume. However, modelling the wall as a plate is more convenient. In this chapter, it will be presented how the plate wall can be modelled in order to get results as similar results as with the volume model, and their differences will also be presented. The choices are based on results from different analyses performed with PLAXIS 2D. Numerical and analytical Excel calculation sheets are presented in Appendix C.

6.1 Mesh refinement

Figure 6.1 shows relative vertical displacements between the soil and the excavation wall and shear stresses along the wall for different variations of mesh coarseness. Each of the graphs show five variations of mesh coarseness.

Normally, it is expected that when the mesh is refined and there is a larger number of elements along the foot plate, the behavior becomes less stiff, which allows for larger deformations, which also causes larger vertical acting forces. However, as Figure 6.1 shows, the relative displacement decreases as the mesh is refined, and despite this, the shear stresses increase.

The decrease in relative displacement might be due to the fact that the mesh refinement affects the virtual thickness of the wall. Smaller elements gives a smaller interface thickness. The interface soil is weaker than the rest of the soil, and the decrease of the amount of this weak soil leads to less room for displacement. This can also be seen in Figure 6.2, that shows the vertical relative displacement between the foot plate and the soil.

The three graphs below all shows that the results from the "very fine" and "extra fine" mesh refinements are overlapping. A finer mesh gives a more accurate result, but when the results don't change with further mesh refinement, it is chosen to proceed with the "very fine" mesh refinement due to time consume.

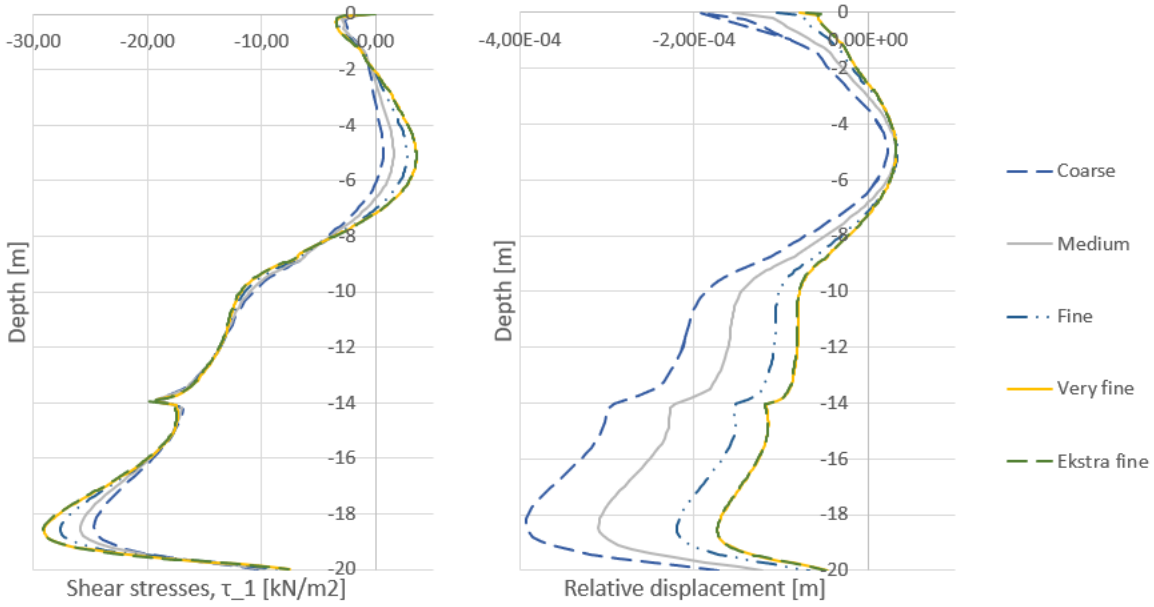

Figure 6.1: Shear stresses and relative displacement of the excavation wall, soil side, second excavation.

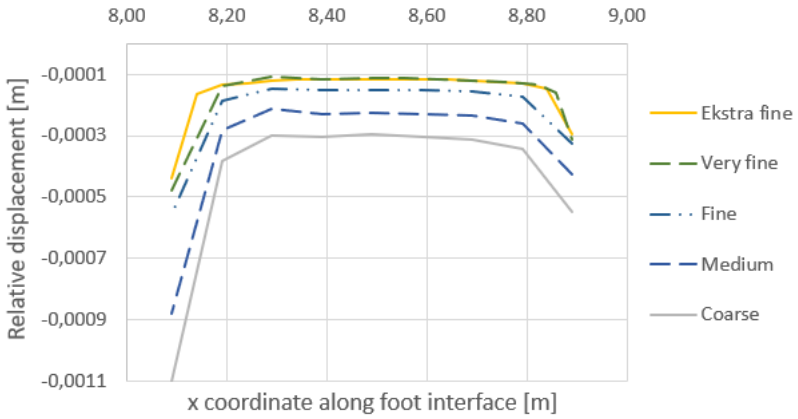

Figure 6.2: Shear stresses along excavation wall on the soil side after the second excavation.

6.2 Optimizing the plate reference model

When modelling the wall as a plate with a horizontal plate at the foot of the wall, the weight of the plate wall need to be reduced compared to the actual weight of the wall. This is because the soil laying above the foot plate will act as an extra weight down on the horizontal plate, in addition to the weight of the wall. To compensate for this, the weight of the wall is reduced. In order to find out how much the weight should be reduced, two different approaches is investigated. When the wall is fully embedded, the weight of the wall is reduced with the weight of the overlaying soil. As the soil is excavated, the weight of the wall is increased as follows:

• The weight of the overlaying soil that is excavated is added to the part of the wall that is no longer embedded.

• The double of the weight of the overlaying soil that is excavated is added to the part of the wall that is no longer embedded.

The two approaches are labeled "half adjusted w" and "adjusted w" respectively. The result of the simulations of these approaches can be seen in Figure 6.3.

It can be seen that the half adjusted weight approach has less shear stresses along the soil side of the wall than the continuum wall. This indicates that this wall has a smaller vertical movement which can be a result of the wall being too light. It is however not realistic to assume that all the weight of the above lying soil is transferred directly down onto the foot plate. The shear stresses in the adjusted weight approach corresponds better with the shear stresses in the continuum wall. After the second excavation the shear stresses along the plate with adjusted weight corresponds well with the continuum wall in the gravel layer, but the stresses are slightly bigger for the plate. The correspondence is not as good in the clay layer, as the shear stresses is decreasing significantly towards the bottom of the wall. This can be interpreted as a result of the foot plate hindering the relative movement between the wall and the soil, which leads to the decreased shear stresses above the foot plate. The decrease in shear stresses is illustrated in Figure 6.3 and it can be seen in Figure 6.4, that the relative movement between soil and wall is significantly smaller for the plate in the clay layer than for the continuum wall. To compare, the results from a simulation with the plate wall without a foot plate is also included in Figure 6.3.

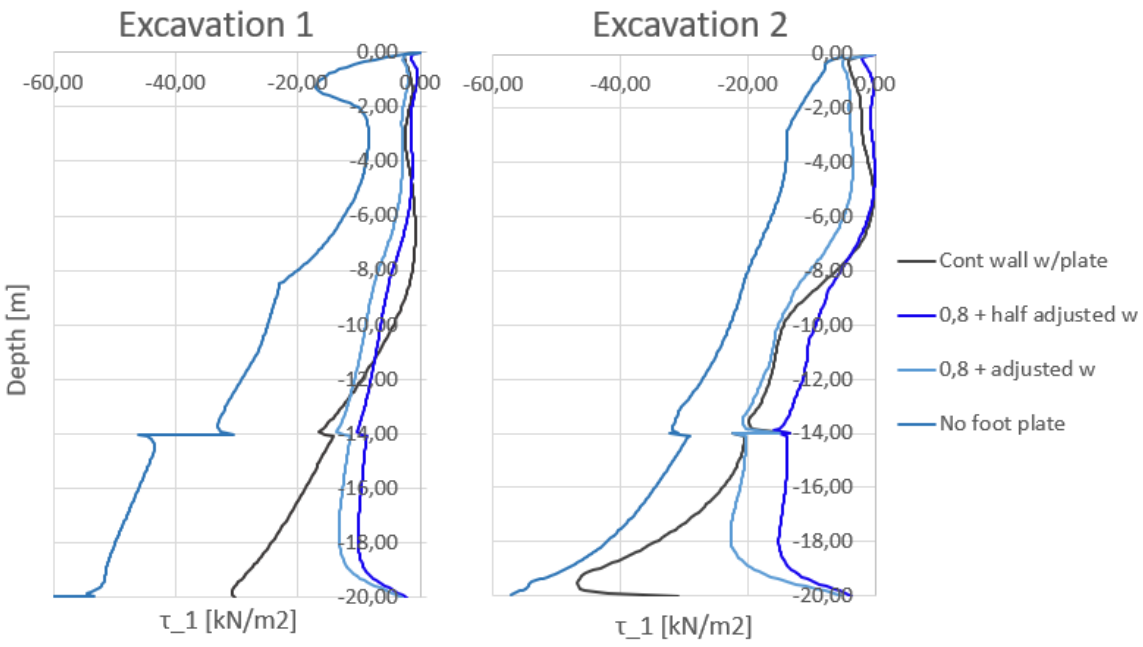

Figure 6.3: Comparison of vertical earth pressure on the soil side along the 0.8 m wide walls.

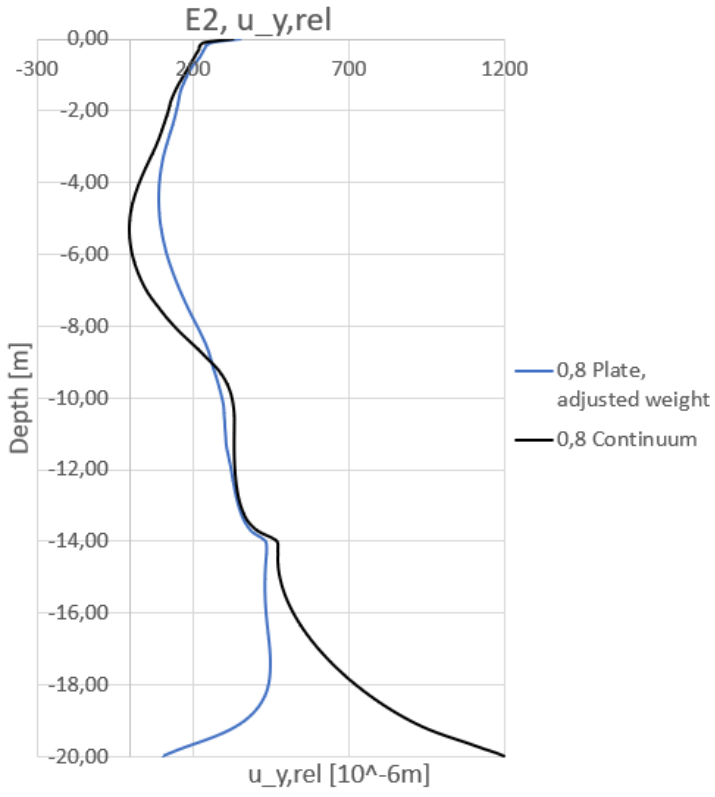

Figure 6.4: Relative displacement between wall and soil on the soil side.

By comparing figures 6.3 and 6.4, one can see that the correspondence between the shear stresses and the vertical relative displacement is pretty good. The wall is stiff and there will not be a large difference in displacement along the wall. The displacements are very small, and there is a little difference between the to models along the wall.

Table 6.1 gives the total integrated shear stresses for a 0,8 m thick wall. These also confirms that the plate wall with adjusted weight is the best fit, but the stresses are somewhat smaller than for the continuum model. Figures B.2- B.5 in Appendix B.1.2 shows that the displacements are larger for the continuum wall than for the plate wall, as expected considering the shear stresses and relative displacement.

Table 6.1: Total shear stresses on 0,8 m thick wall after first and second excavation ont he soil side

Wall type	E1 $[kN/m^2]$	E2 $[kN/m^2]$
$Continuous wall$	-188,79	-290,1
$Plate wall with reduced weight$	-157,62	-255,51
$Plate wall with half reduced weight$	-111,77	-152,42

Another difference between the continuum wall and the plate wall is that the external forces are acting on the edge of the continuum wall and not through the center line, which creates a bending moment. The plate wall has no thickness and therefore, no bending moment is created. In order to make the plate model resemble the continuum model as well as possible, it is chosen to compensate for the off-centered loads in the continuum wall by adding a moment at the top of the plate. This moment equals to the forces acting on the top of the wall multiplied with the distance between the acting point and the center line of the wall. The bending moments of the reference models are presented in figures B.14 and B.15 in Appendix B.3.

The weight and dimensions of the reference plate model is presented in Figure 6.5.

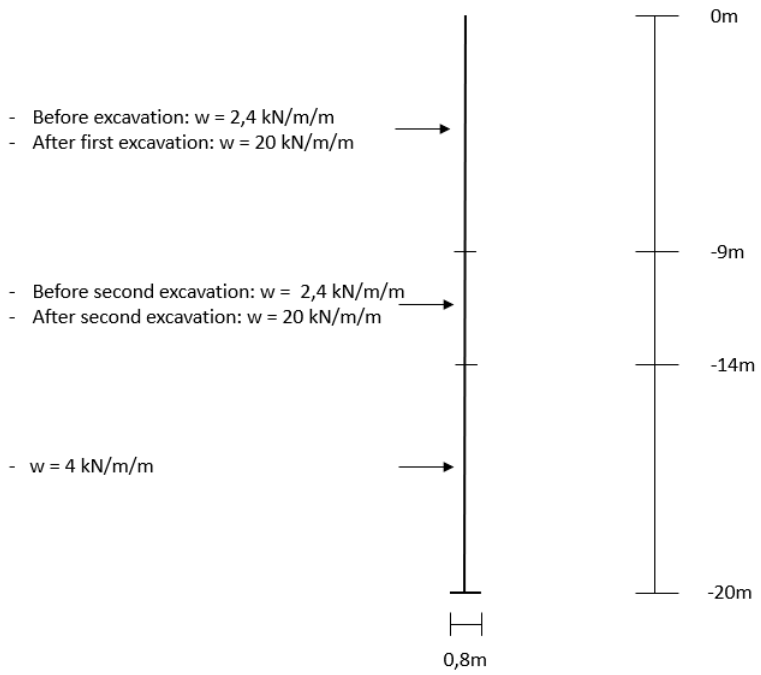

Figure 6.5: Reference plate model

6.3 Comparison of reference models

Figure 6.6 illustrates the comparison of shear stresses along the wall on the soil side calculated with FEM for the plate wall, continuum wall and calculated analytically. Analytically, the shear stresses are calculated for three different scenarios. The "upper bound" represents the situation where the soil is moving downwards relative to the wall, the graph labeled "zero" represents no movement of the wall and the "lower bound" is the situation where the wall is moving downward relative to the soil.

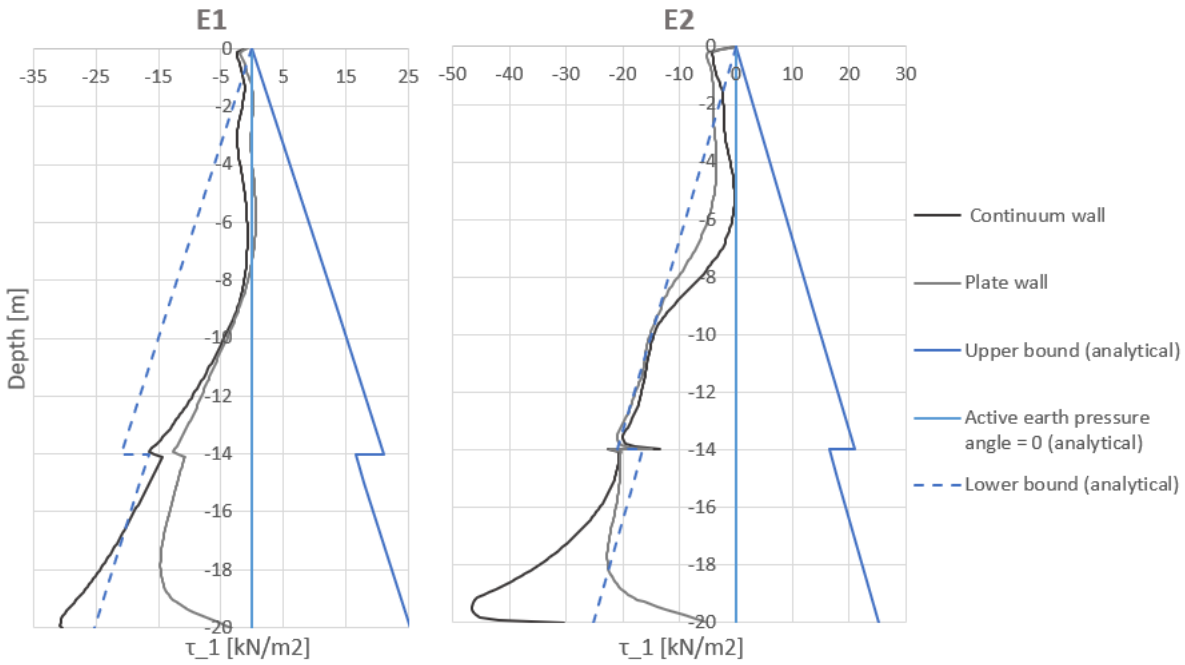

Figure 6.6: Comparisons of shear stresses along the soil side of reference models

When the soil is moving downwards relative to the wall, the earth pressure angle is positive and causes a downward acting earth pressure on the soil side. As figure 6.6 shows, It is the lower bound calculation that fits best with the numerical ones. In the numerical model, the wall is moving downwards relative to the soil, creating upward acting earth pressure, thus can the lower bound calculation represent this the best. In the first excavation (E1), the lower bound calculation stresses are larger than the numerical ones. Considering that the larger part of the numerically calculated earth pressures and the analytically calculated earth pressures are acting upwards, the use of the analytical calculation is less conservative. A reason for the difference is that the earth pressure angle is assumed constant throughout each soil layer alongside the entire wall in the analytical calculations, while in the FEM calculations, the earth pressure angle is allowed to vary alongside the wall.

Figure 6.7 illustrates the difference between shear stresses along the plate wall and the continuum wall. The lower the friction angles, the better the correspondence in the clay layer, but higher friction angles gives better correspondence in the gravel layer. The shear stresses decrease with between 14,8% and 30,2% in the plate model compared to the continuum model after the second excavation in the ϕ variation. After the first excavation the shear stresses decrease with between 42,3% and 43,3%. Appendix C shows the Excel calculation sheets for the

numerical earth pressure and safety factor calculations.

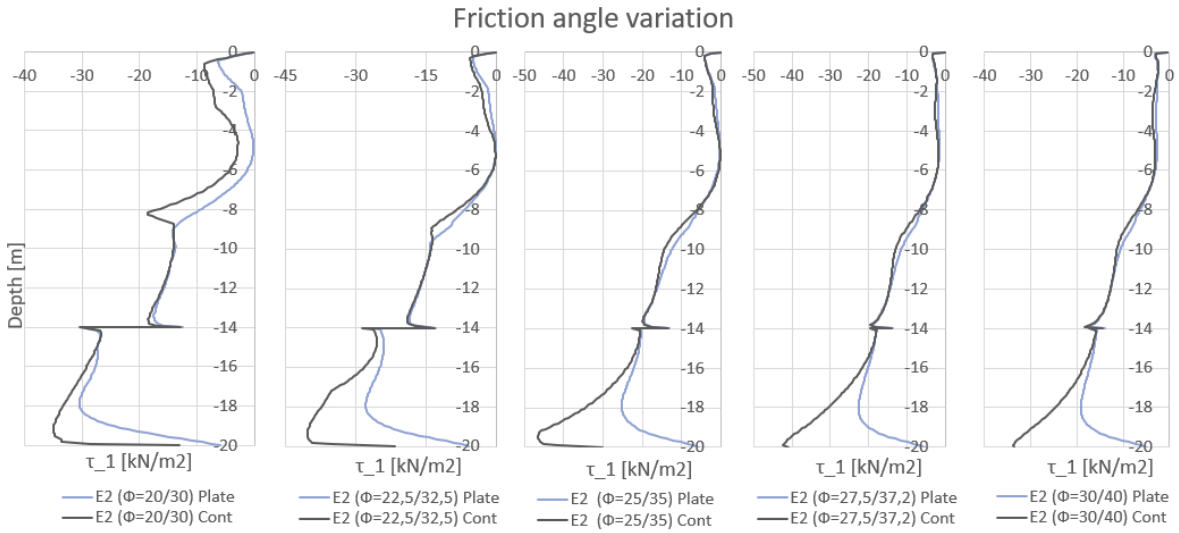

Figure 6.7: Comparison of interface shear stress variation along the soil side in plate and continuum model due to variation of friction angle. Second excavation.

Chapter 7

Interpretation and discussion of Results

This chapter will present and discuss the results of the parameter variations in the analytical model and the FEM models. The parameters that are varied are the friction angle (ϕ) the cohesion (c), and the earth pressure angle (δ). Each parameter variation is presented in three sections; an analytical part and a numerical part that will present the variation of shear stresses due to the parameter variation, and a section presenting the variation of safety factors. In the figures in the analytical sections, the shear stresses on the excavation side is presented on the left side of the zero axis and the shear stresses on the soil side is presented on the right side. Thus, the signs of the size of the shear stress is not correct. In the analytical calculations, the earth pressure on the excavation side is acting upwards, and on the soil side the earth pressure is acting upwards in the lower-bound example and downwards in the upper-bound example. The analytical zero-example is the case where the earth pressure is acting only horizontal. The three different analytical calculations are presented in order to see which one is best comparable with the numerically calculated safety factors.

In the graphs presenting the safety factor results from the friction angle variation, the x-axis pictures a variation of ϕ between 20 and 30 degrees. This corresponds to the variation in the clay layer. However, simultaneously, the friction angle in the gravel layer is varied from 30 - 40 degrees.

The numerical safety factors are calculated by applying partial safety factors from the German Standard to the output earth pressure.

The safety factor figures displays the safety factors calculated analytically and numerically in the three different ways, illustrated by figures 5.1 and 5.2. The figures presenting the safety fac-

tors from the ϕ and c variations contains graphs from the five different calculations below. The figures presenting the safety factor from the δ variation contains the latter two, plus analytical safety factor calculations with earth pressure angles obtained from numerical calculations:

- **Upper bound:** Analytical calculations where $\delta = \frac{1}{2}\phi$
- **Zero:** Analytical calculations where earth pressure angle equals is zero, which gives no vertical acting earth pressure on the wall
- **Lower bound:** Analytical calculations where $\delta = -\frac{1}{2}\phi$
- **Plate:** FEM calculations using the plate model
- **Cont:** FEM calculations using the continuum model

7.1 Friction angle variation

7.1.1 Analytical results

According to the German standard, the maximum earth pressure angle is half of the soil friction angle for diaphragm walls, and when the earth pressure angle increases, so will the shear forces acting on the wall. Due to this, as the friction angle increases, the shear forces can also be expected to increase. As seen in Figure 7.1, this is the case in the clay layer on the passive side. However, in the gravel layer, the vertical earth pressure decreases as the soil friction angle increases. The calculation of initial vertical earth pressure is not affected by the change in ϕ, but it is multiplied with the initial earth pressure coefficient K_0, in order to obtain the initial horizontal earth pressure. K_0 depends on ϕ and decreases as ϕ increases. In addition to that, this initial horizontal earth pressure is multiplied with the active earth pressure coefficient K_a in order to obtain the active earth pressure. As Figure 2.9 illustrates, the active earth pressure coefficients are strictly decreasing as the friction angle increases. These coefficients causes the active earth pressure and therefore also the shear forces on the soil side in the gravel layer to decrease as ϕ increases.

In the clay layer on the active side, the shear stresses change very little when ϕ changes. τ increases from parameter variation 1-3 and decreases from 3-1. In order to get the total horizontal earth pressure, the negative earth pressure contribution due to cohesion must be added.

This earth pressure caused by cohesion is calculated by multiplying the cohesion with the active earth pressure coefficient for cohesion, which decreases as the friction angle increases as shown in Figure 2.9. In this parameter variation, the cohesion is kept constant. This results in decreasing earth pressure because of the cohesion as ϕ is increased. In order to calculate the shear stress, the total horizontal earth pressure is multiplied with the tangent to the earth pressure angle. This earth pressure angle is assumed to be half of the friction angle and will therefore increase when ϕ increases. From parameter variation 1-3 the affect of the increase in earth pressure angle is larger than the effect of the decrease in earth pressure coefficients. This results in increasing shear stresses when increasing the friction angle until 25°. When increasing ϕ beyond 25°, the effect of the decreasing earth pressure coefficients will take over and τ will start to decrease as it does in the clay layer for variation 3-5 and in all the variations in the gravel layer because the friction angle is varied from 30°-40°.

This effect can be explained by the fact that a soil with a higher friction angle is able so stay stable at a steeper slope angle than a soil with a smaller friction angle. The steeper stable slope angle causes smaller horizontal earth pressures to act on the wall, which again causes smaller vertical forces to act on the wall. Figure 7.1 suggests that as the friction angle is increased towards 25° in the clay, the contribution of the effect of the increasing soil friction angle is slightly larger than the effect of the increased slope stability on the active side. This causes the vertical earth pressure to increase when increasing ϕ towards 25°, but at 25°, the increased slope stability becomes the largest contribution, resulting in decreased shear stresses.

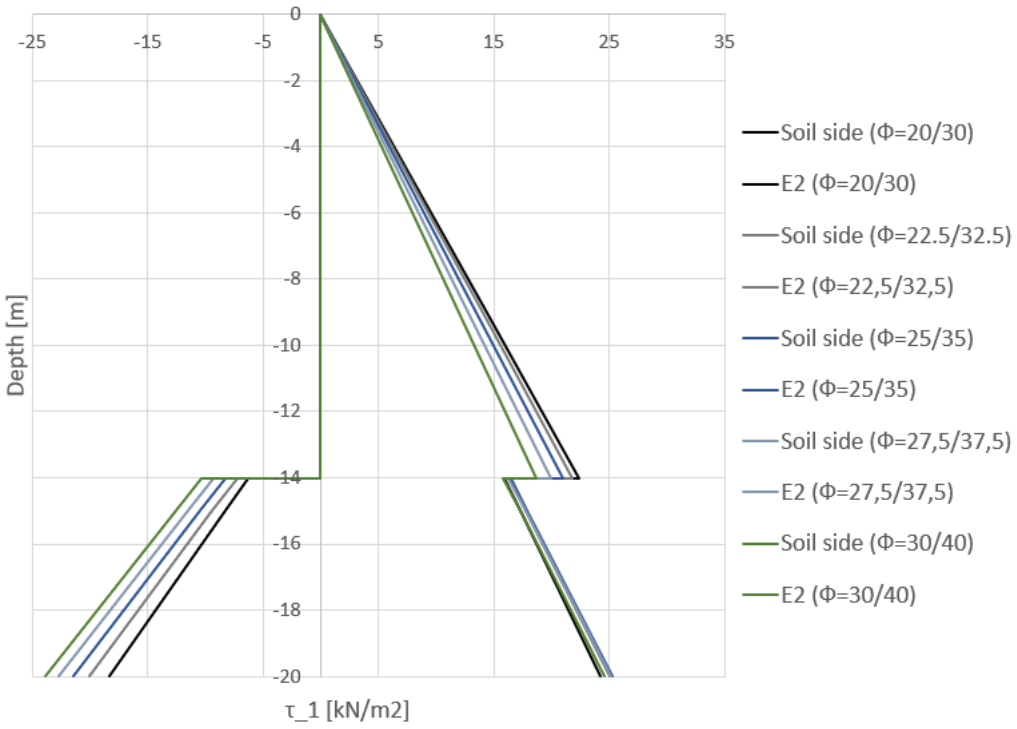

Figure 7.1: Shear stresses along the diaphragm wall according to upper bound shear stresses. Left side: excavation side, second excavation. Right side: soil side.

The two effects described above works in opposite directions on the active side, but on the passive side, on the other hand, the shear stresses seems to still be increasing steadily at $\phi = 30°$. This is because the two effects works in the same direction on the passive side. Cohesion adds shear strength to the passive side and subtracts strength from the active side. Figure 2.11 Shows that the passive earth pressure coefficients are increasing with the increased ϕ, causing the passive earth pressure to increase as opposed to the active earth pressure coefficient.

7.1.2 Numerical results

The numerical calculated shear stresses develops in a different manner than the analytical results. As Figure 7.2 shows, on the soil side, the shear stresses develops in opposite directions at different parts of the wall. Above the excavation level in E1, shear stresses increase as the friction angle increases, and below the excavation level, they decrease. In E2 the shear stresses increases as ϕ increases between -2 and -7 meters, and outside of this, the shear stresses decrease as ϕ increase.

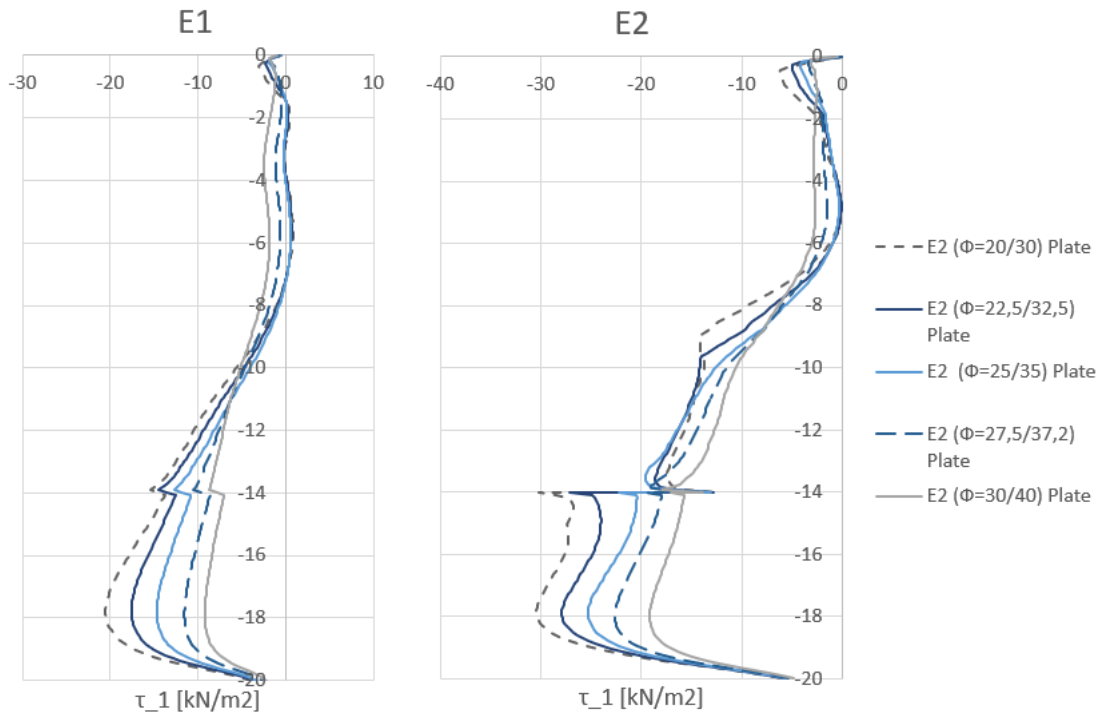

Figure 7.2: Active interface shear stresses along the soil side of the plate wall due to variation of friction angle.

In FEM calculations, there are more factors affecting the stresses than in the analytical calculations. For lower friction angles, the resistance at the foot of the wall is smaller, which can cause a larger downward displacement of the wall. A downward displacement of the wall relative to the soil creates a negative roughness relation between the wall and the soil which causes the shear stresses to act upwards. Smaller friction angles gives larger horizontal stresses which can cause larger horizontal displacements. A horizontal displacement causes the soil to move downwards relative to the wall which creates a positive roughness relation and causes the shear stresses to act downwards. Figure 7.3 illustrates the horizontal displacement and the relative vertical displacement of the wall. The figure shows that down to -8 m after the first excavation step, the wall has close to no relative displacement to the soil, which can come from the combination of vertical and horizontal displacement of the wall. The larger part of this area has slightly positive relative displacement. A positive relative displacement will provide downward acting shear stresses. This corresponds well with Figure 7.2 which shows that there are nearly no shear stresses in this area, and shear stresses are acting upwards for the smaller friction angles.

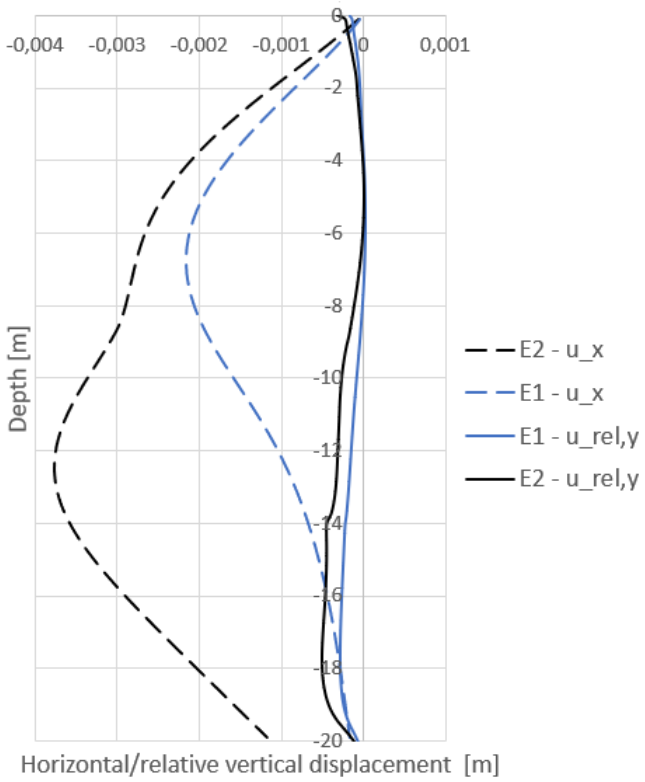

Figure 7.3: Horizontal displacements of wall and relative vertical wall displacements between the plate wall and the soil on the soil side after first and second excavation step

It can be seen in Figure 7.3 that after the second excavation step, the entire wall has larger horizontal displacement, which leads to larger downward movement of the soil. Above -8 m there are still very small relative displacement, but they are slightly larger than after the first excavation step. Due to this, it would be expected that the shear stresses would act downwards in this area, they are however acting upwards. Despite the increase in horizontal displacement in this area, the vertical movement of the wall relative to the soil is negative, and therefore the shear forces are acting upwards. However, the wall and the soil are moving downwards nearly parallel above -8 m, causing the small relative movement, and therefore the shear forces in this area are very small.

As Figure 7.4 shows, the passive earth pressure develops in similar manner along the wall in the FEM calculation as in the analytical calculations. They are however much larger. It can be seen that the flat line at -14 meters is longer in the numerical calculation results. This can be due to the initial earth pressure coefficient. In the FEM calculations, K_0 is set to 0,8 according

to the geotechnical report because of the degree of over consolidation of the clay, while in analytical calculations, normal consolidation is assumed and $K_0 = 1 - \sin\phi$. This provides initial earth pressure coefficients in the range of 0,5-0,66, and as the initial vertical earth pressure is multiplied with K_0 in order to obtain the initial horizontal earth pressure, this initial horizontal earth pressure is smaller for the analytical calculations which, as explained above, also leads to smaller shear stresses.

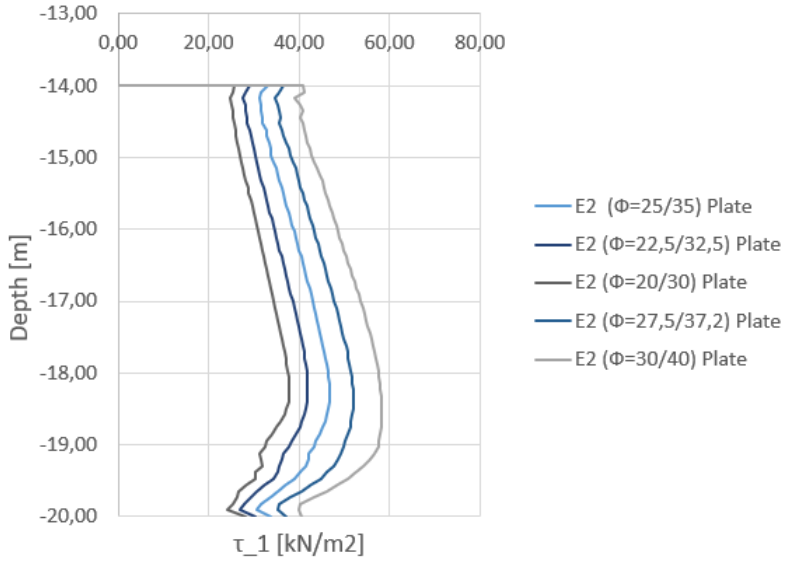

Figure 7.4: Passive interface shear stresses on the excavation side of the wall after the second excavation due to variation of the friction angle

Another reason for the difference between the passive shear stresses, can be that when calculating analytically, horizontal earth pressure at the top of the excavation level is assumed not to be present. While in reality, after the soil is excavated, there is a horizontal earth pressure despite the vertical earth pressure being removed, which is considered by the FEM calculations. The passive earth pressure at the excavation level in Figure 7.1 has a shear stress value larger than zero due to cohesion alone, while in Figure 7.4 this value is a result of the cohesion and the horizontal stress explained above.

7.1.3 Safety factors

The safety factors from the calculations with zero earth pressure angle and earth pressures obtained from the geotechnical report, is constant throughout the friction angle variation. The

forces acting vertically in this case, are the weight of the wall and struts, the external loads acting on them, the tip resistance and the earth pressures obtained from the GTB. These forces are all independent of the change of friction angle in the analytical calculations. In the calculation where all resistances are obtained from the analytical calculations, the safety factors from the zero calculation decreases because the analytically calculated passive earth pressure is taken into account. As Figure 7.4 shows, the shear stresses increase when ϕ increases, giving more resistance forces which increases the safety and decreases the safety factors.

In the upper bound calculations, the safety factors are slightly decreasing as the friction angles increases. The reason for this is that the forces on the soil side in Figure 7.1 are decreasing more in the gravel layer than it is increasing in the clay layer in variations. According to the upper bound calculation when all resistances are obtained from the analytical calculations, the safety factors are larger than 1.0 and therefore indicates that the ground does not have sufficient capacity for the current load situation, and the wall is settling. In the 1st and 2nd calculation, the SF is just below 1.0 in E2. The upper bound is however not correct in this case, because it assumes that the earth pressure along the entire soil side of the wall is acting downwards, while in E1 the wall stretches below the required embedment depth, which would provide resistance forces. In addition, when the safety factor is calculated to be more than 1.0, it indicates that the wall will be settling which means that the earth pressure angle is smaller than the one used in the calculation.

In the lower bound calculations, the earth pressure on the soil side is acting upwards. As illustrated in Figure 7.1, the earth pressure is decreasing in the gravel layer and changing very little in the clay layer as ϕ increases. Only in variation 1-2 the vertical earth pressure increases as much in the clay layer as it decreases in the gravel layer, but when increasing ϕ beyond this point, the total vertical earth pressure is decreasing. The earth pressure on the excavation side of the wall are increasing more or less steadily throughout the five variation steps. The safety factors in the lower bound is more or less constant in the 3rd calculation example and increases slightly in the 1st and 2nd. The reason for the increase is that the resistance forces on the soil side decreases while they remain constant on the excavation side in the 1st and 2nd calculation when the friction angle is increased.

The safety factors calculated from the plate model and the volume model are developing similarly in all three calculation examples, only the plate is giving slightly more conservative

results with safety factors of 0,01-0,09 higher than the volume wall model, meaning it is slightly more conservative.

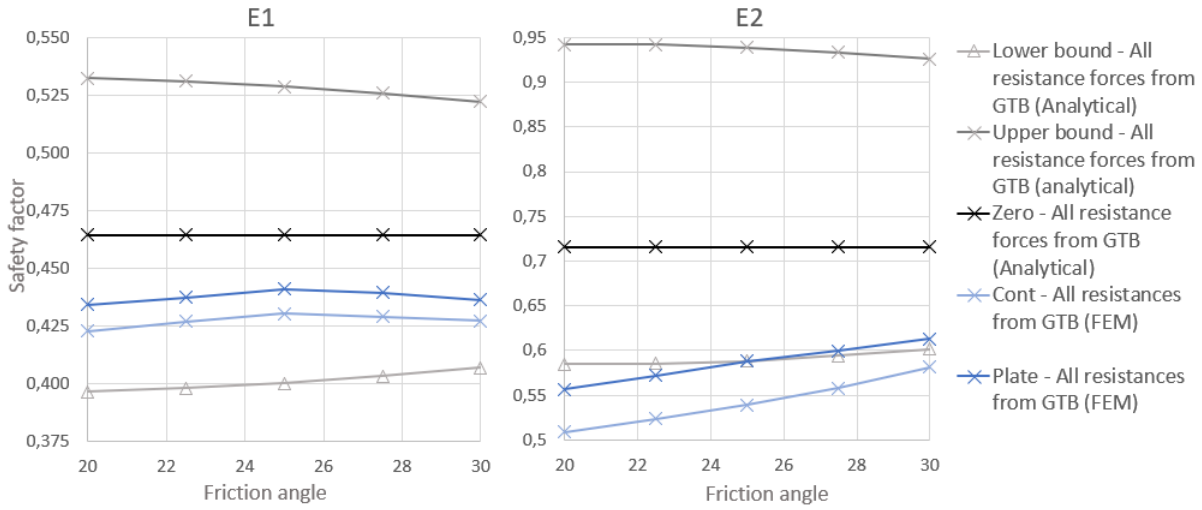

Figure 7.5: 1st calculation: Safety factors due to friction angle variation. All resistances obtained from GTB

In the 1st calculation example presented by Figure 7.5, where all resistances are obtained from the GTB, the safety factors obtained from the plate and continuum models Lays in the middle of the zero and the lower-bound calculation after the first excavation step. This indicates that the wall is moving downwards relative to the soil in the numerical models, causing the earth pressure to act upwards. Considering that all resistance forces are obtained from the GTB, and therefore are constant, this also indicates that the earth pressure angle above the required embedment depth on the soil side is approximately half of the one used for the lower bound calculation. In E1, the numerical SF increases with 0,007 from variation 1-3 and decreases with 0,004 from variation 3-5. These small changes is caused by the change in the shear stress development. In E1, the shear stress increase with increasing ϕ above -10 m and decreases below. Studying Figure 7.2, the shear stresses from variation 1-3 increases more than it decreases above the required embedment depth, and vice versa in variation 3-5. In E2, the numerical SF are increasing steadily with a value change of 0,057 from the first to the fifth parameter variation. The plate model crosses the constant lower-bound line at the third variation and the volume model is below for each variation, but approaching it as ϕ increases. The reason for the constant increase of SF in E2 might be because a significant amount of unchanging passive earth pressure is excavated away, allowing the active earth pressure above the required embedment depth to

affect the SF more. Above -8 m in E2, the vertical earth pressure increases as ϕ increases, and opposite below. Figure 7.2 shows that τ decreases more than it increases in E2, and since the earth pressure is acting upwards on the soil side, this decreases the resistance forces and therefore the SF increases.

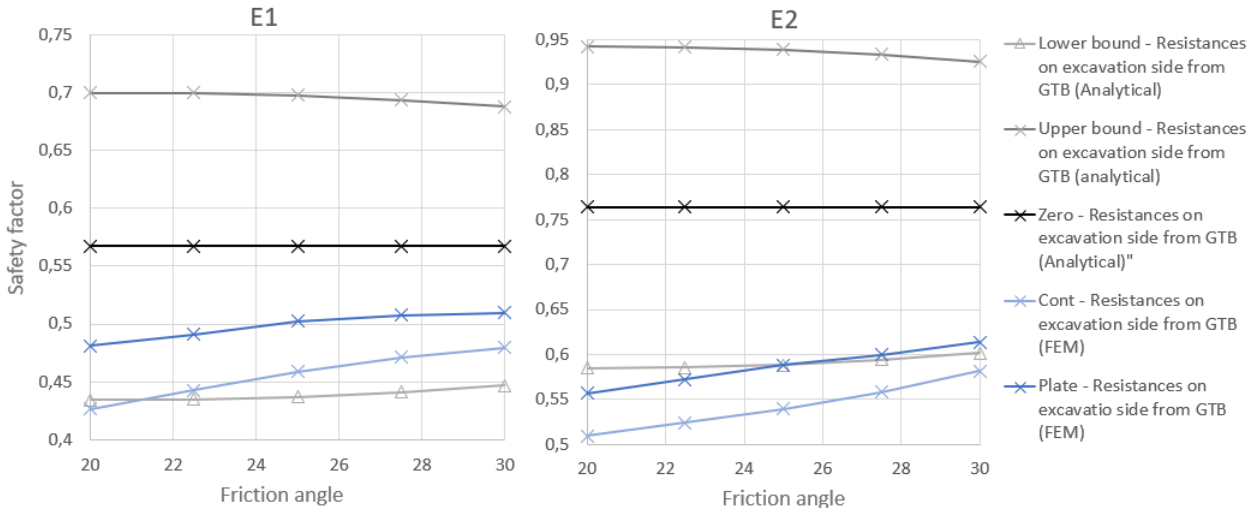

Figure 7.6: 2nd calculation: Safety factors due to friction angle variation. Resistances on excavation side obtained from GTB

In the 2nd calculation, all stresses acting on the soil side are calculated analytically or numerically while the stresses on the excavation side are obtained from the GTB and they are constant throughout the parameter variations. In E1, the safety factors are constantly increasing, but a little less for each variation step. The graph seem to flatten out around $\phi = 30/40°$. The only change in forces acting on the wall is what we can see in Figure 7.2. Studying the E1 graph, we can see τ increases more for each variation above -10 m, and it decreases a little less for each variation below -10 m. It seems like the shear stresses are approaching a more even distribution as the friction angles become larger. The changes above and below -10 m cancels each other partly out more and more for each step causing the graph in Figure 7.6 to flatten. The SF graph from the continuum model also shows a tendency to flatten as ϕ increases, however, slightly slower than the plate model does.

In 2nd calculation E2, the numerical safety factors seem to increase more or less at the same rate throughout the parameter variation. When considering the stresses along the entire soil side calculated by FEM, Figure 7.2 show that despite the stresses increasing above -8 m, they

decrease significantly more below, especially in the clay layer. In these five variations, the total change seem to remain more or less the same for each parameter variation, causing the safety factors to increase with the same rate throughout these variations.

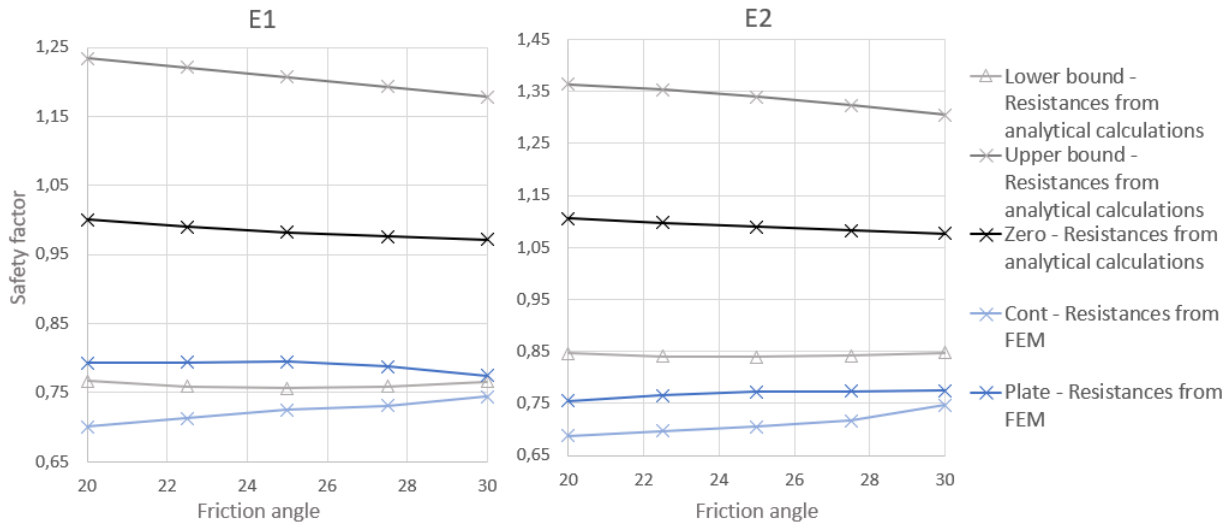

Figure 7.7: 3rd calculation: Safety factors due to friction angle variation. All resistances obtained from Analytical or FEM calculations

In the 3rd calculation, the plate model SF remains constant in the three first variations in E1 and decreases slightly in the fourth and fifth, while in E2 they slightly increase in until the third variation and then flattens out. The volume model increases with approximately the same rate in E1 and also in E2 until the fourth variation. From variation 4-5 it increases a little more. As shown by Figure 7.4, the vertical component of the passive earth pressure increases slightly more for each time ϕ increases. In addition to this, as previously mentioned, the upward acting forces on the soil side are decreasing as ϕ increases. These two changes are affecting the safety factors in opposite directions. The SF will change according to which of the factors have the largest change. In the ϕ-variation, the vertical component of the passive earth pressure is increasing more than what it decreases on the active side in the second excavation. This would in general cause the SF to decrease, but due to the small differences in the changes, the partial safety factors decrease the passive earth pressure and increase the active earth pressure enough to cause the SF to increase from the first to the third variation. The total change in earth pressures increases from variation 3-5 which would cause the SF to increase even more, but the PSF evens the change and causes the graph to flatten.

7.2 Cohesion variation

7.2.1 Analytical results

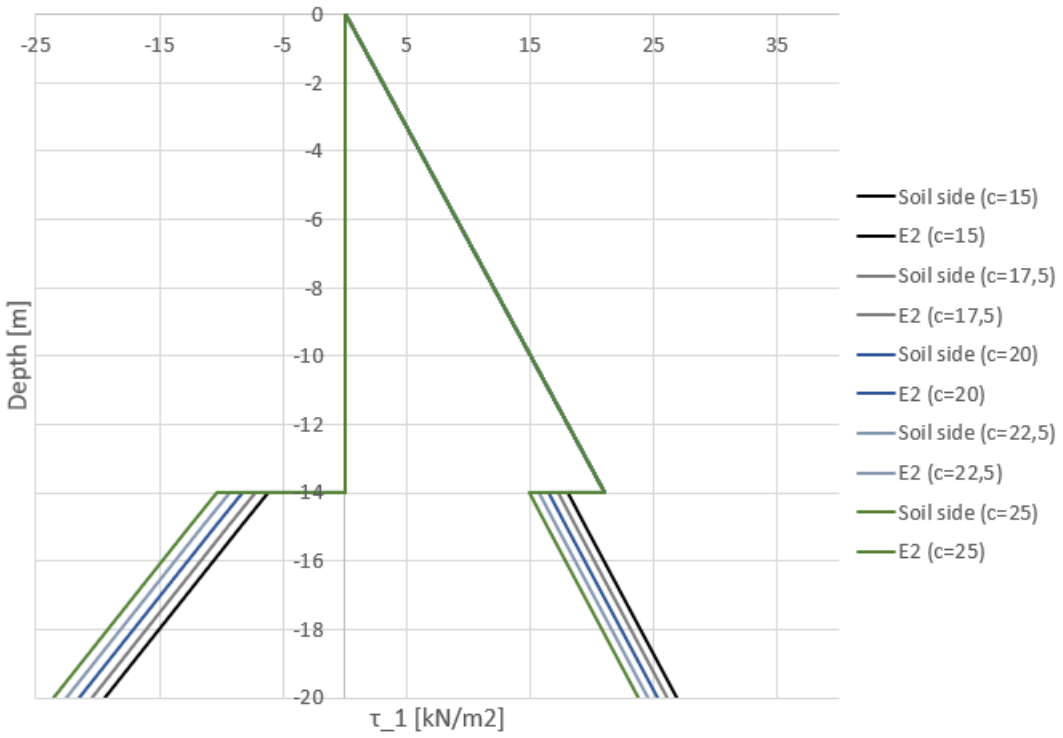

Figure 7.8: Shear forces according to analytical calculations, second excavation, soil side.

It is illustrated in Figure 7.8 how the shear stresses decreases evenly on the soil side and increases on the excavation side of the wall in the clay layer as the cohesion is increased. Cohesion causes inter-particular attraction in the soil which increases the shear strength of the soil. An increase in cohesion will lead to smaller horizontal active earth pressure and larger passive earth pressure acting on the wall because of the increased soil-shear strength. The shear stresses are proportional with the horizontal earth pressures, therefore, when the increasing cohesion causes decreasing earth pressures on the soil side, the shear stresses between the wall and the soil will also decrease on this side. On the excavation side, cohesion leads to larger horizontal earth pressure, and therefore also larger shear forces between soil and wall.

There is no cohesion in the gravel layer, therefore we see no change in shear forces there.

7.2.2 Numerical results

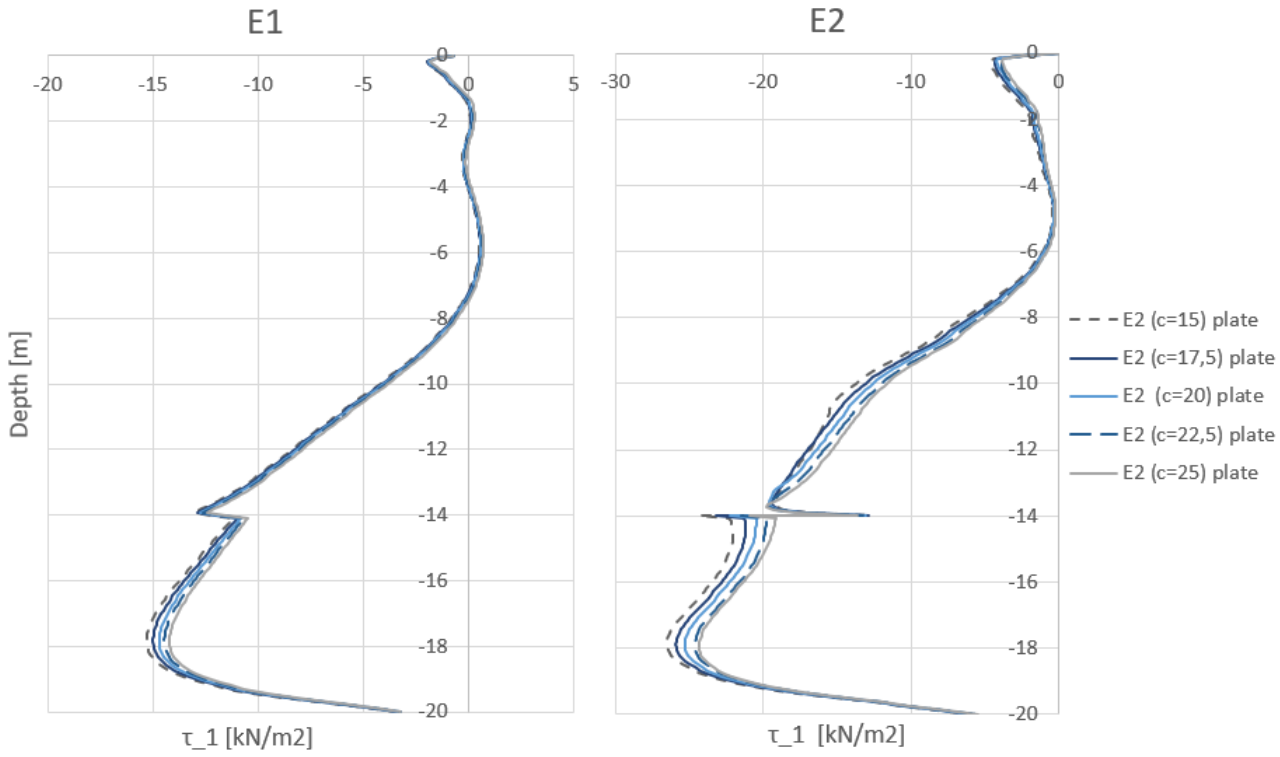

Figure 7.9: Active interface shear stresses according to FEM calculations, first and second excavation, soil side.

In the numerical results, we see the same tendency in the clay layer as in the analytical calculations. The shear stresses decrease as the cohesion increase. Different from the analytical results is the shear stress development in the gravel layer. Despite the cohesion being zero in the gravel, the shear stresses decrease on the soil side as the cohesion increase. This is likely due to wall displacement. As opposed to the analytical calculations, the FEM calculation takes the wall displacement into consideration. The increase of cohesion causes a decrease in downward movement of the wall. As cohesion adds shear strength to the soil, the clay layer will be able to resist the downward movement of the wall better as c is increased. This causes a smaller relative movement between the wall and the soil with the increasing cohesion and therefore we also see a difference in shear stresses between the wall and the gravel. Figure 7.10 confirms that there is both a larger horizontal and relative vertical movement of the wall for the less cohesive soil.

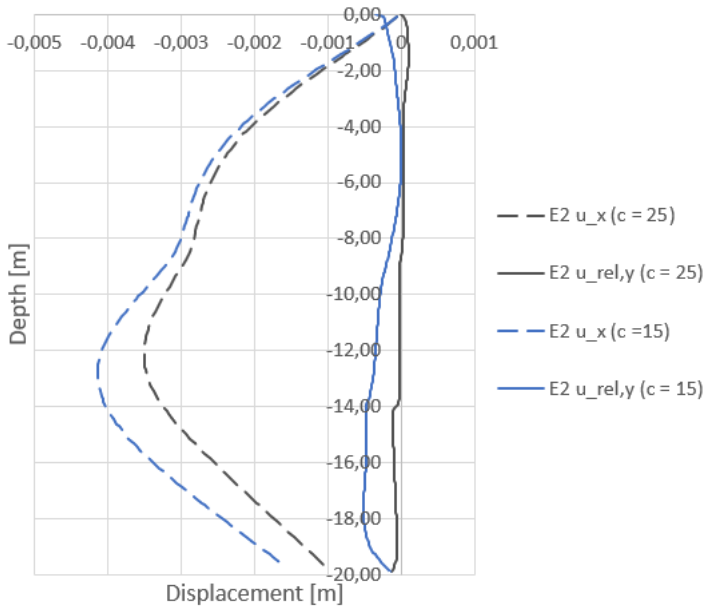

Figure 7.10: Change in horizontal and relative vertical displacement due to change in cohesion, soil side

Figure 7.11 illustrates the development of shear stresses acting on the excavation side on the wall after the second excavation. Due to an increase in shear strength with the increase in cohesion, the soil is able to resist larger forces applied by the wall deformation.

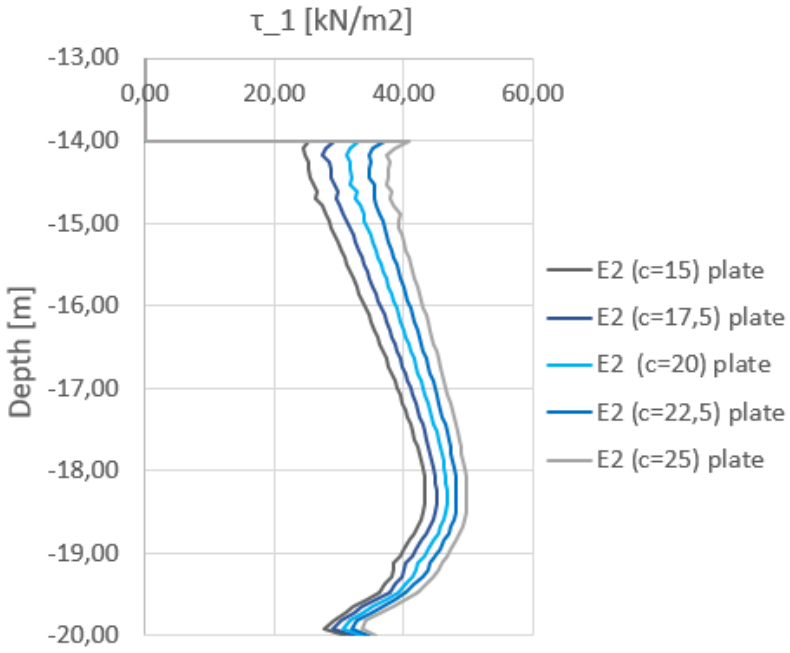

Figure 7.11: Passive interface shear stresses due to variation of the cohesion, excavation side.

7.2.3 Safety factors

Similar as for the ϕ-variation calculations, the safety factors are either constant or slightly decreasing in the upper-bound calculations and either constant or slightly increasing in the lower-bound. The reason for the decrease in safety factors in the upper bound calculations as c increases, is because the amount of downward acting forces decrease, and resistance forces increase when the cohesion increases. In the lower bound calculations, all earth pressures are assumed to act upwards while the downwards acting forces remain constant.

The resistance forces obtained from the GTB remains constant through the parameter variation. In the analytical calculations, the forces acting on the soil side are constant in the gravel layer due to no change in the soil characteristics. Therefore, in the calculation example where all the resistance forces are obtained from the GTB, the safety factors change very little in the analytical calculation because there is only one meter of soil where the cohesion is varied.

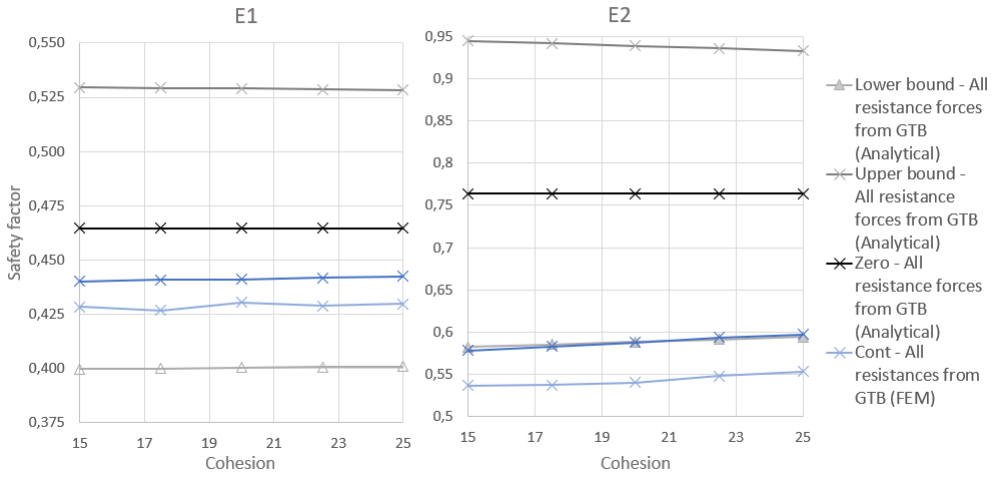

Figure 7.12: 1st calculation: Safety factors due to cohesion variation where all resistances are obtained from GTB.

In the case where the resistances on the excavation side of the wall are obtained from the GTB and the forces acting on the soil side is calculated analytically or numerically, there are less constant resistances, and all the forces on the excavation side is assumed to act in one direction. In the upper-bound case, this means that all forces on the soil side are acting downwards, leading to less resistance forces in addition to the larger amount of downward acting forces. This causes the conservative safety factors of the upper-bound calculations. When a larger amount of forces are included in the analytical or numerical calculations, there is a larger room for change in the

results, as these results varies with the cohesion and the results from the GTB does not.

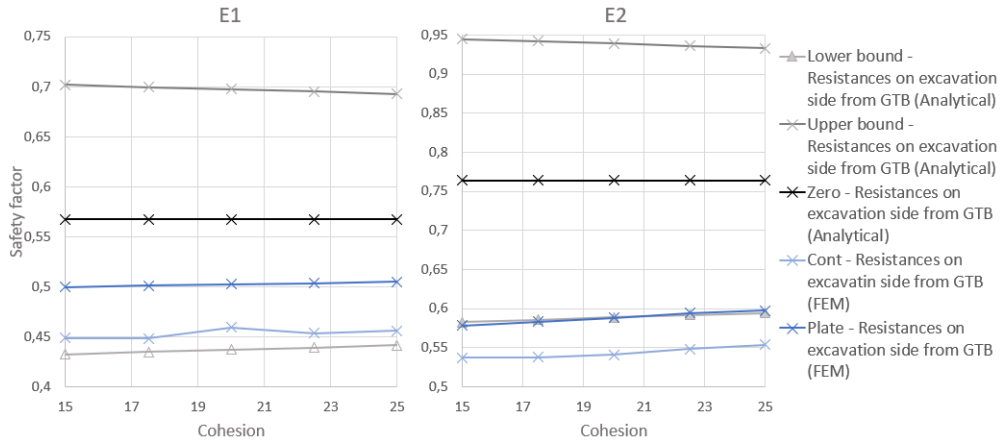

Figure 7.13: 2nd calculation: Safety factors due to cohesion variation where resistances on excavation side are obtained from GTB.

In the 3rd calculation, where the earth pressures acting on both sides of the wall are obtained by analytical or numerical calculations, the change of cohesion affects the earth pressure on both sides of the wall. The upper bound is slightly decreasing as the cohesion increases. This is probably due to the passive earth pressure increasing slightly more than the active earth pressure is decreasing when increasing the cohesion. The upper bound decreases slightly and the zero-calculation decreases slightly.

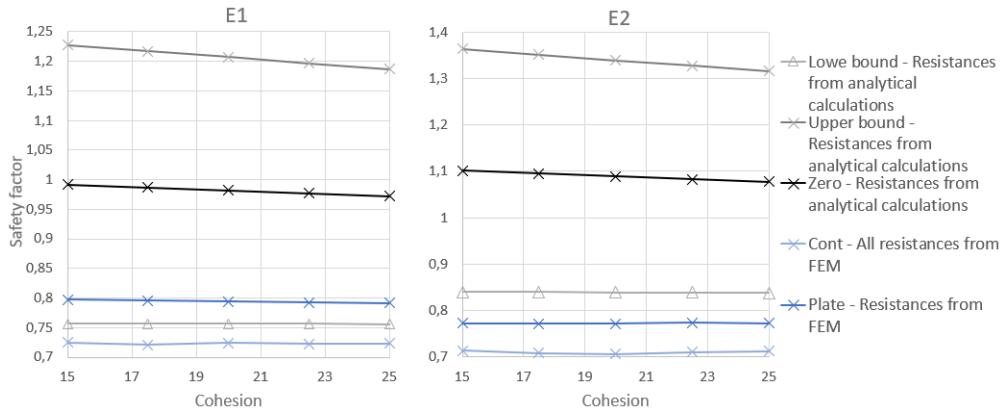

Figure 7.14: 3rd calculation: Safety factors due to cohesion variation where all resistance forces are obtained from analytical calculations

The two numerical models seems to act in similar manners in the different calculations, but

the plate model provides a little higher safety factors than the continuum model, which means it is slightly more conservative. In the calculations where resistance forces are obtained from the geotechnical report, the safety factors according to the numerical calculations are closer to the zero-example after the first excavation, which indicates small earth pressure angles. As less forces are obtained from GTB and more from FEM or analytical calculations, the earth pressure angles seems to increase in the negative direction, leading to more upward acting earth pressure. In the calculation where all resistance forces are obtained from the GTB, the values of the safety factors for the numerical calculations lay approximately in the middle of zero and lower-bound in E1. In E2, the plate model safety factors are overlapping the lower-bound analytical calculation in the 1st and 2nd calculation example. The fact that the numerical calculations has safety factors smaller than the zero-calculation, is an indication of downward displacement of the wall, causing the shear forces to act upwards.

The safety factor values are increasing for the increased amount of earth pressure considered by the analytical or numerical calculations. Only the analytical upper-bound calculation indicates failure with a safety factor larger than 1.0. The reason for this is that all forces on the soil side is assumed to act downwards, which is not the case in this situation.

The safety factors obtained from the numerical and the lower bound calculations are more or less constant in all calculation examples after the first excavation step. They are also constant for E2 in the 3rd calculation. In E2 in the 1st and 2nd calculations, they increase slightly until the fourth variation, but seems to stop increasing after that. The reason for why the SF from the 3rd calculation remains constant, and those from the 1st and 2nd don't, is that in the 3rd calculation the passive earth pressure increases approximately as much as the passive decreases, causing the ratio between the downward acting forces and the resisting forces the same. In the 1st and 2nd calculation, the passive earth pressure is constant, causing the SF to increase as the earth pressure on the soil side decreases when c increases.

7.3 Earth pressure angle variation

7.3.1 Analytical results

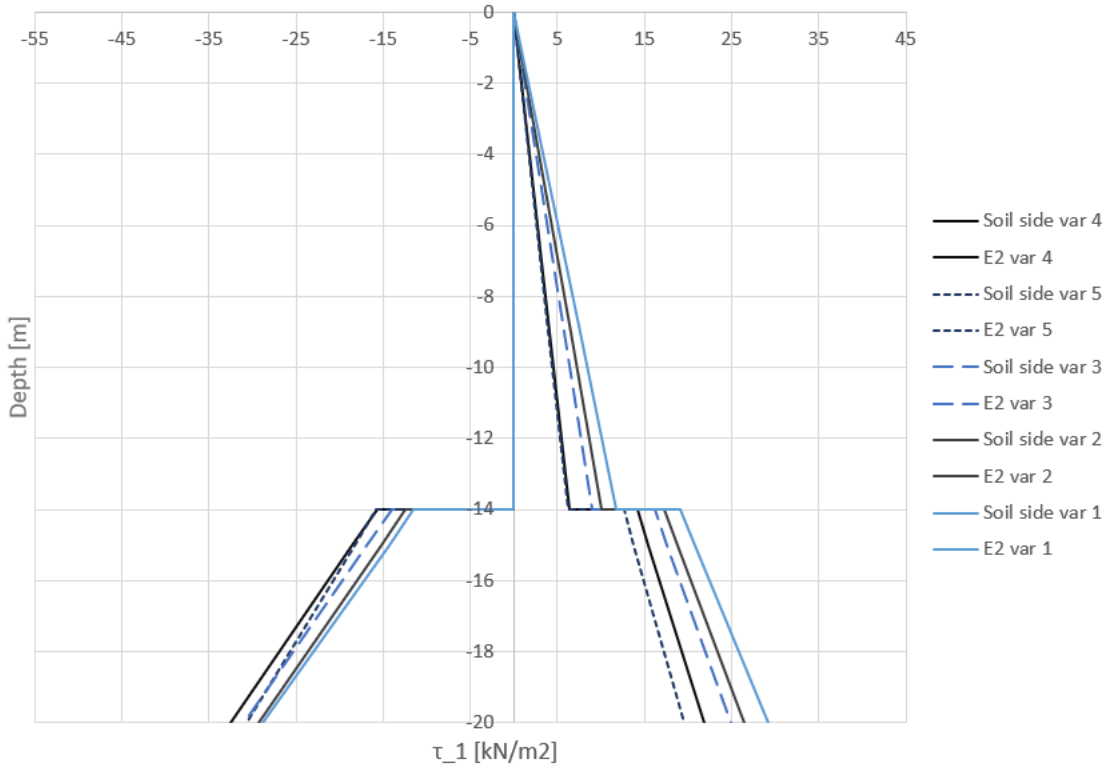

Figure 7.15: Shear stresses along wall according to analytical calculations, 2nd excavation step. Left side: excavation side. Right side: soil side.

It can be seen in Figure 7.15, that as R_{inter} is increased, the shear stresses on the soil side decreases. On the excavation side they increase until $R_{inter} = 0,8$, while the shear stresses when $R_{inter} = 0,9$ is the same as $R_{inter} = 0,8$ at -14 m and about the same as $R_{inter} = 0,7$ at -20 m. The earth pressure angle for the analytical calculations are obtained from the numerical calculations. On the excavation side, the earth pressure angle is calculated by $\delta = \arctan \frac{\tau_{max}}{\sigma}$, where τ_{max} is the maximum shear stresses the wall can mobilize. This provides an earth pressure angle that is larger than the soil friction angle for $R_{inter} = 0,8$ and $0,9$, which is not realistic.

As R_{inter} increases, the earth pressure angle on the soil side decreases. In the analytical calculations, it is the earth pressure angle that is the input parameter. The earth pressure angles are obtained from the numerical output, by calculating the angle of the resultant of the total normal and shear stresses along the wall, in order to keep the results comparable. Therefore, the

development of shear stresses along the wall in the analytical calculation also depends on the numerical calculation. When R_{inter} increases, the wall is able to mobilize larger shear stresses due to the increase in interface friction angle, which would be expected to lead to a larger earth pressure angle.

7.3.2 Numerical results

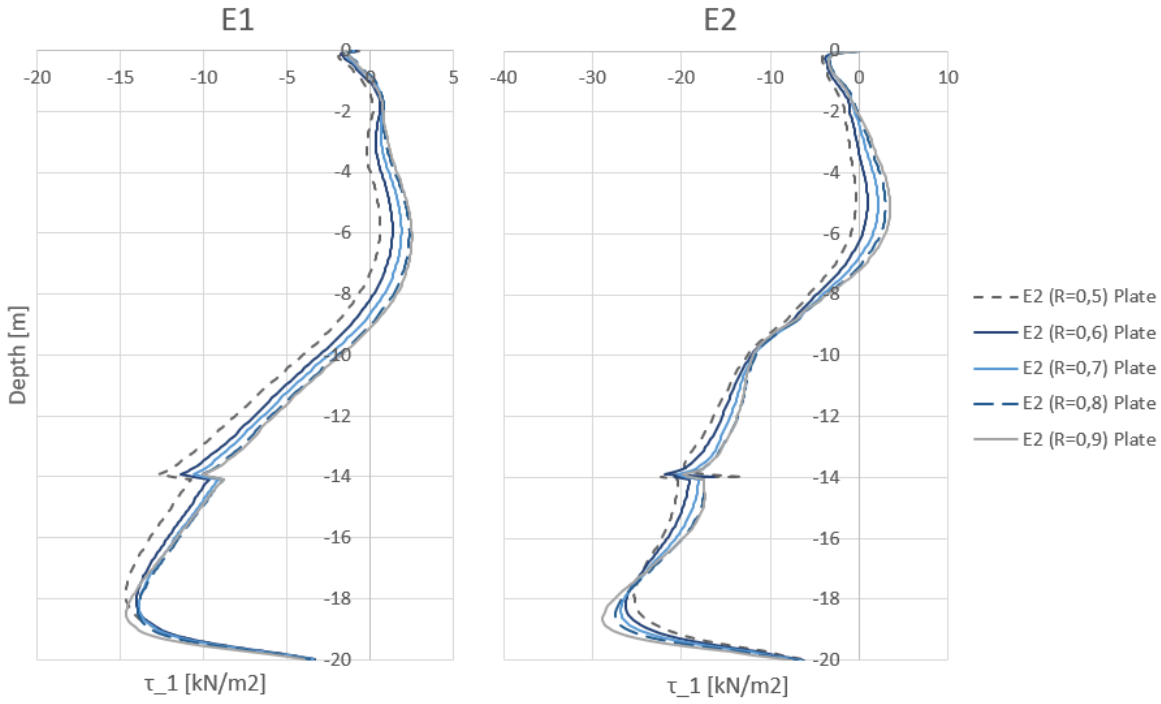

Figure 7.16: Active interface shear stresses on soil side according to FEM calculations, first and second excavation, soil side.

Similar as in the analytical calculations, the shear stresses in the numerical calculations decrease on the soil side as R_{inter} increases, despite the fact that an increased R_{inter} gives an increased ability to mobilize earth pressure. Considering the already small earth pressure angles on the soil side, the ability to mobilize more earth pressure will not affect the vertical earth pressure component much. But as mentioned before, changing R_{inter} causes a change in more than the wall friction angle. When increasing R_{inter}, both the strength and the stiffness of the interface is increased. Increasing the strength and stiffness of the interface, increases the ability of the soil to resist movement of the wall. It can be seen in Figure 7.17 that also in the numerical calculations, the passive vertical earth pressure increases as R_{inter} increases.

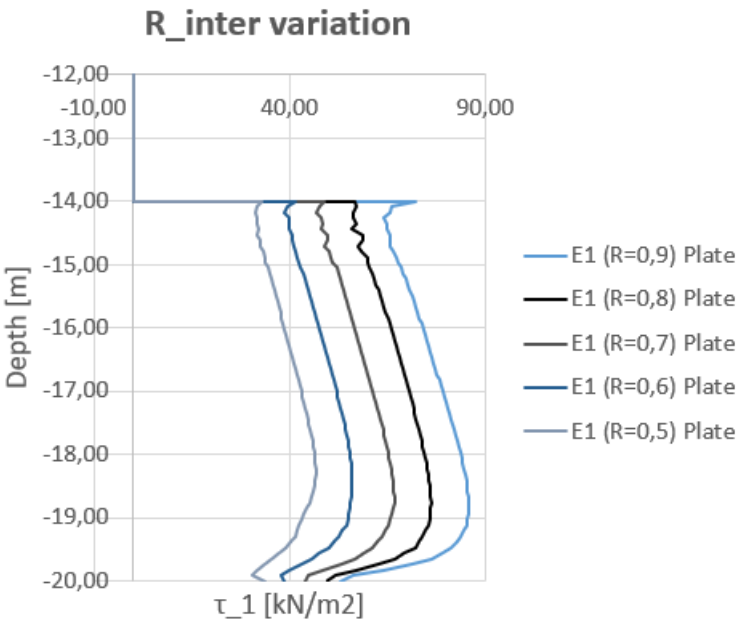

Figure 7.17: Passive interface shear stresses along the wall on excavation side after second excavation for different values of R_{inter}.

As Figure 7.20 shows, the normal stresses acting on the soil side of the wall are changing very little when R_{inter} change. Only at the upper and lower part, there is a slight change of σ. Thus, the decrease in vertical earth pressure does not come from a decrease in the earth pressure in general. However, Figure 7.19 shows that there is a change in relative displacement between the wall and the soil. The wall is mostly moving downwards relative to the soil after both excavation steps. Only between 2 and 9 meters, the soil is moving slightly more downwards than the wall. This behavior can also be recognized in Figure 7.16, where the graph shows positive shear stresses in the same area. This is likely due to the horizontal displacement of the wall. Figure 7.18, shows that there is a larger change in horizontal displacement when excavating the first step then excavating the second step, meaning the soil will move more downwards relative to the wall after E1 than after E2. This fits well with the positive shear stresses and positive relative vertical displacements in figures 7.16 and 7.19. The higher the R_{inter}, the smaller the relative movement between wall and soil. When the relative movement is smaller, so will the earth pressure angles and vertical acting earth pressures be.

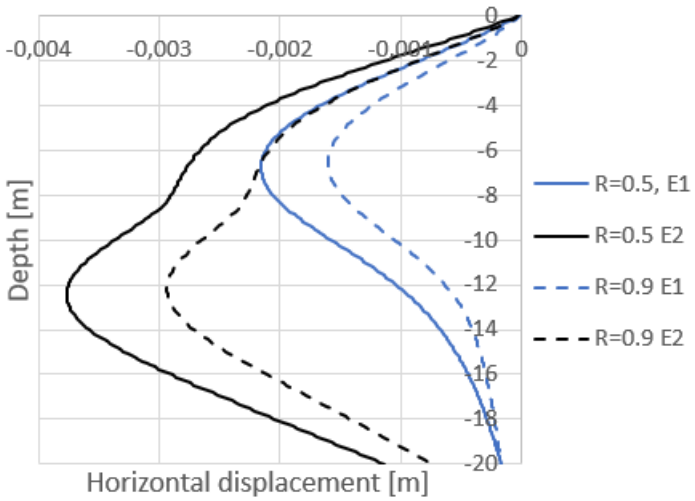

Figure 7.18: Horizontal displacement of the wall after first and second excavation for $R_{inter} = 0,5 and 0,9$

These results also fit well with the Mohr-Coulomb failure criteria. Coulombs law defines the strength limit by the failure line in equation 7.1. Increasing R_{inter} will increase both the cohesion and the friction angle in the interface and increasing these parameters will also increase the strength limit according to Coulomb (Nordal, 2018).

$$\tau_f = c + \sigma * \tan\phi \tag{7.1}$$

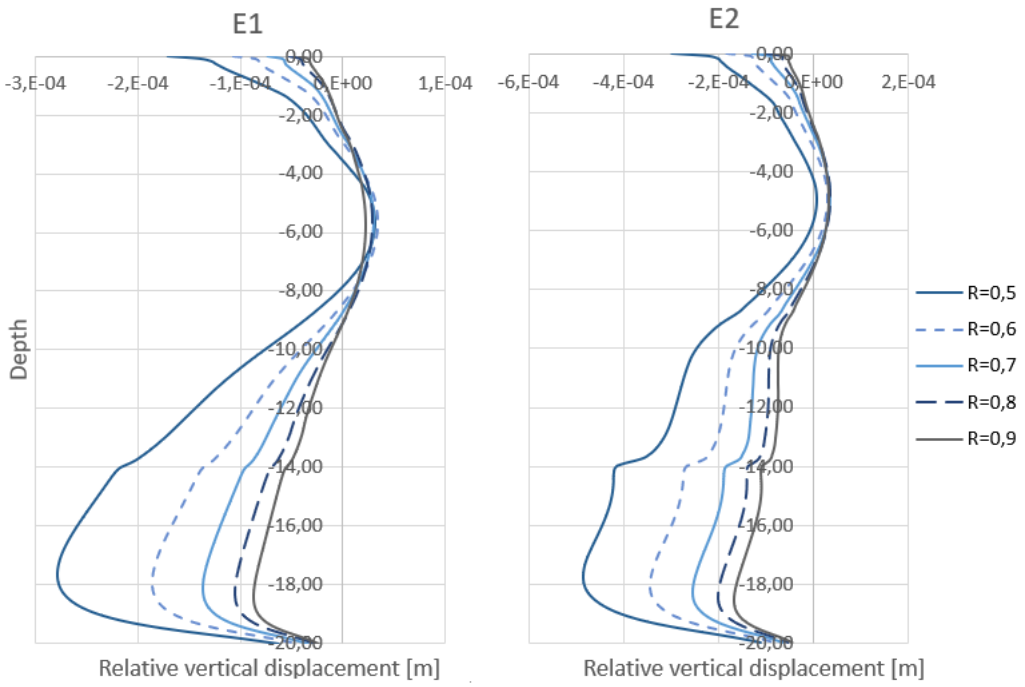

Figure 7.19: Relative vertical displacement between wall and soil on soil side for different values of R_{inter}.

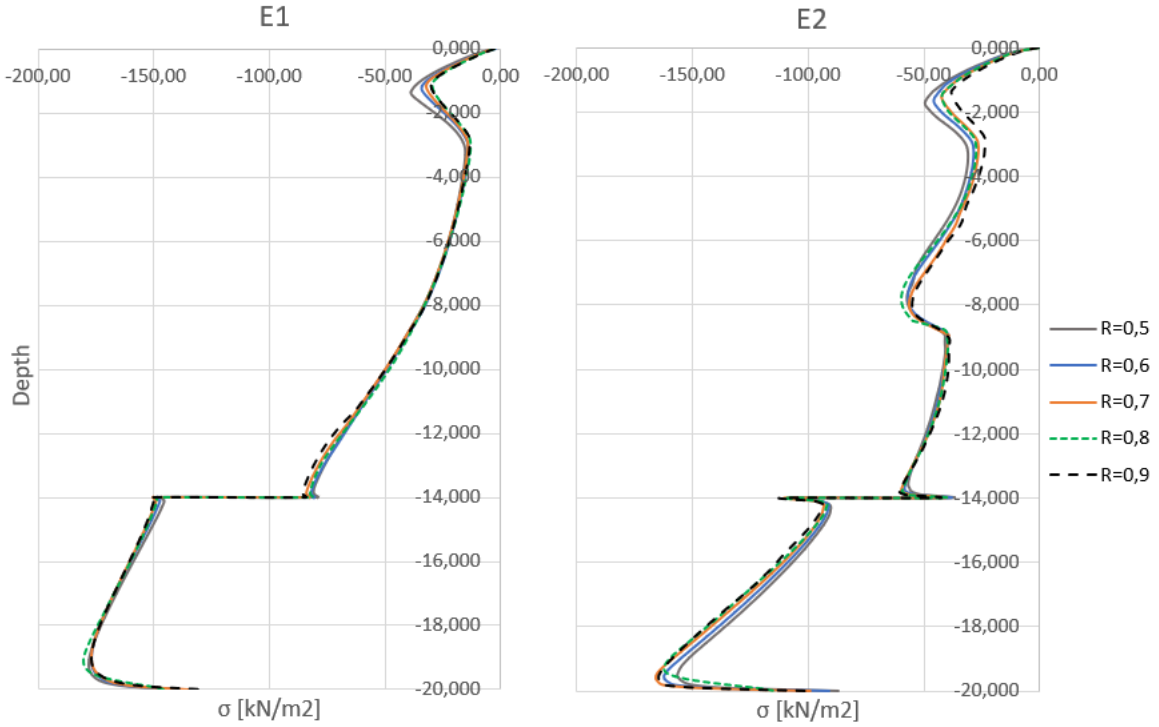

Figure 7.20: Active interface normal stresses along the soil side of the wall after the first and second excavation for different values of R_{inter}.

7.3.3 Safety factors

The safety factors in the 1st and second calculation behave similarly. They increase in all parameter variations, but seem to increase less from $R_{inter} = 0,8$ to $R_{inter} = 0,9$, which indicates that the graphs are flattening out. In the third calculation, the numerical safety factors decrease as R_{inter} increase. The increase in R_{inter} causes a larger increase in passive vertical earth pressure than it causes decrease in active vertical earth pressure. This means that for the 3rd calculation, the total amount of upward acting earth pressure increase as R_{inter} increases, which results in less downward movement of the wall. These effects increases the safety of the system and gives decreasing safety factors for higher values of R_{inter}, as shown in Figure 7.23.

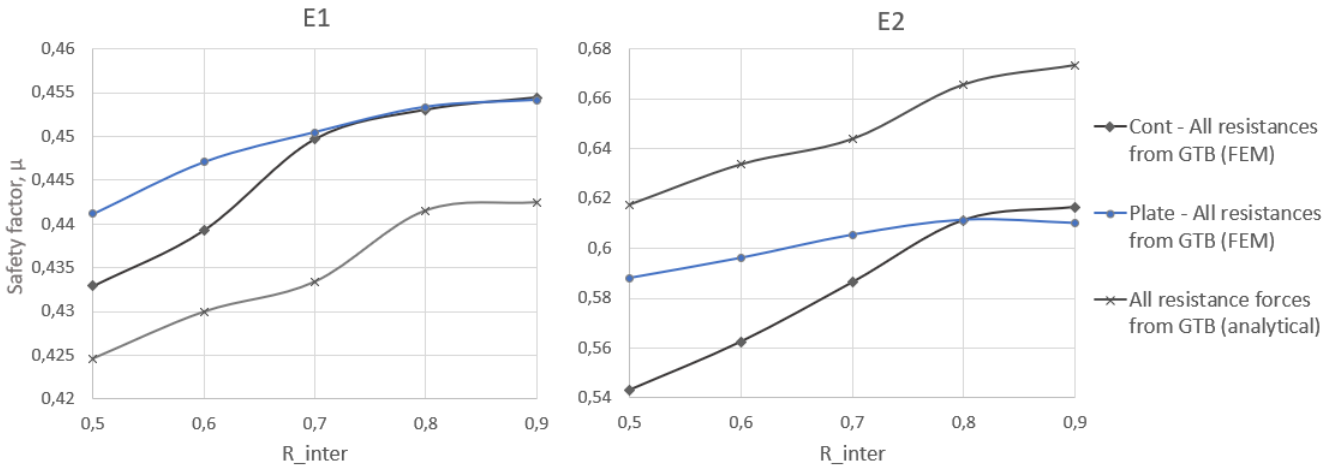

Figure 7.21: 3rd calculation: Safety factors due to earth pressure angle variation where all resistance forces are obtained from GTB.

In calculations 1 and 2, the passive earth pressure is constant, as well as most of the downward acting forces. The upward acting part of active earth pressure is decreasing with the increasing value of R_{inter} and the downward acting part is increasing, causing the safety of the system to become smaller. This means that, as seen in figures 7.21 and 7.22, that the safety factors are increasing for increasing values of R_{inter}, but they increase less in the higher range.

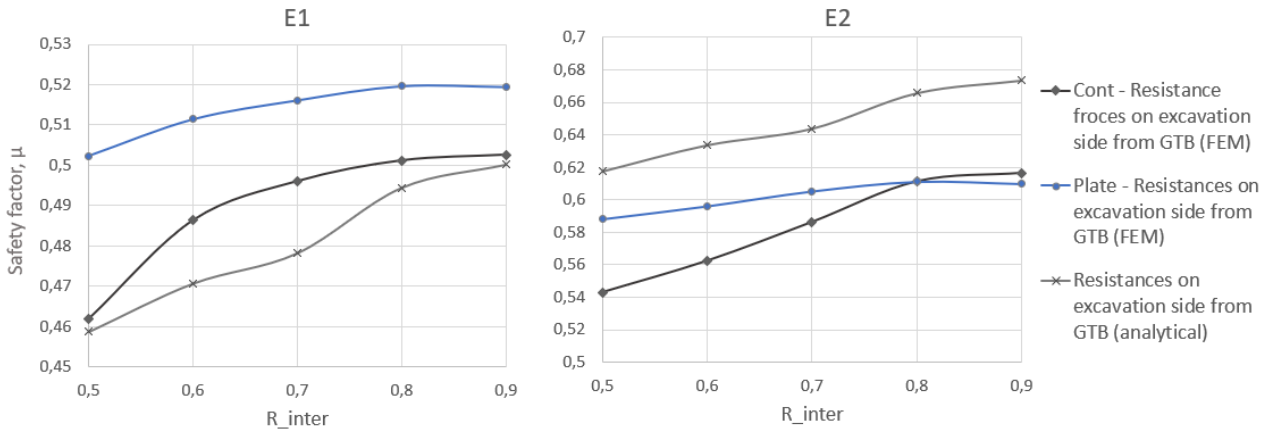

Figure 7.22: 2nd calculation: Safety factors due to earth pressure angle variation where resistance forces on excavation side are obtained from GTB.

In the analytical calculation, the earth pressure on the soil side is decreasing more than the earth pressure is increasing on the excavation side, causing the safety factors to increase in the 3rd calculation. In the numerical calculation, the passive vertical earth pressure is increasing more than the active is decreasing, causing the SF to decrease for all numerical SF except from the continuum calculation in E2. This change very little.

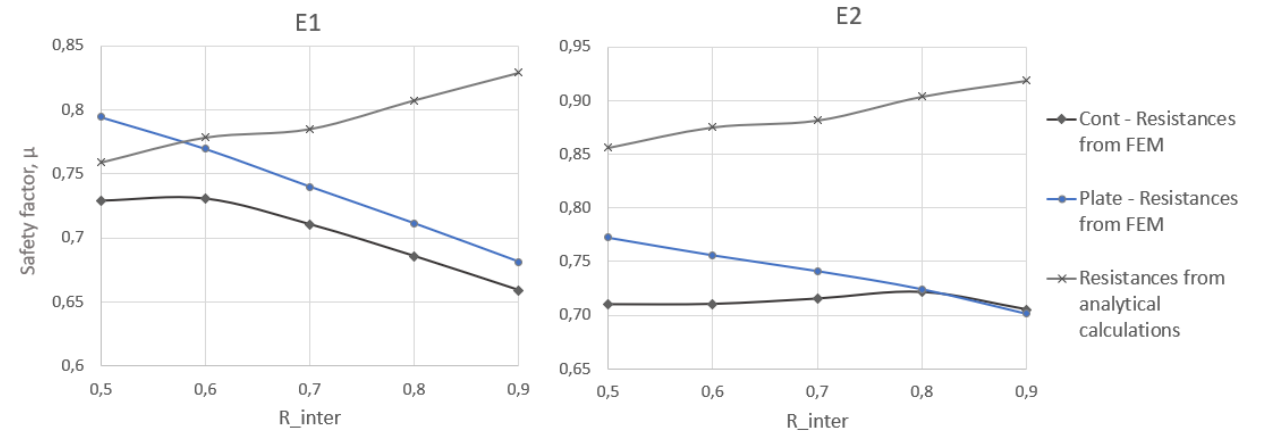

Figure 7.23: 1st calculation: Safety factors due to earth pressure angle variation where all resistance forces are obtained from analytical and numerical calculations.

7.4 Comparison of parameter variations

In this section, the parameter variations are compared in order to see which parameter variation has the larger impact on the safety factor calculation. Only the safety factors from the second excavation are compared.

In the 1st and 2nd calculation types, the ϕ variation causes the largest safety factor difference of 0,072 between the highest and lowest value from the continuum model. Following comes the plate model with a safety factor difference of 0,057. The change in the analytical calculation is 0,017. The lower bound model is the most realistic one to compare with the numerical models. The ϕ variation leads to a spread up to 0,076 between the continuum and lower bound models. In the 3rd calculation type, ϕ causes an SF spread in the continuum model of 0,059, which is the largest difference in SF in the 3rd calculation. The continuum model is closely followed by the upper bound analytical model with an SF difference of 0,058. The plate model differs with 0,019 and the lower bound with 0,008. The numerical results differs from the lower bound up to 0,161. The 3rd calculation and the continuum model is most prone to change due to the variation of ϕ.

In the 1st and 2nd calculation, the variation of cohesion has the largest impact on the plate model and lower bound calculation, which are overlapping. The spread of safety factors are 0,019. The variation is 0,18 for the continuum model. The largest SF difference between the numerical models and the lower bound calculation is 0,043. In the 3rd calculation, it is the upper bound that has the largest SF difference of 0,047, while the rest are close to constant throughout the variation. In the cohesion variation, it is the analytical calculation that is most prone to change when the cohesion changes, but spread between the safety factors of the different models is small.

In the earth pressure angle variation, it is the numerical models that are most prone to change. In the 1st and 2nd calculation, the continuum model SF has a maximum variation of 0,073 and in the 3rd variation, the plate model SF has a variation of 0,070. The largest difference between numerical and analytical safety factors in the 1st and 2nd calculation is 0,075 and for the 3rd calculation the difference is 0,217.

The variation of earth pressure angle causes the largest spread between analytical and numerical safety factors and the variation of ϕ causes the largest spread within one model.

Chapter 8

Summary and Recommendations for Further Work

8.1 Summary and Conclusions

1. **In which way can a diaphragm wall be modelled with plate elements in order to obtain results similar to a continuum model?**

   • In order to avoid loads being transferred through a line, the plate wall is modelled with a horizontal foot plate. When modelling a wall as a plate with a footplate, one must consider the extra weight of the soil laying over the foot plate. This is account for by reducing the weight of the wall by the weight of the overlying soil. As the soil is excavated, the corresponding weight of the soil removed from the foot on both sides of the wall, was added to the wall again.

   • In the volume model, the external loads are added at the edge of the wall, where the struts and slabs are connected to the wall. This eccentricity creates a bending moment in the wall. The plate wall has no thickness and the loads from the struts are therefore transferred through the center line, resulting in no such bending moment. In order to compensate for this, a bending moment corresponding to the moment created by the off-centered load is added at the top of the plate wall model.

2. **To what degree does the foot plate in the numerical plate model affect the results?**

   • The foot plate hinders relative movement between soil and wall in the clay layer. This

results in smaller vertical shear stresses between the clay and wall. In the ϕ variation, shear stresses decrease between 42,3-43,3% after the first excavation and between 14,8-30,2% after the second excavation in the clay layer on the soil side compared to the continuum model.

3. **What are the challenges with numerical calculations considering partial safety factors?**

   • As opposed to the analytical calculation, the earth pressure is not an input parameter in the numerical calculation, but a result of the simulation. According to Design Approach 2 in Eurocode 7, this can be made up for by applying the partial safety factors to the effect of the action instead of the action it self as it is done analytically.

4. **To what degree does the change of friction angle, cohesion and earth pressure angle affect the safety factors?**

   • **Friction angle:** Increasing the friction angle increases the ability of the soil to stay stable at a steeper slope. This leads to smaller vertical earth pressures on the active side and larger on the passive side. When the upward acting forces on the soil side decreases more than the vertical passive earth pressure increases, as it does in this case, the total upward acting earth pressure decreases. Due to this, the safety factor will increase. In the case where the soil moves downwards relative to the wall and the sum of the earth pressures acting on the soil side are acting downwards, downward acting forces will decrease as ϕ increases, which will cause the safety factors to decrease.

   • **Cohesion:** The inter-particular attraction caused by the cohesion is larger for higher cohesion values. This attraction causes the soil stick together, so that it applies less forces to the wall on the active side. It also increases the shear strength of the soil, giving it a better ability to resist movement of the wall, causing smaller horizontal and vertical relative movement.

   • **Earth pressure angle:** The earth pressure angle limits the ability of the wall to mobilize vertical earth pressure. However, changing the earth pressure angle numerically is done by changing the interface value R_{inter}. By changing this value, the stiffness and strength of the soil in the interface area are also changed. Both in the analytical and the numerical calculations, the vertical earth pressure is decreasing on the soil side and increasing on the excavation side as R_{inter} increases, but in the numerical calculations, the passive earth

pressure is increasing more than the active is decreasing. In the analytical calculation, the opposite is the case.

5. **Which parameter has the largest impact on the safety factors?**

   • The variation of earth pressure angle causes the largest spread between analytical and numerical safety factors and the variation of ϕ causes the largest spread within one model.

8.2 Strengths and limitations

The different calculation approaches provides different safety factors, however, the development of the safety factors due to the different parameter variations correspond pretty well, especially the results from the numerical models. The numerically calculated safety factors develop almost parallel to each other in each calculation.

Simplifications are made to both the numerical and analytical models. Terrain loads on the outside of the excavation is not considered in the calculations, and the ground water level is assumed to be below the wall, which is not the actual situation, as illustrated in Figure 4.1. In addition to this, bending moments created by earth pressures, are not considered in the analytical model. The bending of the wall affects the displacement and earth pressures on the wall, which is accounted for in the numerical models. The struts and slabs also affect the behavior of the wall, and except for their weight, they are also not accounted for in the analytical calculations.

The soil above the foot plate makes it difficult to make the weight of the wall correspond with the actual weight of the wall. The foot plate also hinders relative vertical movement between the wall and the soil at the lower part of the wall, leading to smaller shear stresses in the plate model than in the other models.

8.3 Recommendations for further work

If one want to model a retaining wall as a plate with a horizontal plate at the bottom instead of modelling the wall as a continuum, one has to consider the effect that the foot plate has on the soil-structure behavior. In this case, the vertical shear stresses acting on the plate model corresponds well with those acting on the continuum model in the gravel layer, but due to the

foot plate, the results differ a significant amount in the entire clay layer. For further work, it would be especially interesting to look into which parameter variations and which conditions affect the behaviour of the soil around the foot plate.

Recommendations for a further extension of this work is to follow the same procedure and use the same model as in this thesis and investigate more parameter variations for this model. A suggestion of another parameter that can be investigated is if the ideal width of foot plate is the true width of the wall or if it should be slimmer. Another suggestion is to what degree the magnitude of external loads, soil layering and ground water levels affects the earth pressures on the wall.

Further, it would be interesting to see how different geometries of the wall would act different in the same conditions and how anchors would affect the wall behavior compared to the struts. It would also be interesting to investigate whether or not other material models would cause a different correlation of the interaction between soil around the foot of the plate model and between the soil and the foot of the continuum model. The same parameter variations can be repeated for these different situations. In addition, it should be investigated how external loads outside of the excavation pit affects the earth pressure development along the wall. These external loads are not considered in this thesis.

When enough data is gathered, it can be investigated if the difference in the soil structure interaction around the foot plate compared to the continuum model has a repeating pattern. If it does, this can be implemented in the safety factor calculation from the plate model to improve the results.

Appendix A

Additional information

A.1 Acronyms

DA1, DA2, DA3 Design Approach 1, 2 and 3

E1, E2 Excavation step 1 and 2

FE Finite Element

FEM Finite Element Method

GS German Standard

GTB Geotechnical report (GeoTechnischer Bericht)

HS Hardening soil

HSS Hardening Soil model with Small strain

SF Safety factor

SLS Serviceability Limit State

ULS Ultimate Limit State

A.2 Numerical parameter descriptions

Table A.1: Description of model parameters for the HSS model

Parameter	Unit	Desctiption
γ	[kN/m^3]	Density
γ'	[kN/m^3]	Effective density
c'	[kN/m^2]	Effective cohesion
ϕ'	[°]	Friction angle
ψ	[°]	Dilatancy angle
E_{50}^{ref}	[MN/m^2]	Secant stiffness in standard drained triaxial test
E_{oed}^{ref}	[MN/m^2]	Tangent stiffness for primary oedometer test
E_{ur}^{ref}	[MN/m^2]	Unloading/reloading stiffness (default E_{ur}^{ref}=3E_{50}^{ref})
m	[-]	Power for stress-level dependency of stiffness
v_{ur}	[-]	Poisson's ratio for unloading/reloading
p^{ref}	[kN/m^2]	Reference stress for stiffnesses
K_0	[-]	Lateral earth pressure coefficient at rest
R_f	[-]	Failure ratio (default $R_f = 0,9$)
R_{inter}	[-]	Interface strength
$\gamma_0,7$	[-]	Shear strain at which $G_s = 0,722G_0$
G_0^{ref}	[MN/m^2]	Reference shear modulus at very small strains

Table A.2: Description of model parameters Elastic material type for plates

Parameter	Unit	Description
γ	[kN/m^3]	Density
E	[kN/m^2]	Young's modulus
v	[-]	Poisson's ratio
G	[MN/m^2]	Shear modulus
E_{oed}	[kN/m^2]	Oedometer modulus
R_{inter}	[-]	Interface strength
K_0	[-]	Lateral earth pressure coefficient at rest
EI	[kNm]	Flexural rigidity
EA	[MN/m]	Axial stiffness
w	[kN/m/m]	Weight as force per unit of length per unit width

A.3 Analytical parameter descriptions

Table A.3: German Standard approach: parameter description

Parameter	Unit	Description
c	[kN/m^2]	Cohesion
E	[kN/m^2]	Earth pressure
K	[-]	Earth pressure coefficient
ϕ	[°]	Friction angle
δ	[°]	Earth pressure angle
γ	[kN/m^3]	Soil density
p_v	[kN/m^2]	Evenly ditributed vertikal surface loads
β	[°]	Inclination of terrain behind the wall
α	[°]	Inclination of wall

German Standard approach: Indexes

- a Active state
- p Passive state
- h Horizontal component
- v Vertical component
- g As a result of soil density
- c As a result from cohesion

Table A.4: NTNU approach

Parameter	Unit	Description
p'_A	[kN/m^2]	Active earth pressure
p'_p	[kN/m^2]	Passive earth pressure
p'_V	[kN/m^2]	Vertical earth pressure
E_a	[kN]	Resulting active earth pressure force
E_a	[kN]	Resulting passive earth pressure force
K_A	[-]	Active earth pressure coefficient
K_p	[-]	Passive earth pressure coefficient
τ_A	[kN/m^2]	Active shear stress
τ_p	[kN/m^2]	Passive shear stress
δ	[°]	Earth pressure angle
ϕ	[°]	Friction angle
ϕ_d	[°]	Design friction angle
γ	[kN/m^3]	Soil density
r	[-]	Roughness
a	[-]	Attraction
q	[kN/m^2]	Terrain loads
z	[m]	Depth below terrain surface

Appendix B

Supplementary results

This chapter presents the numerical results of the reference models that are used in the safety factor calculations and the wall behavior analysis. The results given are mesh deformation, vertical deformation, interface normal- and shear forces on soil side and excavation side and internal forces of the plate wall.

B.1 Deformations

B.1.1 Deformed mesh

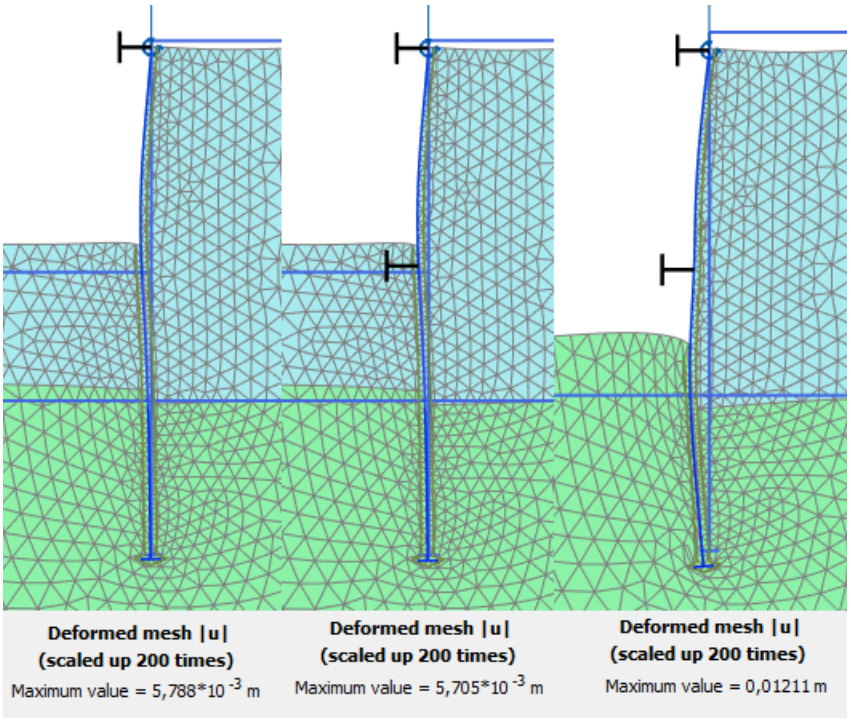

Figure B.1: Deformed mesh after first excavation, activation of lower strut and after second excavation respectively.

B.1.2 Vertical displacements

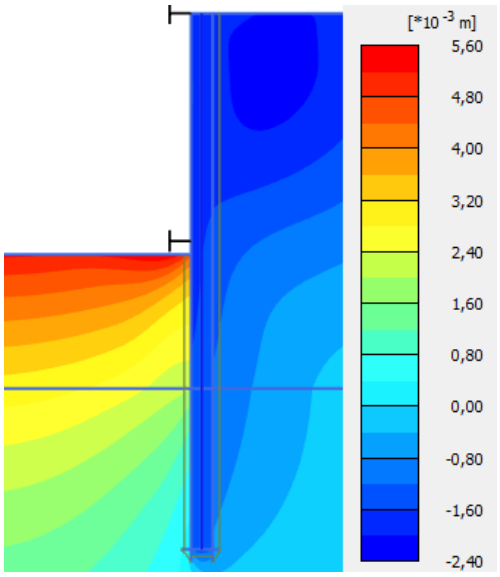

Figure B.2: Vertical displacement of 0.8 m wide continuum wall phase 3: 2,173 mm

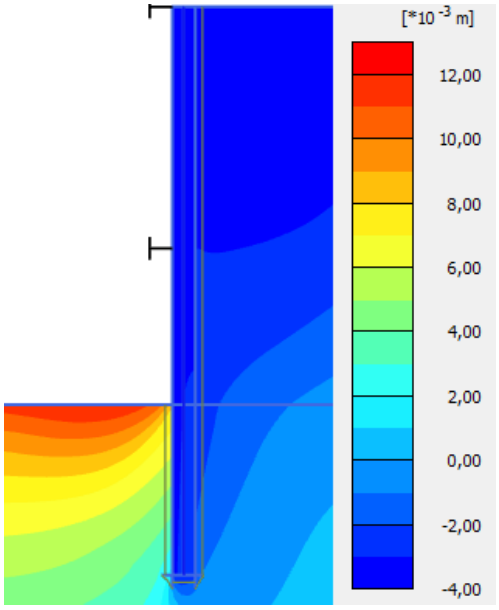

Figure B.3: Vertical displacement of 0,8 m wide continuum wall phase 4: 3,884 mm

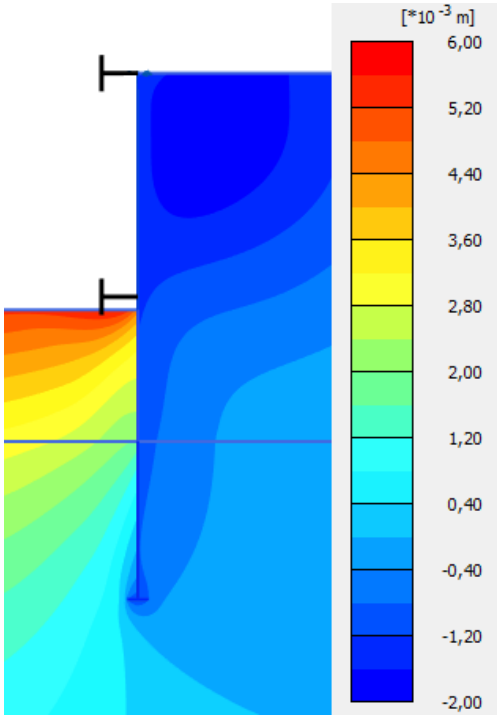

Figure B.4: Vertical displacement of wall with 0,8 m wide foot plate and with half adjusted weight phase 3: 1,509 mm

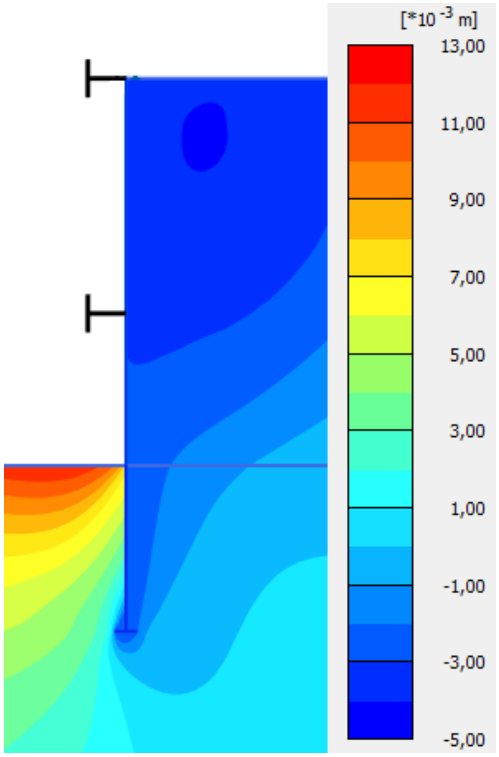

Figure B.5: Vertical displacement of wall with 0,8 m wide foot plate and with half adjusted weight phase 4: 3,501 mm

B.2 Interface stresses

B.2.1 Soil side

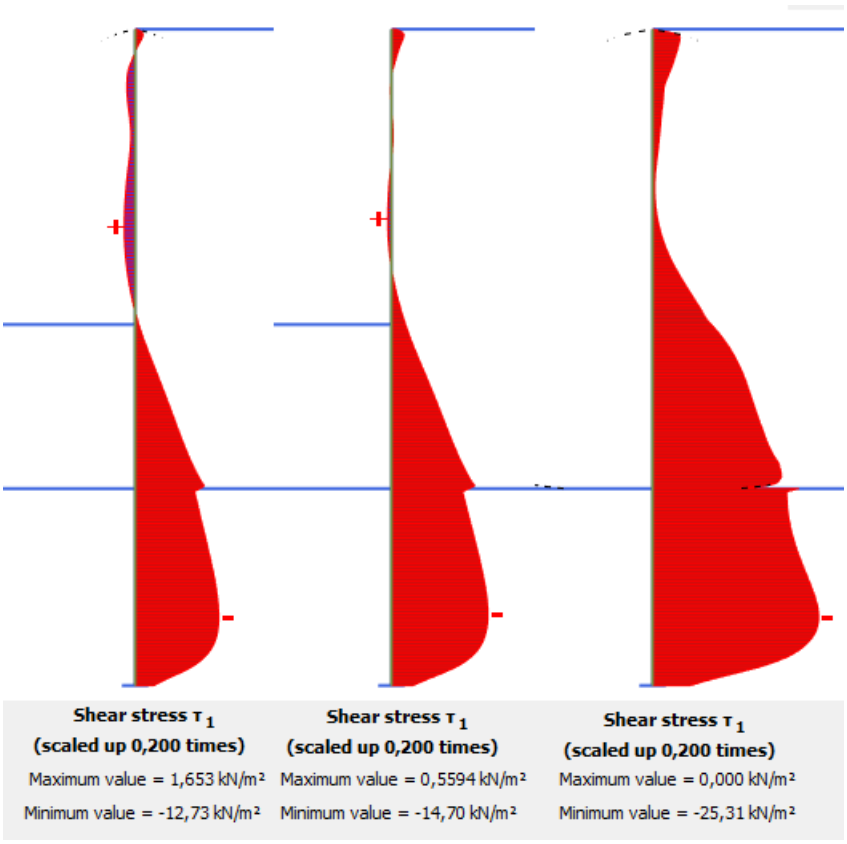

Figure B.6: Interface shear stresses along the soil side of the reference plate model after the first excavation, activation of lower strut and second excavation respectively.

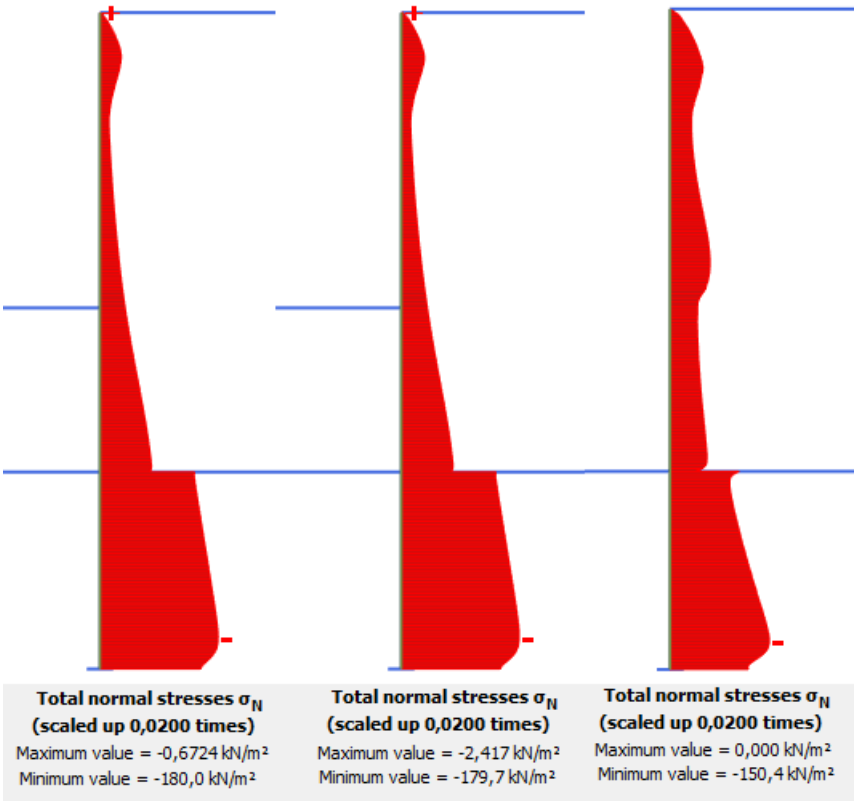

Figure B.7: Interface normal stresses along the soil side of the reference plate model after the first excavation, activation of lower strut and second excavation respectively.

B.2.2 Excavation side

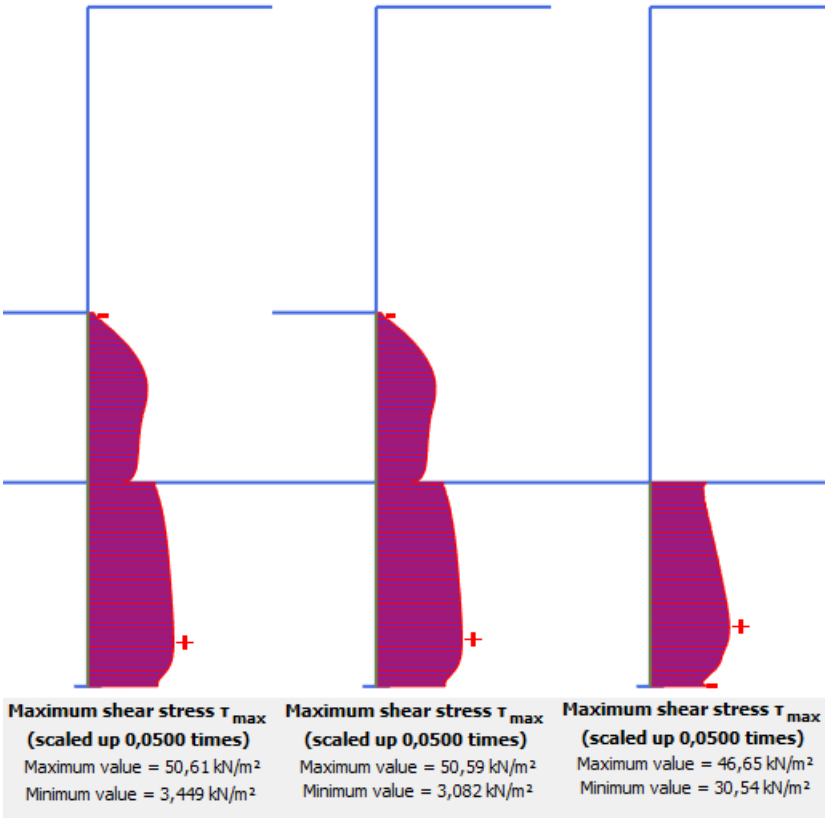

Figure B.8: Interface maximum shear stresses along the excavation side of the reference plate model after the first excavation, activation of lower strut and second excavation respectively.

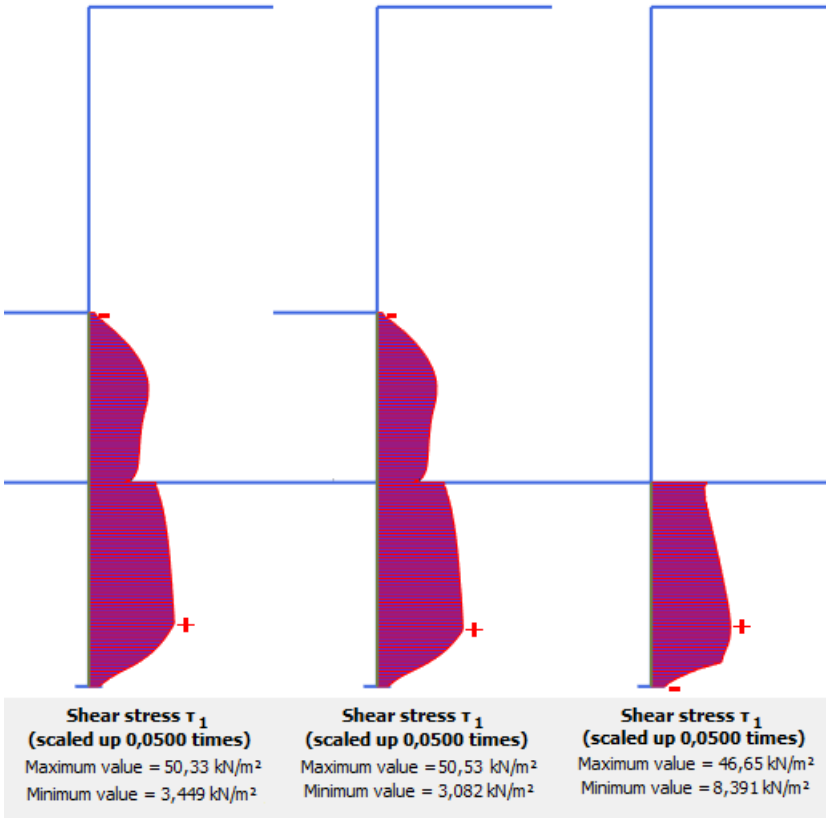

Figure B.9: Interface shear stresses along the excavation side of the reference plate model after the first excavation, activation of lower strut and second excavation respectively.

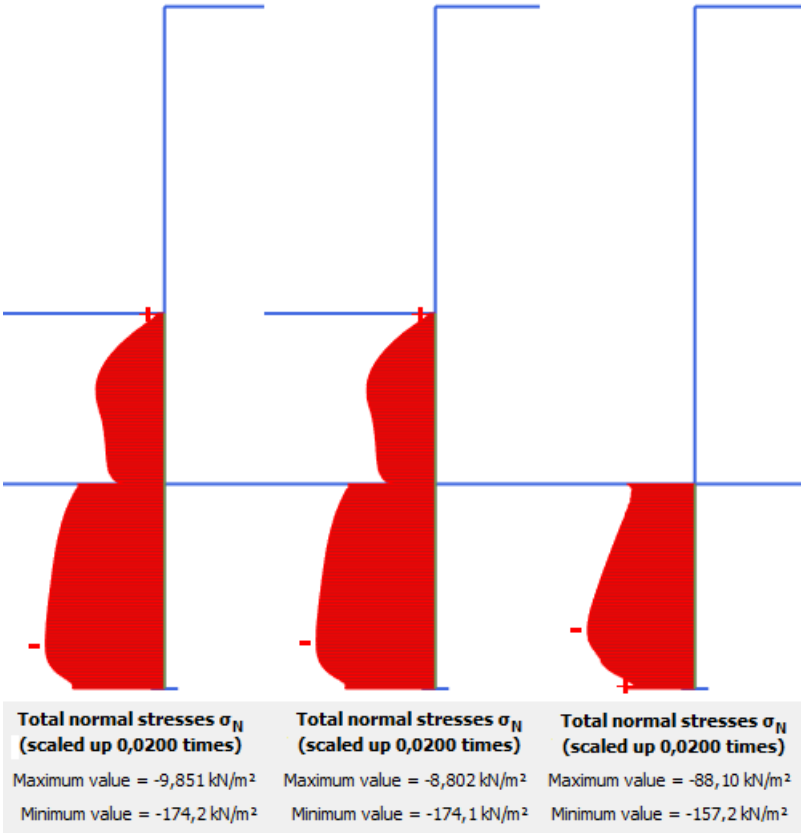

Figure B.10: Interface normal stresses along the excavation side of the reference plate model after the first excavation, activation of lower strut and second excavation respectively.

B.3 Internal forces and relative displacements of reference plate model

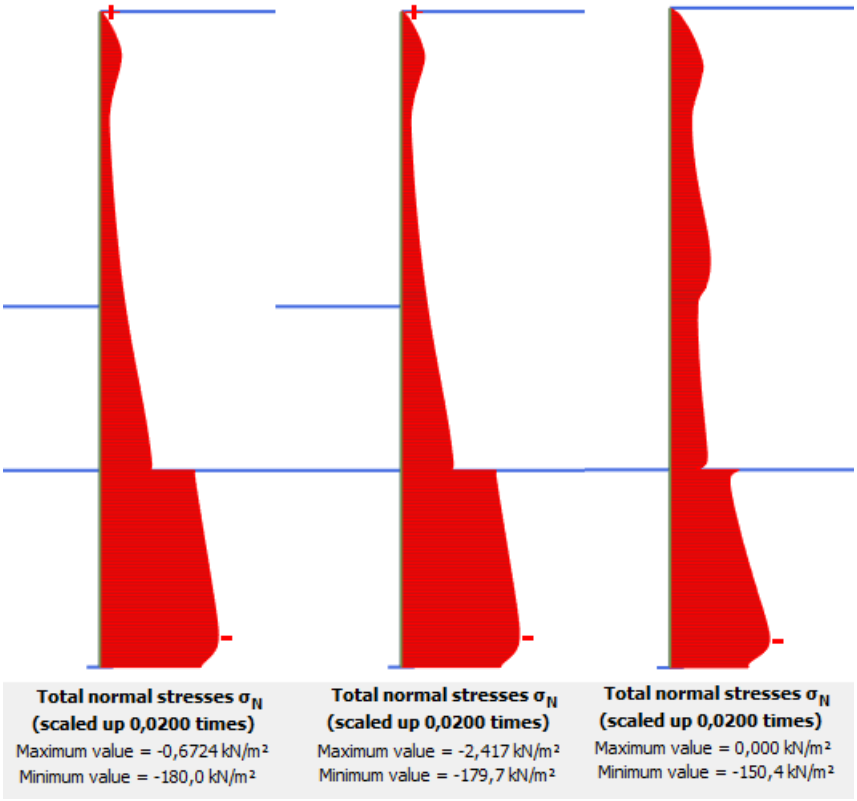

Figure B.11: Interface normal stresses along the reference plate model after the first excavation, activation of lower strut and second excavation respectively.

B.3.1 Normal forces

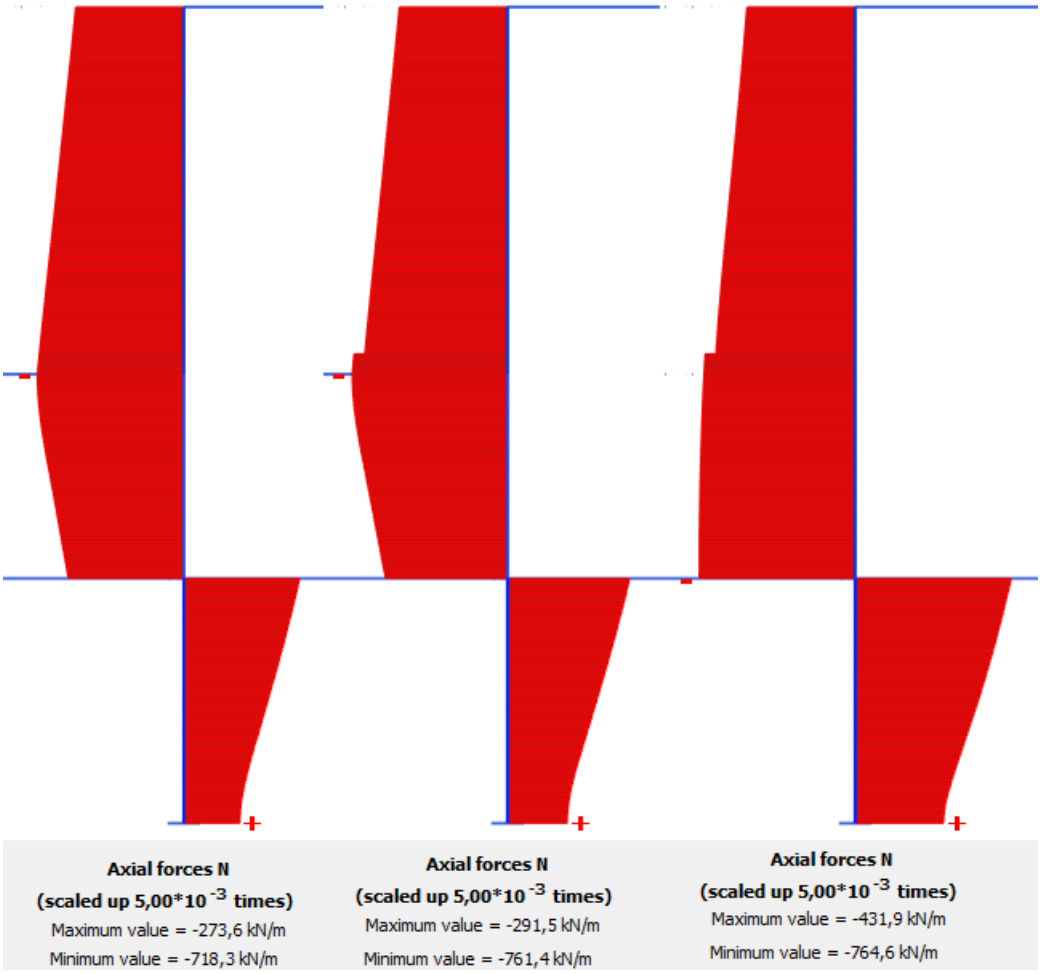

Figure B.12: Normal forces in the reference plate model after the first excavation, activation of lower strut and second excavation respectively.

B.3.2 Shear forces

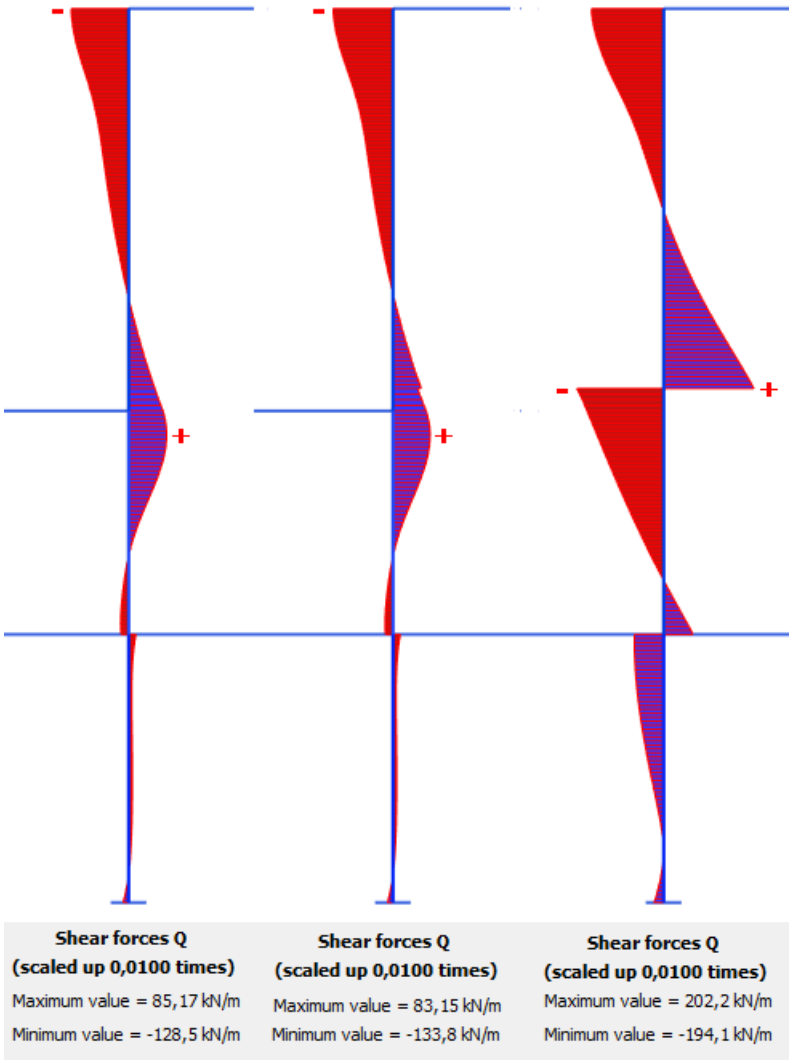

Figure B.13: Shear forces in the reference plate model after the first excavation, activation of lower strut and second excavation respectively-

B.3.3 Bending moment and relative displacement

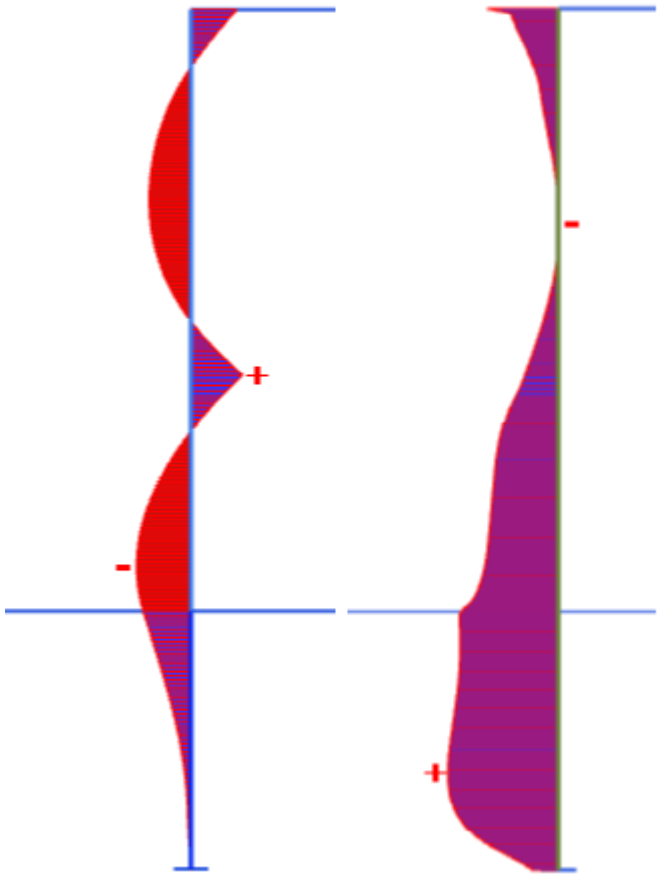

Figure B.14: Bending moment and relative displacement between wall and soil of reference plate model

B.3.4 Bending moment and relative displacement

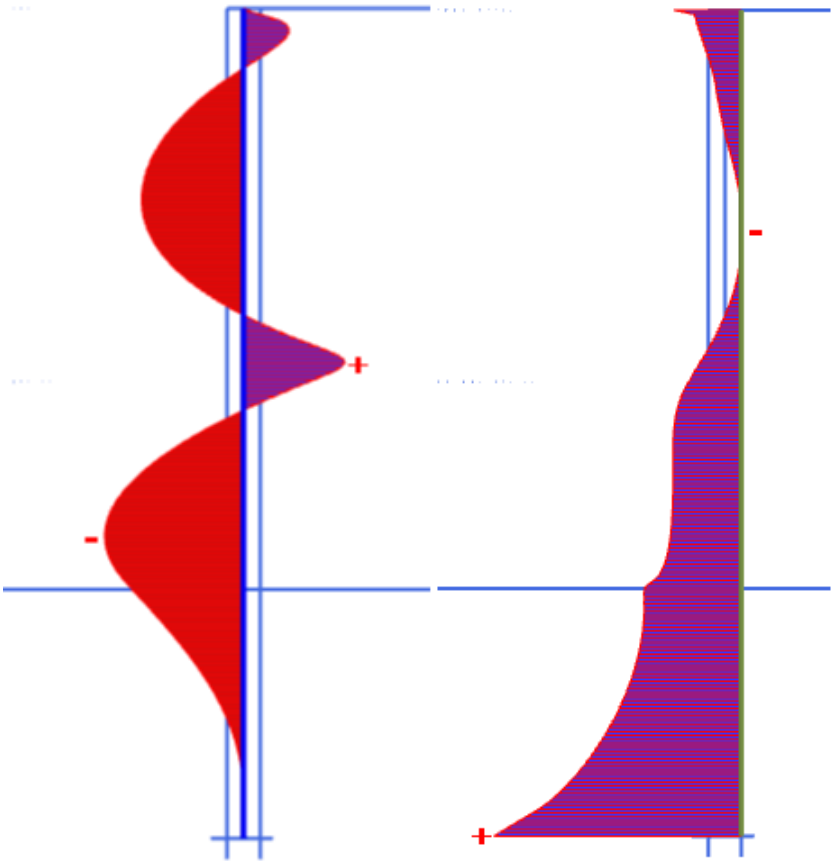

Figure B.15: Bending moment and relative displacement between wall and soil of reference continuum model

Parameter variation: Maximum and minimum bending moment and relative vertical displacements

Table B.1: Relative displacements and bending moments on plate wall as a result of variation of ϕ

ϕ	20°/30°	22,5°/32,5°	25°/35°	27,5°/37,5°	30°/40°	Unit
$Max relative displacement$	0,6096	0,5210	0,4985	0,2360	0,1967	$[10^{-3} m]$
$Min. relative displacement$	-0,0103	-0,0101	-0,0031	-0,0006	-0,0249	$[10^{-3} m]$
$Max. bending moment$	283,4	241,1	212,2	212,2	212,2	[kNm/m]
$Min Bending moment$	-276,0	-252,2	-230,2	-207,9	-183,6	[kNm/m]

Table B.2: Relative displacements and bending moments on continuum wall as a result of variation of ϕ

ϕ	20°/30°	22,5°/32,5°	25°/35°	27,5°/37,5°	30°/40°	Unit
$Maxrelativedisplacement$	2,512	1,626	1,196	0,9215	0,7679	$[10^{-3}m]$
$Min.relativedisplacement$	0,1108	-0,0041	-0,0059	-0,0387	-0,0643	$[10^{-3}m]$
$Max.bendingmoment$	236,4	195,4	161,6	141,4	117,5	[kNm/m]
$MinBendingmoment$	-278,6	-249,4	222,5	196,8	171,5	[kNm/m]

Table B.3: Relative displacements and bending moments on plate wall as a result of variation of cohesion

cohesion	15	17,5	20	22,5	25	Unit
$Maxrelativedisplacement$	0,5182	0,5081	0,4985	0,4875	0,4835	[kNm/m]
$Min.relativedisplacement$	-0,0008	-0,0028	-0,0031	-0,0060	-0,0074	[kNm/m]
$Max.bendingmoment$	236,1	216,2	212,2	212,2	212,2	$[10^{-}3m]$
$MinBendingmoment$	-248,6	-238,5	-230,2	-222,2	217,5	$[10^{-}3m]$

Table B.4: Relative displacements and bending moments on continuum wall as a result of variation of cohesion

cohesion	15	17,5	20	22,5	25	Unit
$Maxrelativedisplacement$	0,6871	1,370	1,196	1,167	1,100	$[10^{-3}m]$
$Min.relativedisplacement$	0,0570	0,0705	-0,0059	0,0599	0,0562	$[10^{-3}m]$
$Max.bendingmoment$	191,5	172,8	161,6	142,2	129,8	[kNm/m]
$MinBendingmoment$	-245,5	-234,1	-222,5	-216,9	-210,2	[kNm/m]

Table B.5: Relative displacements and bending moments on plate wall as a result of variation of R_{inter}

R_{inter}	0,5	0,6	0,7	0,8	0,9	Unit
$Maxrelativedisplacement$	0,4985	0,3561	0,2655	0,2072	0,1716	[kNm/m]
$Min.relativedisplacement$	-0,0031	-0,0260	-0,0352	-0,0357	-0,0313	[kNm/m]
$Max.bendingmoment$	212,2	212,2	212,2	212,2	212,2	$[10^{-}3m]$
$MinBendingmoment$	-230,2	-220,8	-211,6	-205,1	202,7	$[10^{-}3m]$

Table B.6: Relative displacements and bending moments on continuum wall as a result of variation of R_{inter}

R_{inter}	0,5	0,6	0,7	0,8	0,9	Unit
$Maxrelativedisplacement$	1,196	0,8645	0,6496	0,4967	0,4362	$[10^{-3}m]$
$Min.relativedisplacement$	-0,0059	-0,0364	-0,0425	-0,0578	-0,0419	$[10^{-3}m]$
$Max.bendingmoment$	161,6	152,9	140,1	128,5	125,3	[kNm/m]
$MinBendingmoment$	-222,5	-207,7	-192,8	-180,3	175,5	[kNm/m]

Appendix C

Earth pressure and safety factor calculations

C.1 Numerical calculations

From Geotechnical report

Characteristic values		Diaphragm wall [MN/m²]
Tip resistance $q_{b,k}$	Quartäre Kiese	2,8
	Tertiäre Sande	1,75
Skin friction $q_{s,k}$	Quartäre Kiese	0,14
	Tertiäre Sande	0,12

Thickness of wall	0,8

Surface resistance on excavation side

E1			E2		
-9	l	Rs,k,i	-14	l	Rs,k,i
gravel sand/silt/clay	5	0,7	geavel sand/silt/clay		
	6	0,72		6	0,72
Sum	11	1,42		6	0,72

Additional surface resistance from earth pressure below the statically required embedment depth

E1			E2		
-9	l	Rs,k,i	-14	l	Rs,k,i
gravel sand/silt/clay	5	0,6	geavel sand/silt/clay	0	0
Sum	5	0,6		0	0

Tip resistance and skin friction on excavation side according to geotechnical report

Resistances	$R_{b,k}$	γ_b	$R_{s,k}$	$\gamma_{R,e}$	$R_{b,d}$	$R_{s,d}$	$R_{c,d}$
	[MN/m]	[-]	[MN/m]	[-]	[MN/m]	[MN/m]	[MN/m]
E1	1,4	1,4	1,42	1,3	1	1,09	2,09
E2	1,4	1,4	0,72	1,3	1	0,55	1,55

Tip resistance according to Geo. report and skin friction on excavation side according to FE

Resistances	$R_{b,k}$	γ_b	$R_{s,k}$	$\gamma_{R,e}$	$R_{b,d}$	$R_{s,d}$	$R_{c,d}$
	[MN/m]	[-]	[MN/m]	[-]	[MN/m]	[MN/m]	[MN/m]
E1	1,4	1,4	0,35	1,3	1	0,27	1,27
E2	1,4	1,4	0,19	1,3	1	0,14	1,14

Soil side under tb,stat according to geotechnical report

Resistances	$R_{s,k}$	$\gamma_{R,e}$	$R_{s,d}$
	[MN/m]	[-]	[kN/m]
E1	0,6	1,3	0,46
E2	0	1,3	0,00

Soil side under tb,stat according to FE

Resistances	$R_{s,k}$	$\gamma_{R,e}$	$R_{s,d}$		
	[MN/m]	[-]	[kN/m]		
E1	0,20	1,3	0,15	statically required embedment depth	[m]
E2	0,00	1,3	0,00		6

Actions

Loads from slabs

	Wslab [kN/m]	AE Nutzlast [kN/m]	E_k (AE) [kN/m]		E_k (AE) [kN/m]	γ_G [-]	E_d (AE) [kN/m]
E1	451	127,35	589	E1	589	1,2	707
E2	451	127,35	589	E2	589	1,2	707

Dead weight of wall

	No water pressure		
	W_{wall} [kN]	γ_G [-]	E_d (SW) [kN]
E1	400	1,2	480,0
E2	400	1,2	480,0

Vertical earth pressure

$E_{v,k}$	total [kN/m]	until t_0 [kN/m]
E1	-150	-65
E2	-268	-268

Earth pressures on soil side from FE-model, Resistances on excavation side from GTB

	$E_{v,k}$ [kN/m]	E_k (AE) [kN/m]	E_k (SW) [kN/m]	γ_Θ [-]	V_d [kN/m]
E1	-150	589	400	1,2	1006
E2	-268	589	400	1,2	865

	Tip resistance $R_{b,d}$ (GTB) [kN/m]	Exc. Side $R_{s,d}$ (GTB) [kN/m]	Soil side $R_{s,d}$ (GTB) [kN/m]	Total R_d [kN/m]
E1	1000	1092	0	2092
E2	1000	554	0	1554

Safety factor

	V_d [kN/m]	R_d [kN/m]	μ [-]
E1	1006	2092	0,48
E2	865	1554	0,56

Earth pressure until statically required embedmentdepth + skin friction beneath the stat. Req. Embedment depth from GTB

	$E_{v,k}$ [kN/m]	E_k (AE) [kN/m]	E_k (SW) [kN/m]	γ_Θ [-]	V_d [kN/m]
E1	-65	589	400	1,2	1109
E2	-268	589	400	1,2	865

	Tip resistance $R_{b,d}$ (GTB) [kN/m]	Exc. Side $R_{s,d}$ (GTB) [kN/m]	Soil side $R_{s,d}$ (GTB) [kN/m]	Total R_d [kN/m]
E1	1000	1092	462	2554
E2	1000	554	0	1554

	V_d [kN/m]	R_d [kN/m]	μ [-]
E1	1109	2554	0,43
E2	865	1554	0,56

All Resistance forces from FE-Modell

	$E_{v,k}$ [kN/m]	E_k (AE) [kN/m]	E_k (SW) [kN/m]	γ_Θ [-]	V_d [kN/m]
E1	-150	589	400	1,2	1006
E2	-268	589	400	1,2	865

	Tip resistance $R_{b,d}$ (GTB) [kN/m]	Exc. Side $R_{s,d}$ (FE) [kN/m]	Soil side $R_{s,d}$ (GTB) [kN/m]	Total R_d [kN/m]
E1	1000	270	0	1270
E2	1000	145	0	1145

	V_d [kN/m]	R_d [kN/m]	μ [-]
E1	1006	1270	0,79
E2	865	1145	0,76

4.7 Finite-element method (R 103)

12. For analysis according to R 84 (Section 4.9), which guarantees that the downward-acting vertical forces in the embedment zone of the wall can be transmitted to the subsurface with sufficient safety, the vertical component of the characteristic earth pressure is obtained by integration of the vertical stresses across the rear of the wall.

4.9 Verification of the transmission of vertical forces into the subsurface (R 84)

1. It shall be verified that the downwardly directed vertical actions can be transmitted from the wall to the subsurface and that the wall will not sink. For this purpose it shall be verified that according to the limit state condition:

   $V_d \leq R_d$

   the sum V_d of the design values of the downwardly directed components of the actions are at most as great as the sum R_d of the design values of the resistances.

2. The following shall be observed for soldier pile walls, sheet pile walls or in-situ concrete walls with a free earth support according to R 14 (Section 5.3) or R 19 (Section 6.3):

   a) The downwardly directed characteristic actions, e.g. the weight density of the wall, permanent forces acting immediately on the wall, the vertical component of the earth pressure determined using the positive angle of inclination and, where applicable, the vertical component of the anchor forces, shall be converted to design values using the partial safety factors γ_G and γ_Q, separated into permanent and variable actions. See R 105, Paragraph 5 (Section 4.12) for possible simplifications for determining action effects.
   b) All upward-acting characteristic resistances, e.g. the base resistance and the friction force acting on the excavation side of the wall shall be converted to design values using the corresponding partial safety factors for resistances.
   c) The characteristic base resistances for driven soldier piles, sheet pile walls, bored piles and soldier piles placed in boreholes and grouted at the base, as well as for in-situ concrete walls, are obtained from R 85 (Section 13.10).
   d) Either a skin resistance or the vertical component of the support force B_k may be adopted as the characteristic friction force $R_{v,k}$ on the excavation side of the wall. The following are obtained:
      – the skin resistance of the developed surface A_S of the area and the skin friction $q_{s1,k}$ from
        $R_{v,k} = A_S \cdot q_{s1,k}$

4. Skin friction may be adopted as a resistance for diaphragm walls or sheet pile walls in those regions in which they are extended for the entire length of the excavation or staggered in sections over and above that structurally required. It is not necessary to provide for continuous reinforcement of the structurally extended sections for diaphragm walls.

5. If transmission of the vertical forces cannot be analysed using the initially selected approach, the positive earth pressure angle shall be reduced. If necessary, a negative earth pressure angle shall be adopted, assuming a corresponding force transmission is possible at all. The associated earth pressure increase shall be taken into consideration. Accordingly, the embedment depth and the design action effects shall be determined once again using the altered data. When adopting a negative earth pressure angle the upward-acting characteristic vertical component E_{aVk} of the earth pressure is adopted as a negative action and is therefore subtracted from the remaining characteristic actions V_k.

6. The following apply for determination of the design resistances:

   a) The partial safety factors γ_p for pile resistances may be adopted on the resistances side.
   b) If the settlements of the retaining wall need to be kept to a minimum, e.g. for excavations adjacent to structures, the characteristic values of the resistances shall be reduced with the aid of a calibration factor $\eta \leq 0.80$. It may also be necessary to analyse serviceability according to R 83 (Section 4.11).

C.2 Analytical calculations

Analytical earth pressure calculation according to DIN 4085

Parameters

Characteristic values		Diaphragm wall [MN/m²]
Tip resistance $q_{b,k}$	Quarternary gravel	2,8
	Tertiary clay	1,75
Skin friction $q_{s,k}$	Quarternary gravel	0,14
	Tertiary clay	0,12

Width of wall	0,8	m			
Friction angle grav	35	deg			
Friction angle clay	25	deg			
Extra loads on wa	165,555	kN/m			
Earth pressure angle gravel ss	17,5	deg	Earth pressure angle gravel es	17,5	deg
Earth pressure angle clay ss	12,5	deg	Earth pressure angle clay es	12,5	deg

Top layer	Value	Unit	Bottom layer	Value	Unit
Cohesion, c	0	kN/m2	Cohesion, c	20	kN/m2
Friction angle, phi	0,61	rad	Friction angle, phi	0,44	rad
Earth pressure angle soil side	0,31	rad	Earth pressure angle soil side	0,22	rad
Earth pressure angle exc. Side	0,31	rad	Earth pressure angle exc. Side	0,22	rad
Soil density, gamma	22	kN/m3	Soil density, gamma	20	kN/m3

External loads [kN/m]	
Wwall,d	480
Wslabs,d	541,2

Gravel				Clay			
Active earth pressure coefficients		Passive earth pressure coefficients		Active earth pressure coefficients		Passive earth pressure coefficients	
Kagh = Kaph	0,39	**Kpgh**	1,77	**Kagh = Kaph**	0,44	**Kpgh**	1,21
Kach	0,83	**Kpph**	2,99	**Kach**	1,08	**Kpph**	2,05
K0 = K0gh	0,43	**Kpch**	3,12	**K0 = K0gh**	0,58	**Kpch**	2,61

beta	0	Alpha	0

Pass. earth pr. ang.	Coefficients according to Pregel/Sokolowski: Gravel			Coefficients according to Pregel/Sokolowski: Clay		
	ipg	ipp	ipc	ipg	ipp	ipc
≤ 0	0,502	0,850	0,850	0,704	0,920	0,920
> 0	2,596	0,498	1,000	1,951	0,619	1,000
	gpg	gpp	gpc	gpg	gpp	gpc
	1	1	1	1	1	1
	tpg	tpp	tpc	tpg	tpp	tpc
	1	1	1	1	1	1

Initial earth pressure

Initial vertical earth pressure e0gv [kN/m2]				Initial horizontal earth pressure e0gh [kN/m2]			
depth, z [m]	Soil side	E1 excavation side	E2 excavation side	depth, z [m]	Soil side	E1 excavation side	E2 excavation side
0	0			0	0		
-9	-198	0		-9	84,4	0	
-14	-308	-100	0	-14	131,3	-46,9	0
-20	-428	-240	-120	-14	177,8	-63,5	0,0
				-15	189,4	-75,1	-11,5
				-20	247,1	-132,8	-69,3

Weight of wall [kN/m]	Tip resistance [kN/m]
1021,2	1000

Active and Passive earth pressures

	Soil side (Active earth pressure)				Excavation side E1 (Passive earth pressure)				Excavation side E2 (Passive earth pressure)			
	initial Active earth pressure	Earth pr. Due to cohesion	tot.dim. Hz. Earth pr.	Tot. Dim vertical earth pr.	Initial passive e	due to c	tot.dim. Hz. Earth pr.	Tot. Dim vertical earth pr.	Initial passive e	due to c	tot.dim. Hz. Earth pr.	Tot. Dim vertical
0	0		0,00	0	0		0	0	0		0	0
-9	32,94		42,83	13,50	0		0	0	0		0	0
-14	51,25		66,62	21,01	-82,90		-59,21	-18,67	0,00		0,00	0,00
-14	78,65	-21,57	74,21	16,45	-76,72	-52,12	-92,02	-20,40	0,00	-52,12	-37,23	-8,25
-15	83,76	-21,57	80,85	17,92	-90,67	-52,12	-101,99	-22,61	-13,95	-52,12	-47,19	-10,46
-20	109,30	-21,57	114,04	25,28	-160,41	-52,12	-151,80	-33,65	-83,69	-52,12	-97,01	-21,51
	Integration	gravel	147,04					-46,67				0,00
		clay	125,20					-162,17				-89,27
		total	272,24					-208,84				-89,27

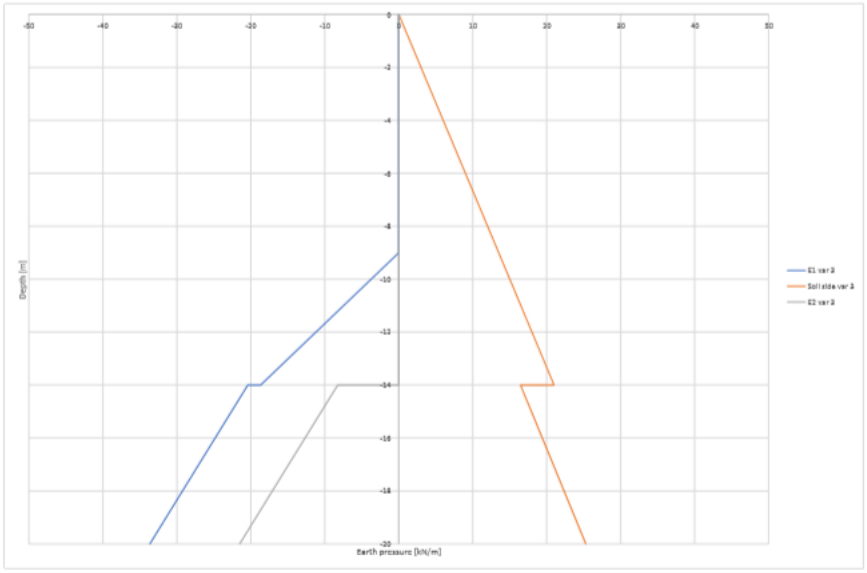

Downward acting forces down to required emb depth (E1)
17,19

Capacities

All resistance forces based on the calculations above

	Downward acting forces	Resistances	μ
E1	914,52	1208,84	0,76
E2	914,52	1089,27	0,84

Resistance forces on excavation side from geotechnical report

	Downward acting forces	Resistances	μ
E1	914,52	2092,31	0,44
E2	914,52	1554,00	0,59

All resistance forces from geotechnical report

	Downward acting forces	Resistances	μ
E1	1022,53	2554,00	0,40
E2	914,52	1554,00	0,59

Bibliography

(2014). Eurocode 7 geotechnical design - part 1: General rules.

Aarhaug, O. R. (1984). *Geoteknikk og fundamenteringslære 2*. NKI forlag.

Bathe, J. K. (1982). *Finite Element procedure in engineering analysis*. Prentice-Hall.

Brinkgreve, R., Kumarswamy, S., and Swolfs, W. (2017). *PLAXIS 2D Reference Manual*, v20 edition.

Brinkgreve, R. and Post, M. (2013). On the use of finite element models for geotechnical design.

Deutsches Institut für Normung (DIN) (2010). Din1054: Baugrund – sicherheitsnachweise im erd und grundbau – ergänzende regelungen zu din en 1997-1.

Deutsches Institut für Normung (DIN) (2017). Din 4085: 2011-05: Baugrund des erdes.

DGGT (2013). *Empfehlungen des Arbeitskreises Baugruben (EAB)*. Deutsche Gesellschaft für Geitechnik (DGGT), 2nd edition, translation of the 4th german edition edition.

DGGT (2014). *Empfehlungen des Arbeitskreises Numerik in der Geotechnik (EANG)*. Deutsche Gesellschaft für Geitechnik (DGGT).

Emdal, A., Grande, L., and Nordal, S. (2013). Geoteknikk beregningsmetoder. Trondheim, Norwgian University of Science and Technology: Geotechnical Division.

Eskandari, L. and Kalantari, B. (2011). Basic types of sheet pile walls and their application in the construction industry—a review. *EJGE*, 16:1533–1541.

Godavarthi, V., Mallavalli, D., Peddi, R., Katragadda, N., and Mulpuru, P. (2011). Contiguous pile wall as a deep excavation supporting system. *Leonardo Electronic Journal of Practices and Technologies*, (19):144–160.

Mathisen, K. M. (2018). Lecture notes in finite element method in strength analysis.

Nordal, S. (2018). Geotechnical engineering advanced course. Trondheim, Norwgian University of Science and Technology: Geotechnical Division.

Osman, A. S. and Bolton, M. D. (2011). A new design method for retaining walls in clay. *Canadian Geotechnical Journal*, 3(41):451–466.

Padfield, C. J. and Mair, R. J. (1984). *Design of retaining walls embedded in stiff clay*. Construction Industry Research and Information Association.

Sadeghi, K., Sofy, S., and Baiz, Z. (2018). Application of sheet piles in offshore structures. *Asian journal of applied sciences*, 7(1):10–18.

Soilmec (2019). Diaphragm walls.

Veidirektoratet (2014). *Håndbok V220: Geoteknikk i veibygging*. Statens Vegvesen.

Voit, T. (2016). 3D - FEM modelling of a deep excavation. Master's thesis, Graz University of Technology.